
[All ETDs from UAB](#)

[UAB Theses & Dissertations](#)

1989

Characterization Of Ion Beam Sputter-Deposited Calcium-Phosphate Films.

Earnest Douglas Rigney Jr
University of Alabama at Birmingham

Follow this and additional works at: <https://digitalcommons.library.uab.edu/etd-collection>

Recommended Citation

Rigney, Earnest Douglas Jr, "Characterization Of Ion Beam Sputter-Deposited Calcium-Phosphate Films." (1989). *All ETDs from UAB*. 4407.
<https://digitalcommons.library.uab.edu/etd-collection/4407>

This content has been accepted for inclusion by an authorized administrator of the UAB Digital Commons, and is provided as a free open access item. All inquiries regarding this item or the UAB Digital Commons should be directed to the [UAB Libraries Office of Scholarly Communication](#).

INFORMATION TO USERS

The most advanced technology has been used to photograph and reproduce this manuscript from the microfilm master. UMI films the text directly from the original or copy submitted. Thus, some thesis and dissertation copies are in typewriter face, while others may be from any type of computer printer.

The quality of this reproduction is dependent upon the quality of the copy submitted. Broken or indistinct print, colored or poor quality illustrations and photographs, print bleedthrough, substandard margins, and improper alignment can adversely affect reproduction.

In the unlikely event that the author did not send UMI a complete manuscript and there are missing pages, these will be noted. Also, if unauthorized copyright material had to be removed, a note will indicate the deletion.

Oversize materials (e.g., maps, drawings, charts) are reproduced by sectioning the original, beginning at the upper left-hand corner and continuing from left to right in equal sections with small overlaps. Each original is also photographed in one exposure and is included in reduced form at the back of the book. These are also available as one exposure on a standard 35mm slide or as a 17" x 23" black and white photographic print for an additional charge.

Photographs included in the original manuscript have been reproduced xerographically in this copy. Higher quality 6" x 9" black and white photographic prints are available for any photographs or illustrations appearing in this copy for an additional charge. Contact UMI directly to order.

U·M·I

University Microfilms International
A Bell & Howell Information Company
300 North Zeeb Road, Ann Arbor, MI 48106-1346 USA
313/761-4700 800/521-0600

Order Number 9009508

Characterization of ion beam sputter-deposited Ca-P films

Rigney, Earnest Douglas, Jr., Ph.D.

University of Alabama at Birmingham, 1989

U·M·I
300 N. Zeeb Rd.
Ann Arbor, MI 48106

CHARACTERIZATION OF ION-BEAM
SPUTTER DEPOSITED
CA-P FILMS

by

E. DOUGLAS RIGNEY, JR.

A DISSERTATION

Submitted in partial fulfillment of the requirements for the
degree of Doctor of Philosophy in the Department of
Biomedical Engineering in the Graduate School,
The University of Alabama at Birmingham

BIRMINGHAM, ALABAMA

1989

ABSTRACT OF DISSERTATION
GRADUATE SCHOOL, UNIVERSITY OF ALABAMA AT BIRMINGHAM

Degree Ph.D. Major Subject Biomedical Engineering
Name of Candidate E. Douglas Rigney, Jr.
Title Characterization of Ion-Beam Sputter Deposited CA-P Films

Recent studies have demonstrated that calcium phosphate compounds, such as tricalcium phosphate (TCP) and hydroxylapatite (HA), as well as some calcium and phosphorus containing glasses, have the potential of developing a bond to living bone. Coatings of these materials have been applied to the surfaces of dental and orthopaedic implant devices with the intention of stabilizing the implant/bone interface.

Calcium phosphate films were produced on titanium and NaCl substrates at low temperature using ion beam sputter deposition and ion beam assisted deposition (IBAD). Films were subsequently annealed at 600°C and quenched to room temperature in deionized water or allowed to cool to room temperature within the furnace. Other films were hot isostatically pressed (HIP) at 600°C and 117 MPa. The films were analyzed using Auger electron spectroscopy (AES), transmission electron spectroscopy (TEM), selected area diffraction (SAD), and energy dispersive spectroscopy (EDS).

Bond strength on the titanium substrate was determined using z-axis bond strength tests.

The coatings produced by sputter deposition and IBAD were determined to be amorphous calcium phosphate with a lower phosphorus content than the HA starting material. Post-deposition furnace treatments produced crystalline films which were primarily a combination of TCP and CaO. As-sputtered coatings were found to be very adherent in bond strength tests, while heat treated specimens had significantly lower bond strengths.

Since tricalcium phosphate is usually resorbed at a more rapid rate by the body than hydroxylapatite, the coatings produced in this study would probably not be stable enough to be functional as bioactive implant coatings. However, the sputter deposition process remains a viable alternative for coating application. By altering the sputtering parameters and starting materials, a slowly reactive, adherent coating could be produced using ion-beam sputter deposition.

Abstract Approved by: Committee Chairman

William R. Jacobs

Program Director

Mark J. W. Colleson

Date

9/15/89

Dean of Graduate School

Anthony R. Bernard

DEDICATION

This dissertation is dedicated to my wife Renita. It has been as much her effort as it has been my own.

ACKNOWLEDGEMENTS

I want to thank my advisors, Dr. Bill Laceyfield and Dr. Linda Lucas, for their continued patience, support, and encouragement throughout the course of this work. They have been more than advisors; they have been my friends.

I greatly appreciate the invaluable help of Mr. Mark Koopman with Auger electron spectroscopy, and I am also very grateful to Dr. Scott Walck for his guidance and assistance in the preparation and analysis of the transmission electron microscopy specimens.

This study was made possible through equipment obtained by the EPSCoR grant from the National Science Foundation.

TABLE OF CONTENTS

	<u>Page</u>
ABSTRACT.....	ii
DEDICATION.....	iv
ACKNOWLEDGEMENTS.....	v
LIST OF TABLES.....	viii
LIST OF FIGURES.....	ix
LIST OF SYMBOLS.....	xi
 CHAPTER	
I. <u>INTRODUCTION</u>	1
II. <u>ION-BEAM SPUTTER DEPOSITION</u>	5
<u>History and Development</u>	5
<u>The Kaufman Ion Source</u>	8
<u>Ion Production</u>	11
<u>The Sputtering Process</u>	15
<u>Sputtering of Alloys and Compounds</u>	22
<u>Particle Energy and Distribution</u> ...	24
<u>Film Growth</u>	27
<u>Sputter Cleaning</u>	31
<u>Ion-Beam Assisted Deposition</u>	33
<u>Adhesion</u>	35
<u>Competitive Coating Processes</u>	39
<u>Droplet Transfer</u>	40
<u>Atom-by-Atom Transfer</u>	42
<u>Literature Survey</u>	48
<u>Hypotheses and Objectives</u>	67
III. <u>MATERIALS AND METHODS</u>	72
<u>Materials</u>	72
<u>Material Preparation</u>	72
<u>Sputter-Coating Procedure</u>	76
<u>Post-Deposition Treatments</u>	79

TABLE OF CONTENTS (Continued)

	<u>Page</u>
<u>Methods</u>	80
<u>Transmission Electron Microscopy</u>	80
<u>Auger Electron Spectroscopy</u>	81
<u>Energy Dispersive Spectroscopy</u> ..	83
<u>Bond Strength Testing</u>	83
IV. <u>RESULTS</u>	86
<u>Auger Electron Spectroscopy</u>	86
<u>Energy Dispersive Spectroscopy</u>	101
<u>Transmitted Electron Spectroscopy</u> ..	113
<u>Bond Strength Test</u>	124
V. <u>DISCUSSION</u>	131
<u>Summary</u>	143
VI. <u>CONCLUSIONS</u>	145
VII. <u>RECOMMENDATIONS</u>	148
<u>LIST OF REFERENCES</u>	151

LIST OF TABLES

TABLE		<u>Page</u>
1.	Chemical Analysis of ASTM F 67 Titanium Grade 2.....	75
2.	Ca/P Ratios for the Ion-Beam Sputter Deposited Coatings.....	108
3.	Average Bond Strength Values and Statistics.....	126

LIST OF FIGURES

<u>Figure</u>	<u>Page</u>
1. The Kaufman Source (Thornton 1982a).....	9
2. Ionization Process in the Kaufman Source (Kaufman 1984).....	12
3. Potential Through the Ion Optics (Kaufman 1984)..	16
4. Spatial Distribution of Sputtered Atoms (Kaufman 1984).....	26
5. Zone Model of Film Growth (Thornton 1982a).....	29
6. Scanning Electron Micrograph of the Sintered Hydroxylapatite Target Material.....	73
7a. Stage Arrangement for Sputter Cleaning.....	77
7b. Stage Arrangement for Sputter Deposition.....	77
8. Position of Bond Test Specimen in Spring Clip....	84
9. Auger Depth Profile of Single-Beam As-Sputtered Coatings.....	87
10. Auger Depth Profile of HA Target Material.....	90
11. Auger Depth Profile of Single-Beam Furnace Cooled Coatings.....	92
12. Auger Depth Profile of Single-Beam Quenched Coatings.....	95
13. Auger Depth Profile of Single-Beam Hot Isostatically Pressed Coatings.....	97
14. Auger Depth Profile of Dual-Beam As-Sputtered Coatings.....	99
15. Auger Depth Profile of Dual-Beam Furnace Cooled Coatings.....	102
16. Auger Depth Profile of Dual-Beam Quenched Coatings.....	104

LIST OF FIGURES (Continued)

<u>Figure</u>	<u>Page</u>
17. Auger Depth Profile of Dual-Beam Hot Isostatically Pressed Coatings.....	106
18. EDS Profile of Single-Beam As-Sputtered Coatings.	109
19. EDS Profile of Dual-Beam As-Sputtered Coatings...	111
20. TEM/SAD of Single-Beam As-Sputtered Films. a. TEM of Single-Beam As-Sputtered Film, b. SAD of Single-Beam As-Sputtered Film, c. TEM of SBAS Film after Electron Beam Heating, d. SAD of SBAS Film after Electron Beam Heating.....	114
21. TEM/SAD of Dual-Beam As-Sputtered Films. a. TEM of Dual Beam As-Sputtered Film, b. SAD of Dual-Beam As-Sputtered Film, c. TEM of DBAS Film after Electron Beam Heating, d. SAD of DBAS Film after Electron Beam Heating.....	116
22. TEM/SAD of Single-Beam Furnace Treated Films. a. TEM of Single-Beam Furnace Cooled Film, b. SAD of Single-Beam Furnace Cooled Film, c. TEM of Single-Beam Quenched Film, d. SAD of Single-Beam Quenched Film.....	119
23. TEM/SAD Dual-Beam Furnace Treated Films. a. TEM of Dual-Beam Furnace Cooled Film, b. SAD of Dual-Beam Furnace Cooled Film, c. TEM of Dual-Beam Quenched Film, d. SAD of Dual-Beam Quenched Film.	122
24. Coating Bond Strength.....	125
25. Photomicrographs of Bond Test Fractures.....	129

LIST OF SYMBOLS

A	Angstrom
d	Distance
D	Density
eV	Electron Volts
E	Kinetic Energy
I	Ion Current
j	Current Density
m	Mass
q	Charge
r	Radius of a Sphere
R_d	Rate of Deposition
s	Sputter Yield
T	Temperature
U	Heat of Sublimation
V	Volume
W	Atomic Weight in Atomic Mass Units
ϵ	Transfer Function
ϵ_0	Permeability of Free Space

CHAPTER I.

INTRODUCTION

Calcium phosphate compounds are naturally occurring minerals in the human body (Bonel et al. 1988; Driessens 1988). Over 90% of tooth enamel is constituted of the calcium phosphate salt hydroxyapatite $[Ca_{10}(PO_4)_6(OH)_2]$. Other calcium phosphate phases such as whitlockite are also present to a lesser extent in enamel (Woltgens 1983). Human bone is 60% anorganic material by weight. Although bone contains a variety of calcium phosphates and carbonates as well as magnesium, sodium and potassium, most of this portion is hydroxyapatite (HA) (Bonel et al. 1988; Van Mullem and Maltha 1983).

In the last decade, a number of calcium phosphate containing ceramic materials have found increasing use for biomedical applications (Feenstra and De Groot 1983; Yamamuro et al. 1988). A number of new developments involving both calcium phosphate ceramics have been reported in orthopaedics and dentistry in recent years (Beirne, Curtis, and Greenspan 1986; Cook et al. 1988; De Putter, De Groot, and Silleviss Smitt 1982). These ceramic materials, in spite of their very different levels of chemical reactivity, have been reported to be better tolerated by the

body than the metallic materials in current use (Heimke and Griss 1983). The typical response of the body to a metallic implant is to surround it by a fibrous capsule, often causing poor stress transmission and loosening of the implant (Thomas et al. 1987, Cook et al. 1987). Ultimately this may lead to failure. Bone forms quickly around bioactive ceramic materials containing calcium and phosphorus without a fibrous capsule (Heimke and Griss 1983; Hench 1988). However, these particular ceramics are mechanically brittle and possess relatively low strengths; therefore, they are not suitable for use in bulk form in load bearing implant applications (Bonfield 1988). A metallic implant coated with a bioactive ceramic may be able to achieve interfacial stability within a shorter time period and thereby enable a patient to attain mobility within a shorter period of time (Yamamuro et al. 1988).

Studies by Cook et al. reported that bone grew directly along HA-coated titanium implants in dogs, while a thin fibrous layer was found between bone and uncoated titanium implants (Cook et al. 1987). Interfacial shear strengths, indicative of bone bonding, for HA-coated implants were stronger after only three weeks in situ than the uncoated implants after 32 weeks. The average interfacial shear strength reported for coated implants after 10 weeks was 7.27 MPa, while the maximum interface reached for uncoated implants was 1.57 MPa after 7 weeks (Cook et al. 1988). De Groot et al. have recently reported interfacial shear

strengths between plasma sprayed HA and cortical bone as high as 65 MPa after six months in vivo (De Groot et al. 1988).

Polymethylmethacrylate grout (PMMA), or bone cement as it is commonly called, is frequently used as a secondary fixation material in many current orthopaedic systems such as the total hip or knee prosthesis. A bioactive ceramic coating capable of developing a bond with the surrounding bone might make this unnecessary. Since PMMA is often considered the "weak link" in the development of a successful long-term implant/bone interface, this would be an added advantage (Davies and Harris 1989; Menis, Wixson, and Lautenschlager 1989). The most commonly used technique for coating biocompatible ceramic materials onto metal implants is by plasma spraying (Kay et al. 1986). However, this method has not been completely successful, as problem areas such as non-uniform density and alteration of the ceramic structure have been reported. An electrophoretic deposition process followed by sintering has also been used to form a hydroxylapatite coating on a titanium substrate. However, the sintering of the ceramic coating at the minimum temperature (900°C) has been shown to adversely affect the mechanical properties of the most commonly used metallic substrates (Van Raemdonck, Ducheyne, and De Meester 1984; Ducheyne et al. 1986).

Stainless steel implants have been successfully coated with a soluble glass containing calcium and phosphorus by immersing the metal into the molten glass (Busemi and Hench

1978; Ducheyne 1985). However, attempts to immersion coat titanium implants with selected bioglasses have been less successful (Lacefield 1988). Bioactive glasses are formed from a combination of SiO_2 , CaO , Na_2O , and P_2O_5 . Several studies have shown that such glasses will react to form a bond with living bone (Ducheyne 1985; Hench 1988). Although the glasses are amorphous in structure, it is the development of a calcium phosphate film on the glass surface which leads to the bond between the bone and the bioglass (Ogino, Ohuchi, and Hench 1980; Pantano, Clark, and Hench 1974).

Previous attempts to coat biocompatible ceramic materials onto metal implants by plasma spraying and other more conventional methods have not been entirely successful because of such problems as low adhesive strength, non-uniform coating density, and alteration of the composition or mechanical properties of the coating and/or the substrate materials (Lacefield 1988).

CHAPTER II.

ION-BEAM SPUTTER DEPOSITION

Ion-beam sputter deposition represents a novel approach to the application of bioactive coatings to materials intended for medical or dental implant use. Although the process has been used in the electronics industry for many years (Ghate 1982; Wehner and Anderson 1970), it is new to the production of bioactive coatings.

History and Development

The first record of ion-beam deposition was by Gore in 1852 (Wehner and Anderson 1970). However, the process was superseded by vacuum evaporation in the production and application of thin films for almost one hundred years because the contamination problems inherent in ion-beam deposition could not be easily controlled. Ion-beam deposition became a viable alternative to vacuum evaporation only after the emergence within the electronics industry of the need for film properties not available by any other means (Maissel 1970).

Basically, two types of ion-beam deposition sources are in use today, primary ion-beam deposition and secondary ion-beam deposition or ion-beam sputter deposition. The cathode in a primary ion-beam deposition source is constructed of

the desired film or coating material; consequently, the ion beam consists of the sputtering material itself. The ion-beam energy for this process is usually in the range of 10 to 100 eV (Harper 1978). Primary ion-beam deposition is also known as diode sputtering. If electromagnets or permanent magnets are added to the diode system to control or direct the charged ion plasma, the process is known as magnetron sputtering (Rossnagel and Kaufman 1987, 1988; Thornton 1982a). These processes will be discussed more thoroughly in a following section on competitive deposition processes; however, for the purposes of this paper, secondary ion-beam deposition will be primarily considered. The cathode in secondary ion-beam deposition is a thermionic filament, most frequently made of tungsten or tantalum wire. A higher energy ion plasma is produced by collisions between energetic electrons from the cathode filament and atoms of an inert gas such as argon. The energy of the resultant plasma may range from several hundred to a few thousand electron volts depending on the particular ion source design (Harper 1978). The plasma is formed into an ion beam and directed at a target disk of the desired film material. All the advantages of secondary ion-beam sputter deposition are due to the isolation of the target material and the substrate from the production of the ion plasma (Kaufman 1978). Physical sputtering occurs when material in the form of energetic ions, atoms, or molecules is dislodged or removed from the surface of the target due to the momentum exchange associated with surface bombardment by energetic

ions (Thorton 1982a). Dislodged material in turn is deposited on the substrate surface.

Secondary ion-beam deposition allows for greater isolation of the substrate from the ion generation process than in diode or magnetron sputtering. It also gives the operator greater control over substrate and target temperatures, gas pressure, angle of material deposition, and independent control over the ion-beam current and energy (Harper 1978).

The first modern ion-beam source was developed by Penning in 1940. This device consisted of a cylindrical anode with two cathodes forming the end plates. A single aperture for beam extraction was actually in one of the cathode end plates. A magnetic field of several hundred Gauss applied parallel to the cylinder axis controlled the ion direction. Control of the ion-beam was somewhat limited in this design because the discharge current was not controlled independently of the discharge voltage (Harper 1978).

The duoplasmatron was developed in 1956 by von Ardenne. This ion source allowed independent control of discharge current and voltage, and it generated intense small diameter ion beams up to 20 keV. However, in using a single ion-beam extraction aperture the overall beam current was limited by space charge effects (Harper 1978).

In 1960 Harold R. Kaufman expanded on these two designs in developing an ion thruster system intended for space propulsion (Harper 1978; Kaufman 1978, 1984). He added a

thermionic cathode which supplied electrons at a rate independent of the discharge voltage and a multiple aperture extraction system designed to broaden the ion beam. A multiple aperture system also had the advantage of allowing higher ion currents than single aperture ion sources (Harper 1978).

The Kaufman Ion Source

The ionization process within the Kaufman source can best be described by first describing the components of the system. Figure 1 is a schematic of the Kaufman-type ion source used in the work presented here. It consists of a tantalum wire cathode filament surrounded by a cylindrical anode chamber. An inert gas such as argon is ionized as it passes over the energized cathode. Permanent magnets surround the anode wall, creating a magnetic field used to prevent the ionized plasma from traveling directly to the anode. The screen grid is held at cathode potential while the accelerator grid is held at a potential not more than 25% of the cathode but negative of ground. This potential difference combined with the several hundred small apertures in the two grids serve to align the plasma and accelerate it toward the target (Kaufman 1984). Together the screen grid and the accelerator grid make up the ion optics of the ion source. At these energies the ions and electrons are not usually in thermal equilibrium, and the arrival rate of electrons to the target is not always equal to that of the ions. This results in a charged plasma. A separate neutralizer filament is placed in the path of the plasma to

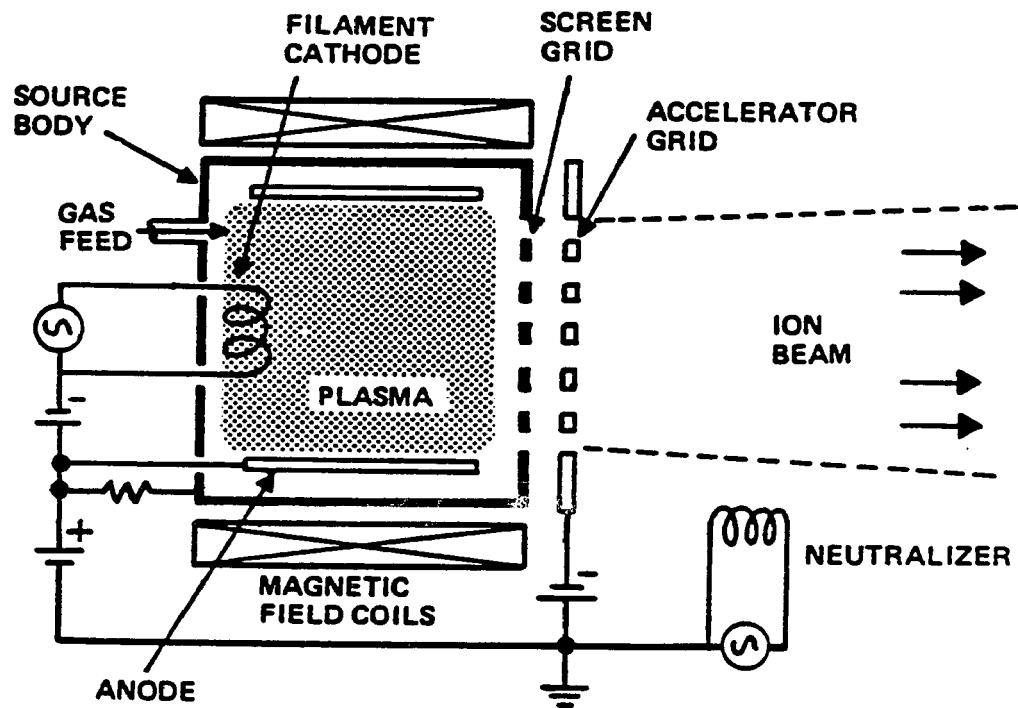


Figure 1. The Kaufman Source
(Thornton 1982a)

add back electrons. Although the electrons do not recombine with the ions to neutralize the plasma, they rapidly distribute throughout it to cancel any net charge (Harper 1978).

It has been stated that a principal advantage of ion-beam sputter deposition is the ability to control discharge voltage independently of current. This allows the operator to achieve a desired level of cathode current and emission without the damaging effects of multiple ionization. The energy for ionization is provided by the discharge voltage. At high discharge voltages, argon can become doubly or triply ionized. A multiply charged ion will acquire more energy passing through the ion optics than a singly charged ion. An Ar^{++} ion will receive twice the energy of Ar^+ . Since doubly and triply charged ions will penetrate the target and substrate more deeply, they will cause more damage to the near surface lattice and also lead to increased film contamination from the ion source. The first ionization potential for argon is 15.8 eV. This means in theory that an electron accelerated to 15.8 eV will ionize an argon atom. The second ionization for argon occurs at 27.6 eV. For a single collision between atom and electron to doubly ionize the argon, the electron must be accelerated to $15.8 + 27.6 = 43.4$ eV. Double ionization can also occur by two independent collisions, but since the mean-free-path for charge exchange at the vacuum chamber pressure of 10^{-4} Torr approaches 15 cm (Harper, Cuomo, and Kaufman 1982), this is not likely. Consequently, if the discharge voltage

is maintained below 43.4 eV, multiply charged ions can be reduced or eliminated from the ion beam (Kaufman 1984).

Ion Production

Ion production in this system occurs by direct-current electron bombardment of the low pressure inert gas atoms. Figure 2 demonstrates schematically the ionization process within the Kaufman source. Neutral gas atoms (1) enter the chamber through the discharge chamber inlet. Energetic electrons (2) from the cathode collide with the atoms (3) of the gas producing ions. Some of the ions (4) travel to surfaces within the chamber and recombine with electrons from those surfaces returning to the chamber as neutrals (5). Some of the ions produced (6) are formed into small beamlets by passing through the holes in the screen grid. As previously mentioned the accelerator grid is held negative to ground. The ion beamlets are attracted to the negatively charged grid, but in normal operation pass on through without impinging on it due to the alignment of the holes in the two grids. The diameter of the the accelerator grid apertures is normally 80% of the diameter of the screen apertures in order to limit the divergence of the beam diameter (Kaufman, Cuomo, and Harper 1982). The total diameter of the ion beam (7) is determined by the sum of the individual beamlets as they pass out of the accelerator grid. The beam is then neutralized by electrons (8) from the neutralizer. The neutralized ion beam has equal densities of electrons and ions within the beam (Kaufman

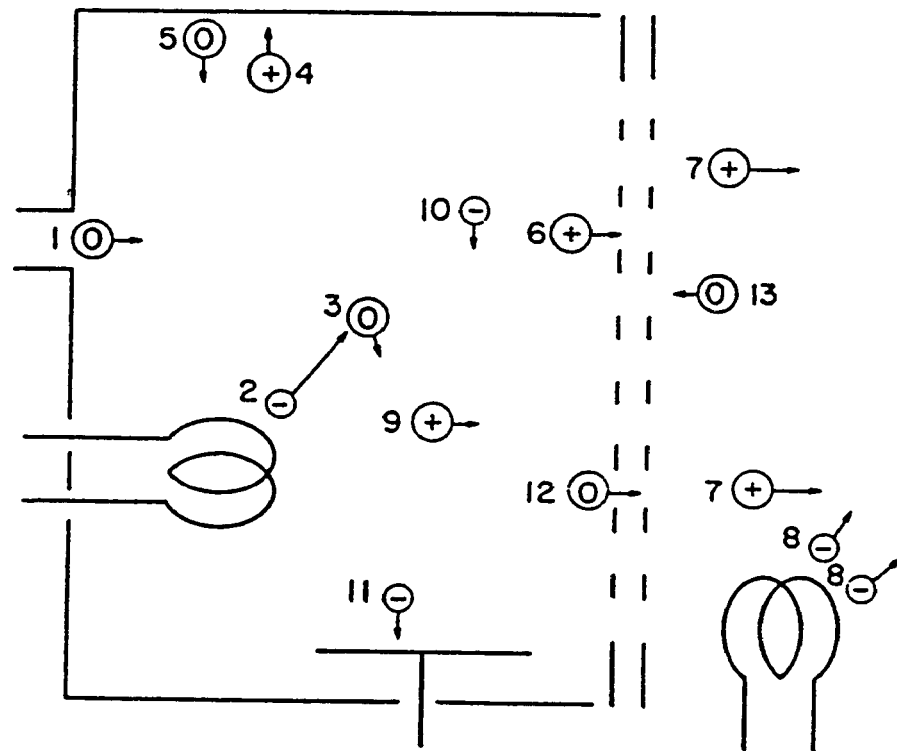


Figure 2. Ionization Process in the Kaufman Source
(Kaufman 1984)

1984). Because the neutralizer filament is within the path of the ion beam, it is physically sputtered by beam ions. This results in shortened neutralizer lifetime and possible contamination of the growing film by the filament material. For small diameter ion beams of a few centimeters or less operating at a minimum of 1000 V, it is acceptable to loop the neutralizer outside the central portion of the ion beam to minimize contamination and increase neutralizer lifetime (Kaufman 1978). Since the ion source used in this experiment was 3 cm in diameter operating at 1000 V, the tungsten neutralizer was looped outside the central portion of the ion beam.

The energetic electrons (2), ions (9), and low-energy background electrons (10) in the discharge-chamber volume are the components of the plasma. The potential within the plasma is generally uniform and is most closely approximated by the anode potential. Since the target is held at ground, the energy of the ion beam equals that of the beam potential as it strikes the target surface. Because the neutralizer is also at ground potential, the accelerator must be negative to prevent the neutralizing electrons from flowing back into the discharge chamber. This phenomenon is known as backstreaming of electrons and can damage the ion optics if not checked. More importantly, the beam power supply cannot distinguish between electrons backstreaming into the plasma discharge chamber and ions being accelerated toward the target. The operator would, therefore, not know if the

beam current was due to ions or backsteaming electrons (Kaufman 1984).

Typically the ion source chamber vacuum is established at a maximum of 6×10^{-6} Torr. Argon is backfilled into the chamber to 4.5×10^{-4} Torr. At this pressure the mean-free-path for electron impact ionization is much larger than the chamber dimensions; therefore, the magnetic field surrounding the anode also serves to increase the probability that an energetic electron will remain within the discharge chamber long enough to collide with a gas atom to create an ion (Kaufman, Cuomo, and Harper 1982). Low-energy electrons (10), however, are not contained by the magnetic field. As such, they are free to diffuse to the anode (11), completing the circuit between the cathode and the anode (Kaufman 1984).

Because the path length between collisions is large, outgoing gas atoms (12) rarely interact with incoming gas atoms (13). However, if different gases are introduced to the vacuum chamber intentionally or through contamination, there will be some inevitable interaction within the ion source. If the partial pressure of the inert gas in the ion source is higher than the other gas, it will dominate but not exclude the other gas or gasses (Kaufman 1984).

The rate of ion extraction and the theoretical basis for most broad-beam ion optics is Child's law of space charge limited current flow. Very simply this states that at some level of operation, the process of removing electrons from the cathode becomes limited by the presence

of other electrons around the cathode (Kaufman 1984; Kaufman, Cuomo, and Harper 1982). For a planar geometry, the space charge limited current density between two planes, such as the ion optic grids, is

$$j = (4 \epsilon_0 / 9) (2q/m) T^{1/2} V^{3/2} / d^2$$

where j is the current density, ϵ_0 is the permeability of free space, d is the distance between the plates, and q/m is the charge-to-mass ratio of the accelerated particles. Child's law can be used to approximate the current capacity of broad-beam ion optics (Kaufman, Cuomo, and Harper 1982).

The potential pathway of the plasma through the ion optics in the source is shown in Figure 3. The broken line indicates the voltage of the plasma and the solid line is indicative of the voltage in the ion source hardware. The ions originate at plasma potential which is close to anode potential. They are accelerated through the total potential V_t between the anode and the accelerator grid and then decelerated to near ground potential. The resultant ion energy in the beam is related to the net voltage difference V_n . The voltage ratio V_n/V_t must be slightly less than 1 to supply a sufficient barrier to the backstreaming electrons from the neutralizer (Kaufman 1978).

The Sputtering Process

The equivalent energy of a singly charged argon ion coming from a gas at 350-400°K and accelerated to 1000 eV is 11,600,000°K (Kaufman 1984; Harper, Cuomo, and Kaufman 1982). This very large amount of kinetic energy is the reason that ion-beam deposition can be used at low

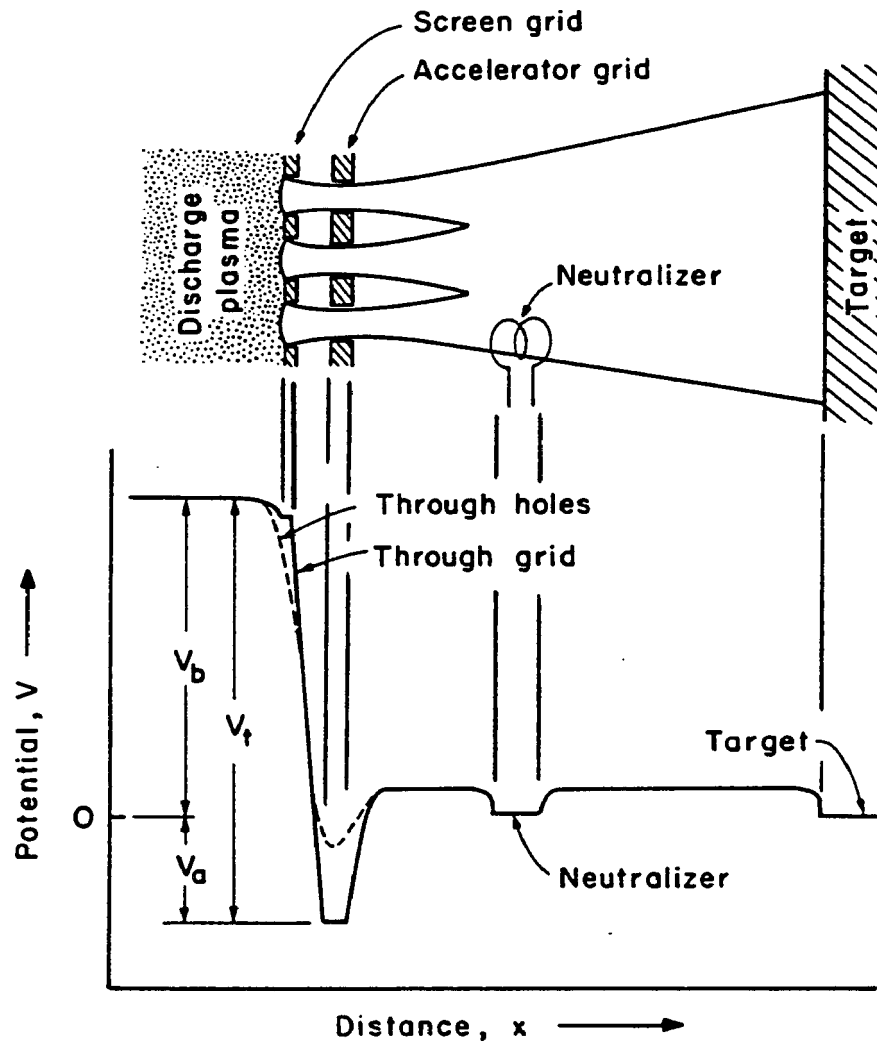


Figure 3. Potential Through the Ion Optics
(Kaufman 1984)

temperatures to produce films of specific properties which would otherwise require high temperature operations. At 10^{-4} Torr for a 1000 eV ion-beam the mean-free-path for ion energy loss is given as 180 mTorr-cm or 1800 cm at operating pressure. The initial loss of energy along this path length is approximately linear. In other words 10% of the ion energy or momentum is lost within 180 cm or 10% of the path length. For almost all vacuum sputter chambers this means the ion beam arrives at the target surface with over 99% of its original momentum (Kaufman 1984; Harper, Cuomo, and Kaufman 1982).

If the kinetic energy of the incoming ions striking the target material exceeds the binding energy of the target atoms, the target atoms are pushed into new lattice positions. At energies exceeding approximately four times the heat of sublimation of the target material, atoms are dislodged and ejected into the gas phase. Since most of the kinetic energy goes into lattice-atom vibrations or displacements, sputtering always involves surface migration of atoms and permanent or temporary damage to the lattice of the target (Wehner and Anderson 1970). At low substrate temperatures this damage layer is amorphous, or nearly so, and usually extends to the depth of ion penetration (Kaufman 1984).

At energies in excess of 100 eV some implantation of the inert species into the target occurs. Kaufman reported argon penetration depths in silicon of 110 and 330 Å at 200 and 1000 eV, respectively (Kaufman 1984). Wehner and

Anderson found penetration of roughly $10 \text{ \AA}/\text{keV}$ for argon in copper (Wehner and Anderson 1970). Mattox and McDonald achieved superior adhesion of cadmium on iron, two mutually insoluble materials, when sputtering with cathode voltages of 1500 V or higher, implying some penetration of cadmium ions or diffusion of its atoms into the iron substrate (Maissel 1970). As ion bombardment continues, equilibrium is eventually reached, and the embedded ions are re-sputtered along with target atoms (Wehner and Anderson 1970). Enhanced diffusion of sputtered material into the substrate is also possible. Tsukizoe et al. found Ag^+ in copper at diffusion depths of 200-300 \AA for implantation energies of 30 and 200 eV. They attributed this to diffusion along dislocations and Frenkel point defects (Harper, Cuomo, and Kaufman 1982).

As previously stated the process of physical sputtering occurs by momentum exchange. If the incoming ion has mass M_i and velocity v_i and impacts a target atom with mass M_t , one of three events may occur. First, the momentum of the ion is imparted to a target atom, driving it deeper into the target. Although the sputtering momentum of the ion is diminished by collisions within the first 10 \AA , computer modeling has shown that the incident ion produces a cascade of collisions over a region of the target material that extends 50 to 100 \AA below the surface (Thornton 1982a; Wehner and Anderson 1970). As the near surface lattice atom is driven more deeply into the target, it may be reflected by a subsequent collision and return to the surface

sputtering atoms from below (Thornton 1982a). In the second event, part of the momentum of the ion is imparted to the target atom, leading to a series of collisions which eventually produce a sputtered target particle. The fraction of momentum imparted to the target atom is given by

$$\varepsilon = 4M_i M_t / (M_i + M_t)^2.$$

By assuming the ion incidence is perpendicular to the target surface, which consists of a random array of atoms, an expression for sputter yield, s , can be developed according to the following:

$$s = (\text{constant}) \varepsilon (E/U) \alpha(M_t/M_i).$$

From this relationship it can be seen that the yield of sputtered material, the amount of target material removed per incident ion, depends directly on the energy transfer function ε . The term $\alpha(M_t/M_i)$ is a non-linear function, E is the kinetic energy of the ion, and U is the heat of sublimation of the substrate material. In contrast to chemical or thermal processes which depend exponentially on activation energy, the main material sensitive factor for sputtering is the heat of sublimation which is a first power dependence. This makes sputtering less sensitive to the material properties of the target than either chemical or thermal evaporation processes (Thornton 1982a).

If the target mass M_t is much greater than the ion mass M_i , incoming ions may be reflected or backscattered. This third possibility is also more likely to occur as the ion-beam angle of incidence approaches 90° , but there is a

chance that ions will be backscattered at smaller angles (Thornton 1982a). Since it is likely that incoming ions are neutralized by field-emitted electrons from the target (Wehner and Anderson 1970), backscattered particles are reflected as neutrals and are not controlled by the electric fields within the chamber. At very low chamber pressures, it is possible that these neutrals strike the substrate surface with little of their original kinetic energy dissipated. Reflected neutrals provide some scrubbing or cleaning effect on the substrate surface, but they also contribute to substrate heating and have the potential of becoming entrapped in the growing coating. They are the major source of inert gas incorporation into ion-beam deposited films (Thornton 1982a; Maissel 1970; Rossnagel and Cuomo 1988).

Aproximately 0.1 to 1.0 atomic percent of the inert gas typically becomes incorporated in the growing coating. In some systems this can be minimized by using a different gas. Bouchier found a reduction from 0.9% to 0.03% gas incorporation in NbTi films by switching from argon to xenon (Harper, Cuomo, and Kaufman 1982). Studies have shown that argon is not likely to stick to a substrate surface unless it arrives there at energies in excess of 100 eV. If the argon back-pressure is increased to a higher level, fewer reflected neutrals will reach the substrate surface with sufficient energy to stick in the growing film (Maissel 1970). Of course, increasing the argon back-pressure also shortens the mean-free-path for energy loss and increases

the likelihood that the ions in the beam will encounter other particles before striking the target.

The following conclusions may be made concerning sputter yield (Harper 1978):

1) Sputter yield, s , increases with ion energy E approximately proportional to $E^{1/2}$ from a threshold of a few tens of electron volts to maximum around 10-20 keV, then decreases at higher energy when implantation becomes primary.

2) Sputter yield generally increases with mass of ion.

3) Sputter yield increases with angle of ion incidence away from normal incidence to a maximum at an angle which depends on ion and target species and energy, then decreases to zero at grazing incidence.

4) Sputter yield depends on the target material, but differences are generally within an order of magnitude. For example, the sputtering rate of tungsten in argon is only a factor of two lower than that of aluminum; however, their evaporation rates at 2000°C differ by more than nine orders of magnitude (Wehner and Anderson 1970).

5) The energy of sputtered particles is in the range of tens of electron volts, with a small fraction at higher energies.

The sputtering rate for an ion beam of current density 1.0 mA/cm² with $s=1$ corresponds to 6×10^{15} atoms/sec/cm² removal rate, which gives about $7 \text{ \AA}/\text{sec}$ for copper, or several monolayers per second (Harper 1978). Typically,

sputter yield ranges from 0.1-3 atoms/ion for ion energies up to 1000 eV (Westwood 1988). The Kaufman source operates at 500-2000 eV to minimize heating of substrates. Usually, a target angle of 45° is used in sputtering to obtain the highest yield. The maximum sputtered flux is then directed normal to the target surface.

Sputtering of Alloys and Compounds

Sputtering of alloys and compounds is a much more complicated process than sputtering of pure elements. The momentum exchange which occurs when an ion collides with the target is a violent one involving great amounts of energy. Usually, the impact energy exceeds the bond strength of the compound, which is normally only a few electron volts. This in turn is sufficient to rupture the bonds and free the individual elemental constituents (Wehner and Anderson 1970). Binding energy affects the sputtering rate in compounds. Most often the sputtering rate of a constituent material in a compound or alloy is not the same as that of the elements alone. The most loosely bound element in the compound is the first to sputter (Thornton 1982a).

The same situation can occur in a two-phase alloy system or in a homogeneous system with precipitates when one phase is more easily sputtered than the other. The result is a textured surface containing depressions or pits in the region of the more easily sputtered phase (Thornton 1982a). It is at this point that the target can reach equilibrium. Because the more easily sputtered phase is in shorter supply in the compound and more difficult to reach in the alloy,

the concentration of the species in the sputtered flux will begin to resemble that of the bulk target (Maissel 1970). It is therefore advisable to initially screen the substrate from the sputtered material until equilibrium is reached. Depending on the target material, 30-100 Å must be removed to reach the proper concentrations of sputtered species (Thornton 1982a).

In most oxide systems, oxygen is preferentially sputtered from the target surface, leaving the near surface volume deficient in that element (Thornton 1982a). Studies of mercury ion bombardment of CuO show it being converted to Cu₂O and then to pure Cu. Iron oxide, Fe₂O₃, is reduced to Fe₃O₄, then to FeO, and finally to Fe. Total reduction depends upon the bond strength and dissociation energy of the compound (Wehner and Anderson 1970). Sputtering in an oxygen environment lessens reduction (Thornton 1982a) but severely limits cathode and neutralizer filament lifetimes in operation (Kaufman 1984). In some instances the presence of oxygen can reduce deposition rates by as much as 50%. This is particularly true in easily oxidized metallic or semi-metallic systems (Maissel 1970).

Although molecules are frequently dissociated during sputtering, the overall chemistry of the final film can be the same as the starting material if the target reaches sputtering equilibrium (Maissel 1970). Several conditions must be met in order for this to occur. First, the target must be cooled to prevent diffusion of the more easily sputtered material to the surface of the target. Second,

the target must not be a material which easily decomposes. Third, the gas phase transport of the constituents must be similar. Fourth, the vacuum chamber must be free of any reactive contaminants, and fifth, the sticking coefficient of each constituent must be similar on the substrate material (Thornton 1982a).

Particle Energy and Distribution

Determining the energy of particles sputtered from the target material is a difficult matter. Energetic reflected neutrals and backscattered ions within the sputtered flux will give the appearance that the flux possesses more kinetic energy than it does (Wehner and Anderson 1970). The average energy of the sputtered particles is generally believed to range from 5 to 40 eV (Thornton 1982a; Westwood 1988). This is 50-100 times higher than particle energies found in vacuum evaporation processes (Thornton 1982a). The distribution of sputtered particle energy is Maxwellian in nature with 10 eV being the most probable energy occurrence. High energy particles populate the low intensity portion of the distribution. Increasing the incident ion-beam energy increases that portion of the particles which are sputtered at higher energy. Ion-beam energy increases above 1000 eV, however, do not produce a commensurate change in the average energy of the sputtered particles (Thornton 1982a).

The average ejection velocity of sputtered particles decreases with increasing atomic mass of the particle. In contrast the average energy of sputtered particles increases with increasing atomic mass. Also, materials with high

sputtering yields usually have lower average ejection energies (Thornton 1982a). The mass of the sputtering gas can affect ejection velocities. Switching from argon to krypton increases average ejection velocities by up to 20%.

The spatial distribution of sputtered material from the target conforms approximately to Knudsen's cosine law (Wehner and Anderson 1970). That is, the distribution of atoms follows the cosine of the angle relative to the target surface normal. Figure 4 shows the distribution and the angle θ . Such a distribution can best be described as coating the inside of a sphere held tangent to the point of ion-beam impact. There is usually a small region of higher than average energy particles opposite the incident ion beam which do not fully conform to the cosine law. This area is caused by glancing angle ion collisions. Theoretically a target stage placed at any point tangent to the sphere will receive uniform deposition. However, practical considerations and chamber design eliminate some locations. The best location is at 90° to the reflection from the beam or up to 30° forward of that. Locations more forward than this are likely to receive non-uniform sputter from the high energy region, while locations below 90° are likely to interfere with the incoming ion beam (Kaufman 1984).

The rate of deposition, R_d , or net yield of sputtered material on a target placed tangent to the sphere shown in Figure 4 can be determined using

$$R_d = 4.95 IW (Y/r^2) D,$$

where I is the ion current in mA, W is the atomic weight in

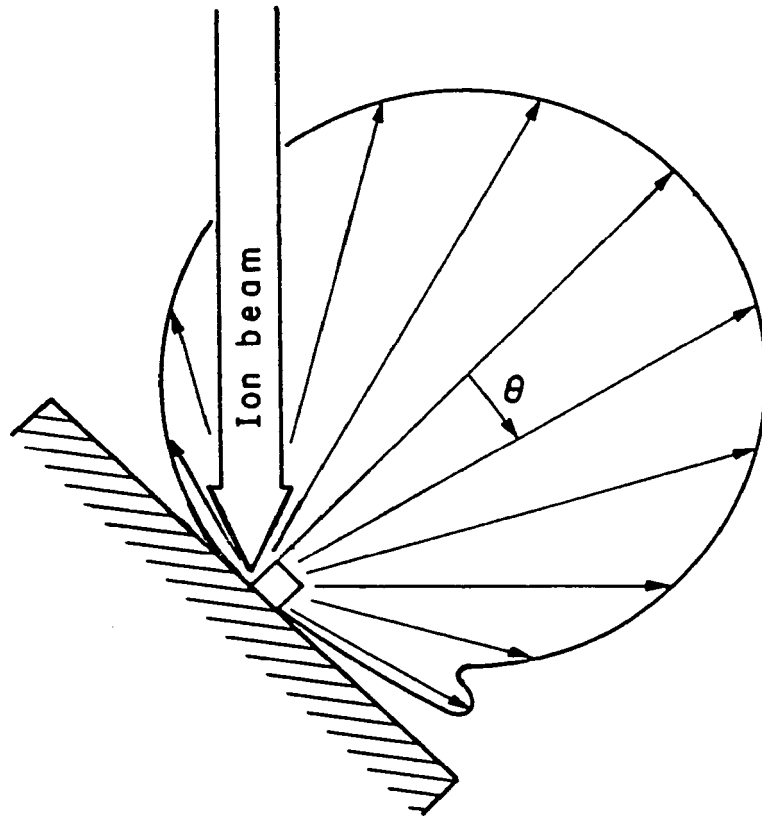


Figure 4. Spatial Distribution of Sputtered Atoms
(Kaufman 1984)

amu, D is the density in g/cm^3 of the target material, Y is the sputter yield from the target in atoms/ion, and r is the radius of the sphere in centimeters. The rate of deposition of a material is considerably lower than its etch rate because of the large angular spread of the sputtered material. It is also not unusual to experience variations in sputter yield from run to run as high as 20-30% using the same ion type, the same ion energy, and the same target materials. Differences as large as a factor of 2 have been reported (Kaufman 1984).

From both computer modeling and experimental work the distribution of sputtered material appears to be independent of ion-beam angle of incidence. However, Rol et al. found that at higher ion-beam energies (20 keV or greater) the spatial arrangement of sputtered materials begins to approach a Gaussian distribution (Wehner and Anderson 1970).

Film Growth

With sputtered atoms arriving at the substrate with a range of energies, a three step process usually occurs. First, when atoms arrive, their kinetic energy is transferred to the substrate lattice, and they form "adatoms" which are loosely bonded to the surface. Second, provided there is enough energy, the adatoms move across the substrate, interacting with the lattice and any other adsorbed species. The adatoms may desorb or be removed through back-sputtering, or if they reach a low energy site, they will become trapped and incorporated in the film. Growth of the film proceeds in this manner with adatoms

arriving, moving over the surface, and becoming trapped in low energy sites. In the third and final step, adatoms rearrange their position within the lattice by bulk diffusion, provided there is enough energy present for this to occur (Thornton 1982a).

Figure 5 shows a zone diagram which models the type of film thought to deposit under varying deposition parameters. The axes of the model are normalized temperature (of the depositing material) and increasing argon pressure or decreasing particle energy since the kinetic energy of the particle is inversely proportional to argon back-pressure. Zone 1 represents atoms arriving on a cold substrate with little or no energy. The resultant region is columnar with voids. The separation of columns increases with increasing gas pressure as the adatoms do not possess enough energy to diffuse over the substrate surface (Westwood 1988). The formation of the voids is due to the shadowing effects of the substrate surface roughness. Since the arriving atoms in this region of the model do not possess enough kinetic energy for surface diffusion, preferential growth occurs at high points in the surface topography. As film growth proceeds, the creation of the void structure is self-propagating because the presence of coating peaks increases the shadowing of valleys or depressions. This makes it increasingly difficult to produce a fully dense film (Thornton 1982a).

Zone T is a transition region in this model. It is essentially Zone 1 without the voids. The structure is

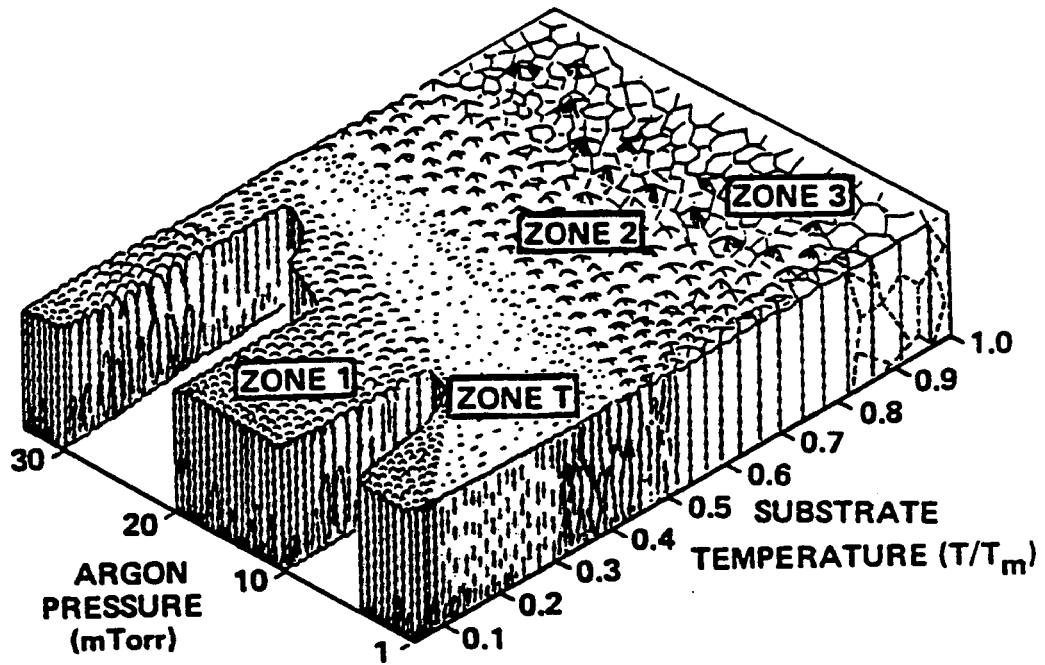


Figure 5. Zone Model of Film Growth
(Thornton 1982a)

still basically columnar, but the increase in adatom mobility and energy produces a denser film because the depositing particles are more likely to diffuse across the substrate surface. In the end the film may have the appearance of fibrous, poorly defined grains (Thornton 1982a; Westwood 1988).

In Zone 2 surface mobility continues to increase and grain growth occurs. The surface of the dense film becomes rougher. Zone 3 is dominated by bulk diffusion mechanisms and characterized by the presence of equiaxed grains (Thornton 1982a). This process occurs at temperatures much higher than those used in sputtering. However, temperatures in this region are necessary to achieve epitaxial growth of the film on the substrate (Westwood 1988).

Neugebauer presented the following nine step process for complete film coverage of a substrate (Neugebauer 1970):

1. Adsorption of adatoms to the surface.
2. Formation of subcritical embryos or clusters of critical size.
3. Formation of critically sized nuclei.
4. Growth of these nuclei to a critical size while depleting the surrounding area of adsorbed adatoms.
5. Concurrently, critically sized clusters will develop in regions which are not depleted of adatoms.
6. Clusters grow and touch, coalescing into a single "island" covering less area than the sum of the original clusters.

7. Secondary nucleation begins when newly arrived adatoms adsorb onto the freshly exposed area.

8. Islands grow together leaving channels or holes of exposed substrate.

9. These channels and holes are filled by secondary nucleation to form a continuous film.

Sputter Cleaning

Proper surface preparation is important to achieve an adherent, continuous film with the desired properties. Usually, substrates are washed in detergent prior to deposition to remove water soluble contaminants. They may also be solvent cleaned to dissolve or emulsify any organic surface contaminants. Sputter-etching or direct ion-beam bombardment of the substrate surface prior to deposition may be performed to remove any adsorbed gasses from the substrate which are not removed by other cleaning processes. The primary advantage to this process is that it is performed within the controlled environment of the vacuum chamber immediately prior to deposition (Mattox 1982). If the vacuum system is continually operated while high purity gas is bled into the chamber, adsorbed gasses will be flushed out of the system without reforming on the substrate surface (Maissel 1970). Ion bombardment removes adsorbed surface impurities by momentum transfer, causing the molecules to dissociate as the activation energy for adsorption is overcome (Thornton 1982b). Sputter cleaning enhances film adhesion by removing surface impurities which

form diffusion barriers and prevent bond formation (Rossnagel and Cuomo 1988; Thornton 1982a).

Direct ion bombardment of the substrate may also have other effects on subsequent film growth. It can create defect sites along the surface which have lower activation energies and may act as nucleation sites for film growth. Since ion bombardment removes foreign material from the surface by sputtering, it can be used to sputter off any metal oxide layer (Thornton 1982b). If performed long enough, this will produce a clean metal surface for coating. However, if the coating material is an oxide, removal of the metal oxide may not be desirable. Metal oxide can form an interfacial layer between the substrate and the coating with an intermediate coefficient of thermal expansion which is conducive to good adhesion. This is particularly true of metal substrates which are strong oxide formers. If the deposit is also an oxide, a chemical reaction may develop between the film and the substrate surface, enhancing film adhesion (Mattox 1982).

Sputter-etching can also be used to microtexture the surface of a material. The damage layer produced by direct ion bombardment of the substrate surface produces a textured surface which can also enhance the mechanical adhesion of the film to the substrate (Wehner and Anderson 1970). By using sputter-resistant screens or masks, patterns can be etched into the surface of a material. Etching patterns may reach depths as great as 600 μ m (Picha and Siedlak 1984).

Ion-Beam Assisted Deposition

Interesting film properties may also be achieved by adding energy to the growing film by ion bombarding the substrate during sputter deposition. This process, known as ion-beam assisted deposition or IBAD (Rossnagel and Cuomo 1988), has been shown to suppress the development of the porous Zone 1 type of film. Use of IBAD results in the formation of a more dense transition zone film at lower temperatures and gas pressures than is normally required to achieve that structure (Thornton 1982a). This is thought to occur because simultaneous bombardment provides additional nucleation sites for film formation (Rossnagel and Cuomo 1988). The incoming ion beam may also strike peaks forming on the substrate surface and redistribute that material into the valleys (Thornton 1982a). The addition of high energy ions enhances surface diffusion on the substrate, allowing more mobility of the sputtered atoms. It may cause local bond breaking, recrystallization, or local heating of the growing film. The grain size of polycrystalline metal films is usually significantly smaller when deposited under simultaneous ion bombardment, and the amount of grain size reduction increases with increasing ion energy (Rossnagel and Cuomo 1988). Compounds can be formed at lower temperatures using IBAD than by rf sputtering or traditional evaporation methods. Fan was able to produce conductive, transparent Sn-doped In_2O_3 films at temperatures below 100°C (Harper, Cuomo, and Kaufman 1982). High temperature crystal structures have also been produced at lower temperatures.

In the sputtering of ferroelectric materials, perovskite was produced using IBAD at 400°C.

Ion-beam assisted deposition does, however, have some distinct disadvantages. The ion energy required to suppress Zone 1 and produce transition zone films of greater density is usually large enough that a significant amount of resputtering of the depositing film will also occur. As much as 30-60% of the growing film may be lost during IBAD (Thornton 1982a); however, at energies below 200 eV the potential for resputtering is small and the additional ion energy may improve film purity by removing loosely adherent atoms (Rossmagel and Cuomo 1988). Weissmantel used IBAD to produce hard, transparent carbon films from graphite. Without IBAD the films were almost always gray, soft, and graphitic (Harper, Cuomo, and Kaufman 1982). Preferential sputtering of one or more of the constituents of an alloy or compound may also occur with IBAD and can alter the composition of the deposited film. Harper and Gambino found that codeposited Gd-Co alloy films were deficient in Gd when they used IBAD. They also discovered that the resputtering rate of the Gd from the deposited film was significantly different from the sputtering rate of elemental Gd. The sputtering ratio of Gd to Co in elemental form is 0.37, but the resputtering ratio in the alloy film ranged from 2-6. These researchers used this knowledge to tailor the makeup of the alloy film to a desired Gd-Co ratio (Harper, Cuomo, and Kaufman 1982).

Increased potential for inert gas entrapment is another problem with IBAD (Rossnagel and Cuomo 1988). Argon contents as high as 30 atomic percent have been discovered in ion-beam assisted films (Thornton 1982a). Harper and Gambino found 14 atomic percent argon in the GdCo alloy films described above when using an ion bombardment energy of 500 eV (Harper, Cuomo, and Kaufman 1982).

In a process called reactive deposition, IBAD may be used to intentionally add back to a film a volatile element (such as oxygen or nitrogen) lost during sputtering. Most often this involves adding 10-20% reactive gas to the inert gas in an attempt to restore film stoichiometry to that of the target material (Harper, Cuomo, and Kaufman 1982). As the film is deposited on the substrate, it is simultaneously bombarded with high energy reactive ions which will aid in the formation of a compound film. A new copper oxide phase was reported by investigators bombarding a depositing copper film with oxygen. Others have reported the formation of diamond-like carbon films by bombarding depositing graphite with a mixture of methane and argon. They were able to control the structure of the carbon films, ranging from graphite to diamond-like, by varying the mixture of argon to methane in the gas (Rossnagel and Cuomo 1988).

Adhesion

Sputtering processes have become known for the superior adhesion of the films produced by this method. This good adhesion is thought to be due principally to the cleaning effects of the ion beam which removes contamination and

creates nucleation sites (Thornton 1982b). The term adhesion refers to a gross effect which is dependent on the bonding between film and substrate, as well as the microstructure at the interface, and upon fracture mechanisms (Mattox 1982). The bonding between film and substrate is dependent on the nature of the two materials in question. If it is chemical, it may be fairly strong with a bond strength of several eV. Because of the possibility of polar attraction, it may be Van der Waals in nature and have attachment strengths below a single eV. Electrostatic attraction is a third possibility resulting from charge layers between the coating and substrate. Combinations of the three bond types are also possible.

Van der Waals forces alone should account for bond strengths in the realm of $5 \times 10^8 \text{ N/m}^2$, but intrinsic stress present in most all deposited thin films can equal or exceed this value, thereby resulting in much lower adhesive strengths. Interface regions are also similar to bulk materials in that they are riddled with microstructural flaws which prevent them from reaching theoretical strengths (Thornton 1982b).

The microstructure at the interface may be classed as mechanical, abrupt, compound, or diffusion. A mechanical interface refers to a film deposited on a roughened surface. Mechanical interlocking between the film and substrate will provide some increased adhesive strength, but care should be taken in roughening the substrate surface. If it is too rough, shadowing from projections will result in a porous

film with decreased adhesive strength because it cannot sustain high stress (Mattox 1982).

An abrupt interface is one characterized by little or no chemical interaction or diffusion between the film and substrate. A distinct boundary remains between the two layers. In contrast, compound interfaces are formed between materials which interact chemically to produce a transition layer of constant composition between the coating and substrate. Diffusion interfaces occur between materials with considerable solid solubility in one another. The interface region is distinguished by a gradual change in composition and intrinsic stress from the film to the substrate (Thornton 1982b).

Almost all sputter deposited films are in a state of stress which is the sum of thermal stress and intrinsic stress. Thermal stress is caused by the difference in the coefficients of thermal expansion between the film and substrate materials. Intrinsic stress refers to the accumulated effect of atoms within the film which are out of place in relation to their site of minimum energy (Thornton 1982b). The development of stress in sputtered films is multi-factorial. It could be caused by recoil implantation of energetic neutrals, entrapment of inert gas, changes in the purity of the film, enhanced surface mobility, or local thermal spikes during deposition (Rossnagel and Cuomo 1988). While thermal stress is a constant and can be relieved by post-deposition annealing in some films, intrinsic stress increases with film thickness. Below a coating thickness of

approximately 5000 Å, intrinsic stress is essentially constant and thermal stresses dominate (Thornton 1982b). At larger film thicknesses, however, the intrinsic stress takes over. Intrinsic stress as high as 10^9 N/m² has been found in some films (Thornton 1982b) which may exceed the yield stress of the bulk material (Mattox 1982). Consequently, a thin film may be more likely to adhere to the substrate than a thicker one (Mattox 1982). The magnitude and direction of intrinsic stress is determined by processing variables such as inert gas pressure and deposition angle; it can, therefore, be controlled to some extent (Mattox 1982; Thornton 1982b).

Deposition studies using several metals indicated that intrinsic stress in films was compressive at low inert gas pressures (0.6 mTorr) and became tensile at higher chamber pressures (10-20 mTorr). This transformation was somewhat dependent on the sputtering material. Nickel films exhibited a change from compressive to tensile at chamber pressures as low as 1.5 mTorr. Tantalum, on the other hand, exhibited compressive intrinsic stress values up to around 15 mTorr. The effect of the angle of deposition was also to an extent dependent on the sputtering material, but the study showed in all cases that a normal angle of incidence produced compressive films. As the angle of deposition moved toward a grazing incidence the films were more likely to exhibit tensile stresses (Thornton 1982b).

Compressive intrinsic stress can be beneficial if the coefficient of thermal expansion between the coating and the

substrate is very large or if the film is a ceramic or refractory material (Mattox 1982). Ion-beam assisted deposition has been used by some investigators to create the proper compressive stress in the film. Hirsch and Varga found that concurrent bombardment of the substrate during Ge deposition produced more adherent films. They attributed this to lower intrinsic stress in the coatings. Through a series of experiments they were able to determine the effects of varying energy on the film stress. They found that by controlling the energy of the arriving atoms of the film material, they could convert the intrinsic stress from tensile to compressive (Rossnagel and Cuomo 1988). In a similar experiment Sun discovered that the magnitude of compressive stress increased with increasing incident ion energy (Rossnagel and Cuomo 1988).

Competitive Coating Processes

Coating deposition processes can be subdivided into two types which are categorized by the material transfer mechanism. These subdivisions are droplet transfer and atom-by-atom transfer. The divisions are indicative of the size of the discrete particle transferred to the substrate surface during the deposition process. Plasma spraying, flame spraying, and electric-arc spraying are all droplet transfer processes. Physical vapor deposition (PVD), chemical vapor deposition (CVD), electrodeposition, ion sputtering, and ion plating are considered atom-by-atom transfer processes (Bunshah 1982b).

Droplet Transfer

Plasma spraying is commonly used to apply protective thermal barrier coatings to aircraft and power generation turbine blades (Herman 1988; Miller 1984). It is also frequently used to apply bioactive coatings to implant surfaces (Cook et al. 1987; Thomas et al. 1987). Plasma spraying is accomplished by striking an electric arc between negative and positive electrodes. An inert gas such as argon is fed at a high flow rate through the arc exiting as a high velocity, high temperature plasma at the positive electrode (Herman 1988). The deposition material in the form of a powder is fed tangentially into the jet at the positive electrode where it is rapidly heated up to its melting point and accelerated to the substrate surface within the thermal plasma (Tucker 1982). Accelerated particles can reach speeds of up to 260 m/s depending on powder flow rate and particle size (Herman 1988), while temperatures within the plasma commonly reach 25,000°C or more (Tucker 1982). The molten powder particles impact the substrate with a tremendous force and are immediately quenched to its surface temperature. Cooling rates of 1,000,000°C per second have been reported. Although the substrate may be cooled during processing, the bulk of the material does not usually see temperatures over 150°C (Herman 1988). The resultant coating is constructed from individual molten particle impacts on the substrate. This means the coating consists of many layers of thin overlapping "lenticular splats" (Tucker 1982).

Plasma spraying offers a very rapid deposition rate. Coatings range in thickness from 5-50 μm and can be as thick as 5 mm (Herman 1988). The process is also versatile since it can be carried out within an environmental chamber or in air (Tucker 1982). It is a line-of-site process, which means it is difficult to coat intricate shapes or pieces with internal cavities. While this is not as much of a problem if the coating is performed in air, since the gun nozzle can be manipulated around the substrate, it is a limitation when coating within an environmental chamber or a vacuum. In theory any material which can be produced in powder form can be plasma sprayed; however, the material must be stable at thermal plasma temperatures. If it decomposes in the arc or dissociates at its melting point, the coating may be substantially different from the starting material. Vaporization of all or part of the injected powder can be a problem. Typically, powder sizes used in plasma spraying range from 5-60 μm in diameter, but a narrow particle distribution is usually used to achieve as uniform a coating coverage as possible. Also, very small particles stand a good chance of being vaporized in the intense heat of the thermal plasma, while overly large particles may not fully reach a molten state as they are accelerated to the target. Under the right conditions plasma spraying can produce a coating reaching 95% of the theoretical density of the starting material. However, if the starting material is easily oxidized, the density will be compromised by included

oxygen unless the operation is performed in a vacuum (Tucker 1982).

Flame spraying is a similar deposition process, but the powder is fed into a combustible gas such as acetylene, ignited at the nozzle, and sprayed to the substrate. Combustion temperatures are not as intense as in plasma spraying, and coating contamination from the acetylene is a potential problem (Bunshah 1982a).

In electric-arc spraying the starting material is not a powder but wire electrodes. The arc is struck at a converging point between the two wires. As the tips of the wire melt, molten particles are sprayed to the substrate surface. The wire starting material is continuously fed to the arc point (Bunshah 1982a).

Atom-by-Atom Transfer

Atom-by-atom transfer processes generally can be said to have three process steps in common:

1. Production of the depositing species, usually as gaseous or vapor phase.
2. Transport of the species to the substrate surface.
3. Condensation or collection of the material onto the substrate surface followed by film nucleation and growth.

These processes are distinguished by the extent to which each step can be individually controlled (Glang 1970; Bunshah 1982b).

Physical vapor deposition (PVD) is basically an evaporation process and probably the oldest and most common

vacuum coating method. It was from this coating process that the three steps listed above were derived. First developed in the mid-nineteenth century, PVD has seen extensive application in the electronics and semiconductor industries in this century. As with almost all vacuum deposition processes, most of the improvements in this technology in the last twenty years have been in the area of vacuum chamber design. Purer and more complicated films have been achieved since the development of harder and cleaner vacuums (Bunshah 1982b). In PVD, the coating material, in solid or liquid form, is heated by resistance or induction under vacuum until a vapor or gaseous phase is produced. The vapor spreads outward from the source material, coating everything within the chamber, including the substrate. Transport is considered molecular at low pressures where the mean-free-path is larger than the distance between the source and the substrate. This is typical of magnetron sources. At higher pressures (20-120 mTorr), transport is largely viscous. This is typical of the higher pressure diode sources. In either case the energy of the incident particle condensing on the substrate is only about 0.5 eV (Bunshah and Deshpandey 1988).

The three process steps occur in such close proximity to the substrate in chemical vapor deposition (CVD) that they cannot be independently controlled (Bunshah 1982b). Gaseous precursors are pumped into a reactant chamber containing the substrate material. The contents of the

chamber are heated to a temperature sufficient to cause a chemical reaction which will produce a deposit of the desired composition on the substrate (Blocher 1982). CVD allows the production of high temperature materials at significantly lower temperatures. TiB_2 , which has a melting point of $3225^{\circ}C$, can be produced by reacting $TiCl_4$, BCl_3 , and H_2 at $900^{\circ}C$. Although the substrate must be held at a somewhat lower temperature than the reaction to get condensation on the surface, it still is subjected to a considerable portion of the reaction temperature. The heat of the substrate gives the depositing adatoms more mobility to find nucleation sites (Besmann, Stinton, and Lowden 1988). CVD deposition rates are exceeded only by plasma spraying. Films are produced at rates as high as several tens of $\mu m/hour$ (Besmann, Stinton, and Lowden 1988) and may be as thick as 25 mm with or without a supporting substrate (Blocher 1982). The limiting factor for CVD is the availability of a chemical reaction that will produce the desired film composition. The substrate must also be able to withstand the chamber temperature and must be chemically stable in the presence of the reacting gasses. Substrate and coating material combinations are also limited to those materials with only minor differences in coefficients of thermal expansion since the film and substrate must cool together from the deposition temperatures. If the difference in α values is too great, stresses could develop on cooling which might lead to coating delamination (Blocher 1982). By ionizing the reacting gasses into a plasma,

metastable phases can be formed at much lower substrate temperatures. Ionized gasses can also be directed and accelerated to the substrate with an electric field (Bachman, Gartner, and Lydtin 1988). The process called plasma-assisted chemical vapor deposition enables the incident particle to strike the substrate at higher energy than conventional CVD. It is, however, a more cumbersome deposition process with more parameters to control (Besmann, Stinton, and Lowden 1988).

Electrodeposition refers to electrolytic deposition and electrophoretic coating. The former involves submerging two electrodes in an aqueous solution of a dissociated ionic salt. When a potential is placed across the electrodes, positive ions are attracted to the cathode, creating a film. In electrophoretic deposition the substrate is immersed in a colloidal suspension dissociated into positive and negative ions. An electric field is applied such that the substrate becomes the anode. The negative colloidal particles are attracted to the positively charged substrate and are discharged onto the surface. Most of the time this process requires a post-deposition treatment such as sintering to achieve an adherent film (Bunshah 1982a).

Glow discharge sputtering is the process most similar to ion-beam sputtering (Vossen and Cuomo 1978). In its simplest form the coating material is the cathode or negative electrode, and the substrate is the positive electrode or anode. This configuration is usually called a

diode (Thornton 1982a; Vossen and Cuomo 1978). If a magnetic field is used to collimate and direct the plasma, the system is called a magnetron (Thornton and Penfold 1978; Waits 1978; Westwood 1988). In both configurations the vacuum chamber is evacuated to 10^{-4} to 10^{-7} Torr and then backfilled with an inert gas of known purity to 1-100 mTorr. An electric discharge is ignited so that the inert gas becomes ionized in the region of the cathode. A potential difference of 500 to 5000 V is set between the substrate and the target material or cathode. The gas ions impact the cathode and sputter off target material in atomic form by a momentum transfer process. This process has been described more completely in the previous section on ion-beam sputter deposition. Target particles are generally scattered in all directions with a portion of them impinging on the substrate surface with energies of 5-30 eV (Westwood 1988). Diode sputtering can be differentiated from ion-beam sputtering because the creation of the plasma occurs at the target surface. This limits the control that the operator has over the process. Since the target is the negative electrode, positive ions remain attracted to its surface while negative ions are accelerated away. Ion-beam sputtering is not subject to such separation effects (Wehner and Anderson 1970). Since the substrate is also within the plasma it is exposed to a substantial number of energetic neutral-gas atoms. These atoms strike the film as it deposits on the substrate with the same energy as the ions striking the

target. As much as 70% of the depositing film can be resputtered under certain charged conditions (Maissel 1970).

The major limitation of glow discharge systems is the inability to separately control ion current and ion voltage (Harper 1978; Rossnagel and Kaufman 1988). As ion energy is increased with voltage, current must increase accordingly (Rossnagel and Kaufman 1987, 1988). The working gas pressure must also be increased to maintain a glow discharge at high current levels (Thornton 1982a). As was shown in the film growth zone model in Figure 5, increases in working gas pressure make production of a fully dense, adherent film more difficult (Westwood 1988).

The dc diode or magnetron configuration cannot be used to sputter nonconducting materials because such surfaces will become charged. Charge accumulation leads to sparking and the subsequent damage of target and substrate (Thornton 1982a). In order to remedy this situation radio frequency (rf) methods are used to sputter insulators (Wehner and Anderson 1970).

Since there is an inevitable difference in the mobility of electrons and ions within a plasma, the target surface will always be slightly negative to the floating potential of the plasma by 20 to 50 eV. In fact, all surfaces which are capacitively coupled to the discharge will be negative to the floating potential of the plasma. If an alternating voltage is applied to the cathode, more electron current will flow when the electrode is positive relative to the plasma than will ion current when it is negative relative to

the plasma potential. In order to prevent charging, the net current flow to the electrode must be zero in each rf cycle. For this to occur there must be a negative bias on the cathode so that the electron current on the positive side of the cycle equals the ion current on the negative side of the cycle, i.e., no net surface charge. The measured negative bias needed to achieve this is equal to the zero-to-peak voltage of the rf signal (Thornton 1982a). Radio frequency sputtering can be used on both conductors and insulators, but it is a more complex process than diode sputtering with more processing parameters. Resputtering of the deposited film and preferential sputtering of film constituents are each more likely to occur in rf sputtering. The bias on the substrate attracts energetic argon ions to its surface (Westwood 1988).

Ion plating is a general term which applies to any atom-by-atom transfer process where an ionized gas is directed and accelerated to a substrate material using an electric field (Bunshah 1982a).

Literature Survey

The use of ion beams and ion sputtering in the production and modification of thin films has become widespread throughout many industries. Films and coatings can be directly produced by ion-beam deposition (Zuhr et al. 1989; Yamauchi et al. 1988) or by a combination of ion beams known as ion-beam assisted deposition (IBAD) (Seaward, Barbee, and Tiller 1986). It is also common to use an ion source in conjunction with another deposition process such

as chemical or physical vapor deposition to modify the film as it is deposited onto the substrate (Hubler et al. 1989; Jaulin et al. 1989; Roy et al. 1989).

Various processes have been utilized in the electronics industry to develop or enhance semiconductor and superconductor thin films (Lau 1989; Lichtenwalner, Anderson, and Rudman 1989; Seaward, Barbee, and Tiller 1986; Taga and Ohwaki 1989; Yamauchi et al. 1988). Sputter deposition has also been used to produce and modify solid lubricant films (Cuomo 1986; Jiankun et al. 1989; Lince and Fleischauer 1987) and wear resistant coatings (Carosella et al. 1989; Hirvonen and Hirvonen 1989; Greenwald, Hirvonen, and Jaggi 1989). Sputter deposition and ion-beam processing have enlarged the list of materials used for optical thin films (Donovan, Carosella, and Van Vechten 1989; al-Jumaily et al. 1989; Williams et al. 1989). Corrosion resistant coatings and even diamond-like carbon films have recently been fabricated by ion-beam deposition (Deutchman and Partyka 1989; Greenwald, Hirvonen, and Jaggi 1989; Lee, Fisher, and Schulz 1988; Nowak, Levy, and Chang 1986). Frequently ion-beam processes are used to fabricate thin films with metastable or difficult to achieve crystal structures (Kaufman, Biancaniello, and Kreider 1988; Kay, Parmiagiani, and Parrish 1987; Huang et al. 1985). Some very recent work has investigated the application of these processes for possible biomedical uses (Legg and Solnick-Legg 1988; Picha and Siedlak 1984; Solnick-Legg and Legg 1989).

Yamauchi et al. sputter deposited thin films from the piezoelectric ceramic $\text{Ba}_2\text{Si}_2\text{TiO}_8$ known as Fresnoite (Yamauchi et al. 1988). Using argon as the working gas and an rf magnetron, they deposited films on fused quartz, cleaved NaCl, and silicon with a range of substrate temperatures from 60-175°C. The resultant films were determined by electron microprobe analysis to be slightly deficient in barium and enriched in titanium. In all cases the as-deposited films proved to be amorphous or nearly amorphous in structure. Only the films deposited on fused quartz at 175°C showed some evidence of widely scattered Fresnoite crystals within an amorphous matrix. The authors subsequently annealed films at 750°C, 900°C, and 1000°C for ten hours. After heat treating they appeared polycrystalline in bright-field TEM micrographs with grains approximately 50 nm in diameter. Electron diffraction patterns showed a diffuse halo with some discrete spots suggesting that the films were crystalline but still contained some amorphous regions. Even samples annealed at 900°C and 1000°C for ten hours had amorphous regions dispersed throughout the crystals.

Lee, Fischer, and Schulz used rf magnetron sputtering to deposit amorphous metallic films onto 1008 steel for enhanced corrosion resistance (Lee, Fischer and Schulz 1988). The target material used was Allied Chemical alloy 2826A ($\text{Fe}_{32}\text{Ni}_{36}\text{Cr}_{14}\text{P}_{12}\text{B}_6$) which exhibits very good corrosion resistance in both acidic and basic environments. However, it has had little practical application because it is

manufactured as an amorphous metal ribbon by rapidly cooling the melt on a rotating copper wheel. A 4000 Å film was deposited onto the polished steel substrates using ion-beam sputter deposition alone and with secondary ion bombardment or ion-assisted deposition. In both cases the corrosion rate of the 1008 steel was reduced by two orders of magnitude in basic solutions. However, significant corrosion resistance to sulfuric acid was only exhibited by the films produced by ion-assisted deposition. Films fabricated by ion-beam sputter deposition alone contained significant amounts of oxygen as a contaminant and were not as dense as the IBAD films. Energetic ion bombardment during film deposition nearly eliminated the oxygen contamination from the IBAD films, but it also preferentially sputtered phosphorus and iron. As a result the IBAD films from alloy 2826A were not as highly resistant to sulfuric acid corrosion as the target material.

MoS_2 is known to have a low coefficient of friction and has been suggested as a solid lubricant film. Lince and Fleischauer investigated the structure and properties of sputter deposited MoS_2 films. Since its hexagonal, two-dimensional crystal structure is thought to be the reason for the material's lubricity, maintenance of that structure was critical. Films were deposited onto 440C stainless steel substrates at ambient temperature and at 245°C. SEM and x-ray diffraction showed the resultant films contained MoS_2 crystallites oriented with the basal planes perpendicular to the substrate surface. After subjecting

the films to sliding wear studies, the authors noted that the crystallites appeared to reorient such that the basal planes were parallel to the substrate surface. Ambient temperature films exhibited a somewhat greater reduction in sliding friction than the high temperature films. High temperature films were more likely to contain oxygen impurities and were also deficient in sulfur.

Kaufman, Biancanello, and Kreider investigated the effect of various annealing methods on sputter deposited Al-Mn and Al-Mn-Si films (Kaufman, Biancanello, and Kreider 1988). Post-deposition annealing was necessary in this system because the as-deposited films were always amorphous when deposited at room temperature and only "quasi-crystalline" at deposition temperatures between 275°C and 420°C.

The authors found that a metastable Al-Mn intermetallic structure could be formed when the amorphous films were heated in the electron microscope using the electron beam as the heating source. This phase was determined by convergent beam electron diffraction to be an aluminum rich θ -Al₁₀Mn₃. Specimens were also heated within the scope using a heating stage. The θ -Al₁₀Mn₃ phase was found to develop around 450°C. Although the phase diagram predicted the formation of Al₄Mn at this temperature, it was not observed until reaching 610°C.

In the ternary Al-Mn-Si system formation of the β -Al₉Mn₃Si phase began at temperatures as low as 380°C and continued forming up to 630°C. However, α -Al was found to

coexist within the β phase and increased in amount as the annealing temperature increased.

Sputter deposition was also used to produce alloy films from constituent elements which did not exhibit equilibrium miscibility (Rizzo et al. 1989). The literature suggested that amorphous films could not be produced from such systems. The authors were able to sputter deposit amorphous films at room temperature in the Pu-V and Ag-Fe systems despite the fact both systems exhibit solid and liquid phase immiscibility. Films from the immiscible Pu-Ta, Cu-W, and Cu-Mo systems were produced with amorphous and metastable crystalline regions.

Others examined the usefulness of sputter deposited Al_2O_3 films as protective coatings for GaAs laser mirrors (Webb et al. 1989). Uncoated mirrors oxidize with time, which leads to the deterioration of the laser due to scattering and interference effects. The mirror surfaces were sputter cleaned using 100 eV argon ion bombardment prior to deposition. Coatings were sputter deposited using a range of ion-beam energies from 300 to 1000 eV. The authors found no significant difference in the refractive index or compressive residual stress of coatings deposited in this range of ion-beam energies. However, in testing the degradation of the coatings in deionized water, only those deposited at 800 eV proved to be effective in protecting the mirrors. They showed no signs of film degradation even after three hours in deionized water.

In another recent work magnetron sputtering was used to produce SiO_2 thin films (Taga and Ohwaki 1989). Films were sputtered from pure Si and SiO_2 targets using Ar, O_2 , or a combination of the two gases. The properties of the resulting films were dependent on the type of particle sputtered from the target. Films sputtered from the Si target using O_2 as the working gas had the highest density and best electrical properties, but the slowest deposition rate at $22 \text{ \AA}/\text{min}$. Films sputtered from the Si target using a mixed working gas of Ar and O_2 had the highest deposition rate at $204 \text{ \AA}/\text{min}$ and the lowest density and worst electrical properties. Films sputtered from the SiO_2 target using Ar had deposition rates and properties intermediate to the other two groups.

A commercial ion implanter operated at its minimum extraction energy of 35 keV was used to directly deposit transition metal films onto silicon substrates (Zuhr et al. 1989). Since the beam was produced in a Freeman source intended for ion implantation, the authors were able to magnetically mass analyze the ion beam to carefully control the energy and ionization state of the accelerated ions. The beam was passed through three liquid-nitrogen traps and decelerated upon entrance to the deposition chamber by a series of four-element deceleration lenses. The energy of the resultant metal ion beam was 40-200 eV. The authors deposited Co, Fe, Ni, Ti, and W onto both n- and p-type Si substrates at 500°C . They did not subject the films to any post-deposition annealing since they wanted to examine the

properties produced by the sputter deposition process alone. In all cases metal silicides were formed, but the metal/Si combinations could be divided into those in which the metal is the dominant diffuser (Co and Ni) and those in which the Si is the dominant diffuser (Fe, Ti, and W). In the former group the stoichiometry of the silicide varied throughout the thickness of the film. The latter group formed stoichiometric disilicides in each case. Titanium formed a TiSi_2 film with the lowest resistance of the group. The titanium disilicide film was also marked by the greatest amount of Si diffusion.

Lichtenwalner, Anderson, and Rudman combined the unique properties of ion-beam sputter deposition and glow discharge plasma sputtering to produce NbN films (Lichtenwalner, Anderson, and Rudman 1989). Their deposition chamber consisted of a Kaufman ion source directed toward an Nb target and a substrate region surrounded by a glow discharge magnetron. The authors were able to ionize an argon/nitrogen gas mixture over the substrate in order to provide a source of excited and ionized nitrogen to the deposition surface. Films were sputtered from the elemental Nb target using an incident ion-beam energy of 1200 eV. Some samples were deposited with N_2 gas flowing over the substrate, without the operation of the magnetron. Other samples were deposited with the gas ionized by the magnetron.

The films fabricated using only N_2 gas flowing over the deposition surface were determined to be the superconducting

δ -NbN phase. Those films fabricated in the presence of the nitrogen plasma proved to be the hexagonal δ' phase. Although this NbN phase is not superconducting, the authors were the first to produce this structure in a thin film.

Two ion sources may be used simultaneously in the deposition of thin films. Most frequently, this is accomplished by bombarding the target material with the beam from one source while directly bombarding the substrate with the other ion beam as the film deposits (Cuomo 1986). Secondary ion bombardment (also called IBAD) can be performed with noble gas ions to add energy to the depositing film (Kay, Parmigiani, and Parrish 1987). In the formation of compound films, it may be carried out with a reactive gas such as nitrogen, oxygen, or methane (Cuomo 1986; Rossnagel and Cuomo 1988).

Huang et al. determined the effect of secondary Ar ion bombardment on the growth and resultant structure of ion-beam sputter deposited Ag films (Huang et al. 1985). Sputter deposition was performed using a Kaufman ion source set at 700 eV. The secondary ion source energy was used as an experimental variable. Although the authors found preferential (111) orientation in their sputter deposited films, the amount of preferential orientation was much lower in sputtered films than in vapor deposited Ag of the same thickness. Preferred orientation in the sputtered films also decreased with increasing secondary Ag ion energy. Several other effects on structure were discovered to be affected by increasing secondary ion energy. The Ag lattice spacings

perpendicular to the plane of the film reversed from contraction to expansion. Plane stress became compressive rather than tensile, and Ag grain size was reduced by half. Twin fault probability increased by a factor of five while dislocation density increased by an order of magnitude. These effects were found to become insensitive to change at secondary ion-beam energies approaching 42% of the primary ion-beam energy.

Kay, Parmigiani, and Parrish bombarded growing metal films with various noble gas ions to determine the effect this would have on film structure and properties (Kay, Parmigiani, and Parrish 1987). Ion-beam sputter deposition was performed using a Kaufman-type ion source at a constant deposition energy of 700 eV. The secondary ion source bombarded the substrate surface at 500 eV during deposition. The authors used Ar, Ne, and Xe as working gases in their experiment and deposited films from Pd, Pt, and Cu targets. They discovered preferred crystallographic orientation for several ion/metal combinations. In particular, films sputtered from Pd with Xe and those from Pt with Ne showed nearly complete orientation of the (111) lattice planes parallel to the surface. Cu/Xe films also exhibited a similar (111) orientation as well as a secondary increase in (200) orientation. Additionally, some dilation of lattice parameters was discovered in all films produced this way. The amount of lattice dilation was found to increase with decreasing gas/metal mass ratio. The same effects were observed without the second ion source if primary sputtering

occurred in such a way as to produce a significant number of reflected neutrals in the direction of the substrate.

Earlier work by Ziemann and Kay using a dc triode sputtering system to deposit Pd films with Kr gas showed much the same result (Ziemann and Kay 1983). To achieve noble ion bombardment in a diode or triode glow discharge system the substrate must be biased negatively of ground to directly attract the gas ions to the substrate surface (Thornton 1982b). Ziemann and Kay experimented with negative voltages between 0 and 500 V. They found the same preferential orientation of (111) lattice planes parallel to the film surface, dilation of the crystal lattice, and decreasing Pd grain size with higher ion energy bombardment. The authors also found increasing concentrations of Kr in their films with increasing negative bias as well as higher dislocation concentrations in films which were exposed to secondary ion energies above 24 eV/Pd atom.

Nagakubo, Yamamoto, and Naoe used dual ion-beam sputter deposition techniques to produce thin magnetic iron films (Nagakubo, Yamamoto, and Naoe 1989). They investigated the effects of argon gas pressure and film thickness on the magnetic properties of the films. The films were deposited from an ultra-high purity Fe target at 500 or 1000 eV. The secondary ion source bombarded the growing film at 100 eV.

The authors found constant soft magnetic properties in films of 50-1000 nm, but the magnetic properties of films thinner than 50 nm were inferior. Film structure was found to be dense and columnless using single source deposition at

argon pressures below 1.0 mTorr. Above this pressure level the films were usually columnar with voids and had poor magnetic qualities. If the films were bombarded by argon ions at 100 eV during growth, dense noncolumnar structures could be grown up to argon pressures of 1.6 mTorr with good soft magnetic properties. The effect of the two incident ion energies used was not as conclusive. Those films sputter deposited using 1000 eV ion-beam energy had higher electrical resistivity than films sputtered at 500 eV. This was apparently due to the formation of α -Fe crystallites in the higher energy films caused by additional reflected neutral bombardment from the target.

The Kaufman dual ion source method was used to construct $\text{Li}_2\text{O}/\text{Ni}$ multilayer x-ray mirrors (Kataoka et al. 1989). The Li_2O layers were fabricated using a reactive dual ion source method in which lithium was sputtered from a high purity target and deposited onto a fused quartz substrate. Oxygen ions were targeted through the second ion source at the substrate during deposition. The nickel layers were deposited from a nickel target with secondary argon ion bombardment at 50 eV. The reflectivity of the resultant mirror was only about half that of the calculated value. This was due to a higher than expected roughness at the $\text{Li}_2\text{O}/\text{Ni}$ interface. The authors also discovered the presence of up to 15% oxygen in the Ni layers which was probably due to contamination from the oxygen process used in the Li_2O deposition.

Seaward, Barbee, and Tiller deposited silicon carbide films from separate elemental carbon and silicon targets. By using two magnetron sources concurrently they were able to independently control the deposition rates of Si and C to the substrate (Seaward, Barbee, and Tiller 1986). The authors fabricated a series of SiC_x films ranging in composition from carbon rich to silicon rich. The carbon-rich films were found to contain β -SiC particles in amorphous carbon while the silicon-rich films were largely silicon with isolated β -SiC particles scattered throughout. In films with 1:1 silicon to carbon ratios, there was a preferred orientation of the (111) planes and a columnar microstructure. These films were characterized by a refractive index comparable to published values of p-type films deposited on sapphire with sheet resistivity around 2 Ω -cm.

Legg and Solnick-Legg used rf magnetron sputtering combined with higher energy ion implantation to produce thin films from hydroxylapatite (HA) intended for biomedical applications (Legg and Solnick-Legg 1988; Solnick-Legg and Legg 1989). Deposition was carried out in a modified Varian 200/1000 ion implanter with an argon back-pressure of 10^{-3} Torr. The authors first sputtered a thin film layer onto the substrate and bombarded it with 100 keV ions of an inert or reactive gas. The intent of this step was to physically mix the coating into the near surface volume of the substrate. This was followed by deposition of the film to the desired thickness. They called this process enhanced

plasma deposition (EPD). Scratch tracks in films deposited without EPD showed severe film decohesion at the film/substrate interface, whereas films produced with EDP did not.

Since a complex oxide such as HA does not usually sputter in its molecular form, the crystal structure of the starting material was lost during deposition. Although stoichiometry was maintained to within approximately 10% of the Ca:P:O ratios of HA, the as-sputtered films were found to be amorphous or only partially crystalline whether or not EDP was used. Also, very light elements such as hydrogen and to some extent oxygen can be removed with the vacuum. Following film deposition the investigators subjected their films to a proprietary hydration step in an attempt to restore the hydrogen content and convert the films to crystalline. The authors used reflection high energy electron diffraction (RHEED) to check for crystallinity. They were only able to produce crystalline films by using a combination of the enhanced plasma deposition process and the hydration process.

Titanium nitride coatings were produced using a similar process combining ion-beam sputter deposition and ion implantation (Jiankun et al. 1989). The films were grown on polished iron substrates by alternating between ion-beam sputter deposition from a Ti target and ion implantation of nitrogen ions. The resultant films were composed of randomly oriented TiN crystallites with a lower oxygen contamination than that found in films produced by sputter

deposition alone. The authors also found an intermixing of Ti and N up to 40 nm into the depth of the iron substrate. The coatings were hard and adherent with a very low coefficient of friction.

Perhaps the most common use of ion-beam technology in the deposition of thin films is in ion-beam assisted deposition where an ion-beam source is used in conjunction with another deposition process. PVD and CVD have been used as primary deposition methods with Kaufman-type sources used to add energy and mobility to the depositing particles (Jaulin et al. 1989; al-Jumaily et al. 1989). By combining methods, films can be produced with the high deposition rates of PVD or CVD but with structures and properties achievable only through higher energy deposition.

Physical vapor deposition was used simultaneously with ion bombardment to produce titanium carbide and silicon carbide films (Jaulin et al. 1989). In this study films were vapor deposited from bulk SiC and TiC with assistance from Ar ions at 1.5 keV from a Kaufman ion source. The coatings were then bombarded with 100 keV Ar ions to intermix the film atoms with the atoms in the near-surface volume of the chromium steel substrate. The coatings from the TiC starting material were determined to be fine-grained, homogeneous titanium carbide with a face centered cubic crystal structure. As-sputtered silicon carbide films were amorphous without an 800°C anneal. Following heat treatment the films were very fine-grained β -SiC. Friction studies on both coatings showed a decrease in friction when

compared to the bare steel substrates, but the SiC coatings endured the testing regime over six times longer than the TiC coatings.

Ion-beam assisted deposition was also used with electron beam vapor deposition to fabricate optical thin films (al-Jumaily et al. 1989). They deposited films of aluminum nitride and oxynitride as well as silicon nitride and oxynitride while bombarding the substrate surface with nitrogen, oxygen, or a mixture of the two gasses. Silicon nitride has an index of refraction of 2.1, while that of silicon dioxide is 1.42. The authors were able to produce films with values intermediate to these by varying the gas mixture through the ion source and, consequently, the film composition. Similar results were achieved with aluminum nitride and oxynitride, indicating that optical thin films could be produced with specific optical properties by using this method.

Donovan, Carosella, and Van Vechten, working with Hubler and Kant, have combined Kaufman ion bombardment with electron beam evaporation to produce a number of different films with varying optical and mechanical properties (Donovan, Carosella, and Van Vechten 1989; Hubler et al. 1989; Carosella et al. 1989). They produced $\text{Si}_{1-x}\text{N}_x$ films by evaporating silicon onto silicon wafers under a constant nitrogen ion bombardment at 500 eV. The resultant films were amorphous with decreasing indices of refraction as the nitrogen content increased. Subsequent annealing of the films between 450°C and 1100°C resulted in a drop in the

index of refraction in each case due to structural relaxation of the amorphous phase (Donovan, Carosella, and Van Vechten 1989).

Similarly, Carosella et al. vapor deposited $B_{1-x}N_x$ films under constant nitrogen ion bombardment at 250 eV (Carosella et al. 1989). These films were also amorphous or only microcrystalline. The index of refraction was found to decrease with increasing nitrogen content, and the microhardness of the films peaked at a nitrogen/boron ratio of 0.36 but dropped off steadily with increasing nitrogen.

The process described above was also used to produce TiN films (Hubler et al. 1989). Titanium was vapor deposited while nitrogen ions struck the substrate at 500 eV. The authors postulated that nitrogen could be found on the deposited titanium surface in two forms: adsorbed molecular N_2 and reacted N bonded to Ti in TiN. By increasing the ratio of N ions arriving during deposition, the authors found that more N_2 from the ambient chamber gas reacted to form TiN. The arriving ions provided the energy needed to convert N_2 to reacted nitrogen while sputtering away any extra adsorbed nitrogen.

Other investigators have used IBAD with mixed results in attempting to produce TiN coatings (Chang and Kant 1989; Kant et al. 1989; Tetreault, Hirvonen, and Parker 1989). Chang and Kant found that TiN grain size increased with increasing nitrogen ion energy and flux. Kant et al. reported increasing Knoop microhardness values with increasing ion energy bombardment. They also found a

reduction in sliding friction to 0.2 from 0.6 for coated versus uncoated substrates. The coefficient of friction value was independent of the microhardness value, but the endurance of the friction reduction was dependent on hardness. Coatings of intermediate range hardness (1800-2600) afforded longer protection from wear. Those films with values above and below this range did not last as long in the pin-on-disk wear apparatus.

Hirvonen and Hirvonen also used IBAD to deposit boron nitride films (Hirvonen and Hirvonen 1989). Boron was evaporated onto silicon substrates at temperatures from ambient to 400°C with secondary nitrogen ion bombardment between 600 eV and 1000 eV. Only the room temperature films subjected to the highest energy ion bombardment and current density were stoichiometric BN. All the other films were boron rich. These investigators found an unexplainable hydrogen contamination in their films, which had some limiting effect on the mechanical properties.

It was previously mentioned that deposition using IBAD can modify the intrinsic stress of the film. Roy et al. used Ar ion bombardment to modify the intrinsic stress of vapor deposited tungsten films (Roy et al. 1989). The films were produced at substrate temperatures of 300°C, 450°C, and 750°C using 400 eV ion bombardment and varied argon ion current density. Experiments were also conducted at a constant temperature of 450°C using ion bombardment energies of 200 eV, 400 eV, and 600 eV while varying the current density at each potential. Ion current density is

indicative of the flux or flow rate of ions arriving at the substrate surface.

The authors found that film stress remained tensile at 300°C and 450°C with constant 400 eV ion bombardment until the ion current density reached 0.07 ma/cm². In contrast a substrate temperature of 750°C produced compressive film stress with as little ion current density as 0.02 ma/cm². At a constant substrate temperature of 450°C, films bombarded with 600 eV became compressive at 0.03 ma/cm², while the 400 eV films became compressive at 0.08 ma/cm² and films bombarded by 200 eV argon ions remained compressive at all ion flux rates.

Tetreault, Hirvonen, and Parker found very low coefficients of friction ($\mu = 0.10$) for boron nitride films produced by IBAD and vapor deposition (Tetreault, Hirvonen, and Parker 1989). However, friction was found to increase as the B/N ratio increased.

Greenwald, Hirvonen, and Jaggi combined vapor deposition with IBAD to fabricate diamond-like carbon films (Greenwald, Hirvonen, and Jaggi 1989). Carbon was deposited from a graphite source while being subjected to a constant bombardment of 400 eV ions from a Kaufman source. The authors varied the working gas from pure argon to pure methane (CH₄). Although the resulting films had Knoop microhardness values as high as 1600, none of them appeared to exhibit diamond-like carbon bonds.

Hypotheses and Objectives

Calcium phosphate ceramics and glasses containing calcium and phosphorus have been shown to be better tolerated by the body than metallic implant materials. Additionally, these materials are bioactive. They can form a chemical bond with living bone or they may be resorbed by the body, supplying critical calcium and phosphorus to newly developing bone. The inherent brittleness of most calcium phosphate materials, however, makes them unsuitable as implant materials in their bulk form. A number of investigations have been directed at producing metallic implants coated with bioactive calcium phosphate compounds in order to enhance both short-term and long-term implant fixation in bone. The overall objective of this study was to produce thin adherent crystalline coatings of bioactive calcium phosphate on titanium substrates by ion-beam sputter deposition. The following hypotheses and specific objectives were developed to enhance and support the overall goal.

Hypothesis: The ion-beam sputtering process will produce non-stoichiometric or amorphous calcium phosphate thin films from hydroxylapatite ceramic $[\text{Ca}_{10}(\text{PO}_4)_6(\text{OH})_2]$. This deposition process occurs at an energy level (1000 eV) high enough to break the molecular bonds of the hydroxylapatite target material, since they are only on the order of a few electron volts. The sputtered particles are ejected from the target surface in the form of single atoms of Ca, P, and O and as molecular clusters of PO_3 , PO_4 , CaO, CaP, and OH.

Since the energy of the particle arriving at the substrate surface is usually less than 5% of the incident energy of the argon ion beam, diffusion to lowest energy nucleation sites to produce a crystalline material is not likely. If the temperature of the substrate is not high enough to supply energy for diffusion, the resultant as-sputtered film will be randomly oriented and amorphous. Additionally, because the vacuum system operates continuously in this process to maintain a consistently low pressure, any constituent released as a gas during sputtering (e.g., OH and O) would not be expected to survive the transfer to the substrate.

Objective: The structure of as-sputtered films was investigated using transmission electron microscopy (TEM) and selected area diffraction (SAD) to determine if they were amorphous or crystalline. Auger electron spectroscopy and energy dispersive spectroscopy (EDS) were used to determine whether the elements present in the as-sputtered coatings were stoichiometric.

Hypothesis: Crystalline coatings will be produced if sufficient energy is available for surface diffusion of the sputtered particle. Ion-beam assisted deposition (IBAD) raises the energy of sputtered particles deposited on the substrate surface, giving them enough energy in some instances to diffuse to nucleation sites of lowest energy. This process, also referred to as dual-beam deposition, has been shown to alter the structure and composition of

as-sputtered films, producing crystal structures which would normally only be attainable by higher temperature methods.

Objective: Transmission electron microscopy and selected area diffraction were used to determine if the IBAD process could produce crystalline films without an additional post-deposition treatment. Auger and EDS were used to determine if elements present in the dual-beam as-sputtered coatings were stoichiometric.

Hypothesis: Amorphous calcium phosphate coatings will attain crystallinity if sufficient energy for the transformation is available in a post-deposition treatment. Post-deposition heat treatments have been shown to be beneficial in restoring crystallinity to amorphous thin films and coatings deposited by ion-beam sputter deposition, as well as by other coating techniques. Controlled cooling as opposed to quenching has also been shown to affect the amount of material restored to a crystalline structure in systems with sluggish amorphous to crystalline transformations. In earlier work by Lacefield on the bond strength testing of sputter deposited HA coatings, quenching from an elevated temperature in distilled water appeared to transform the coating structure to columnar-shaped crystals (Lacefield 1988).

Objective: As-sputtered films were annealed to produce crystallinity. Half of the films were allowed to cool within the furnace, while the remainder were quenched to room temperature. Transmission electron microscopy and selected area diffraction were used to determine if the heat

treatment produced crystallinity and to determine if the furnace cooling rate was more effective at producing crystalline films. Auger electron spectroscopy was used to determine if the heat treatment produced any diffusion of the HA constituents or the titanium into the coating/substrate interface.

Hypothesis: Ion-beam sputter deposited calcium phosphate coatings will have excellent adherence to the titanium substrate. Most sputter deposited coatings have a reputation for excellent bond strength in their as-sputtered state. If sputtered at low enough vacuum chamber pressure (0.6 mTorr or less), the intrinsic stress of the sputter deposited coating is usually compressive. Such stresses are beneficial to the bond strength of ceramic coatings such as calcium phosphates. Also, heat treatments under pressures of 100 MPa or more have been shown to promote chemical diffusion between a deposited coating and its substrate, thereby improving the bond strength between them (Ducheyne et al. 1986). Hot isostatic pressing at 117 MPa was investigated as a method of promoting chemical diffusion between the sputter deposited HA coating and the titanium substrate.

Objective: Z-axis bond strength tests were performed on all as-sputtered coatings and on all heat treated coatings. Comparison of bond strengths was made between the two deposition methods and between the post-treatment categories. These results were compared to published values for the bond strengths of plasma sprayed HA coatings. Auger

electron spectroscopy was used to investigate the possibility of chemical diffusion at the interface.

CHAPTER III.

MATERIALS AND METHODS

Materials

The deposition target material used in this study was hydroxylapatite $[\text{Ca}_{10}(\text{PO}_4)_6(\text{OH})_2]$ ceramic supplied by Lifecore Biomedical, Inc. (Minneapolis, MN). It was hot pressed and sintered by Cerac, Inc. (Milwaukee, WI) into a 6 mm X 127 mm disk at 1150°C . It was then bonded to a copper backing plate and fixed to the water cooled sputter-coater stage. The target was identified by x-ray diffraction as hydroxylapatite. Figure 6 shows a scanning electron photomicrograph of the surface of the sintered target material. Commercially pure titanium, meeting the ASTM specification F 67 for surgical materials, was used as the substrate material for both Auger electron spectroscopic analyses and coating adhesion testing. Single crystal NaCl was used as the substrate material in preparing samples for transmission electron microscopy. Table 1 gives the chemical analysis of the titanium, which was supplied by Phoenix Metallurgical (Houston, TX).

Material Preparation

Titanium specimens were cut from 10 mm diameter round bar stock to a thickness of 2 mm on a high speed diamond saw.

Figure 6. Scanning Electron Micrograph of the Sintered Hydroxylapatite Target Material



TABLE 1

Chemical Analysis of ASTM F 67 Titanium Grade 2						
Element	N	C	H	Fe	O	Ti
Weight %	0.012	0.007	0.010	0.22	0.21	Bal.

They were wet ground using 240, 400, and 600 grit silicon carbide paper, respectively, and polished using 0.3 μ m alumina powder on a Buehler automatic polisher. A similar procedure was also used in preparing 2 mm X 6.35 mm Ti samples. All titanium specimens were cleaned and degreased in benzene, acetone, and ethanol, respectively, ten minutes in an ultrasonic cleaner. They were then rinsed in distilled, deionized water and passivated in 40% nitric acid for thirty minutes following ASTM Specification F 86.

Once cleaned and passivated the specimens were fixed onto the sputter-coater stage with Mung paste, a conductive adhesive containing silver particles supplied by Commonwealth Scientific (Alexandria, VA). The chamber was closed and evacuated to a minimum of 6.0×10^{-6} Torr. Once this was achieved, high purity (99.999% minimum) argon was back-filled into the chamber to a pressure of 4.8×10^{-4} Torr.

The specimens were ion sputter cleaned for 30 minutes using the secondary ion source at 40.7 mA and 750 V. This procedure produced a clean reactive surface prior to

deposition of the Ca-P film. The specimen stage was held at 90° to the incident argon beam from the secondary source during cleaning. Figure 7a illustrates the physical arrangement of the ion sources, the specimen stage, and the target stage within the sputter-coater chamber during sputter cleaning.

Sputter-Coating Procedure

After sputter cleaning, the specimen stage was rotated into position for deposition or coating. Specimens were coated using one of two methods: single-beam deposition or ion-beam assisted (IBAD) deposition. In the former, deposition was performed by the primary ion source alone. In the latter, deposition was performed by the primary ion source with the secondary source simultaneously bombarding the substrate surface with energetic argon ions.

For single-beam deposition the stage was rotated 80° counter clockwise to place the specimens at the angle of highest incidence with respect to the incoming sputtered material. This was done to achieve the fastest rate of deposition. The target stage containing the hydroxylapatite disk was placed at an angle of 45° with respect to the ion beam from the primary ion source. Figure 7b illustrates the stage arrangement during single-beam sputter deposition. The deposition process was accomplished at a chamber pressure of 4.8×10^{-4} Torr and an ion-beam energy of 1000 V and 40.7 mA. Since the mean-free-path for collisions at this chamber pressure was larger than the distance from the

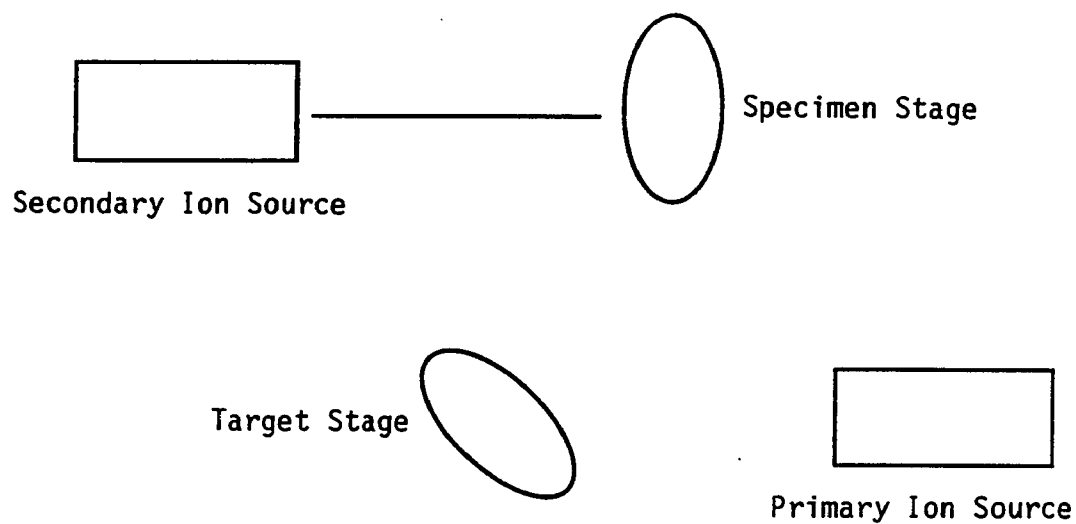


Figure 7a. Stage Arrangement for Sputter Cleaning

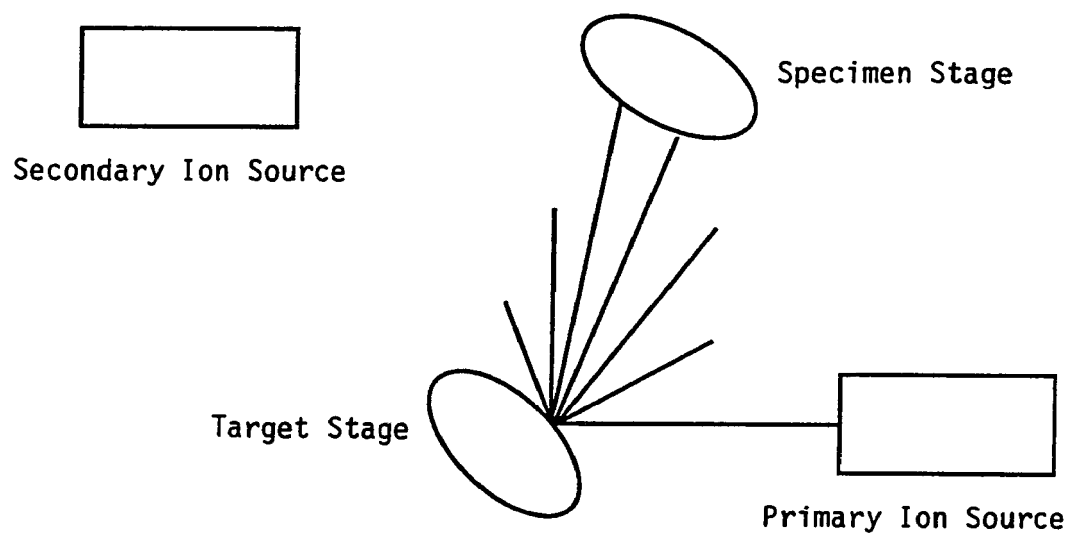


Figure 7b. Stage Arrangement for Sputter Deposition

ion source to the target, the ion beam reached the HA surface with an incident energy very close to 1000 eV. A discharge voltage of 40.7 V was used in all processes to minimize the possibility of double argon ionization.

The majority of ion-beam energy is absorbed by the hydroxylapatite target material as heat. Sputtered particles leave the target with only a fraction of the ion-beam energy. Ion-beam assisted deposition was performed in order to increase the surface energy of the substrate material during deposition. For this procedure the specimen stage was rotated only 60° after sputter cleaning so as to make a 30° angle with the secondary or assist ion beam. The secondary ion source was operated at 700 eV but at very low ion current (4.5-5.5 mA). This was done to minimize the possible resputtering of incoming target material as it deposited on the specimens. Since some resputtering was inevitable, the deposition rate for IBAD was slightly lower. It was thought that the ion-beam assisted process might provide enough energy to allow the depositing material to relax into its lowest energy crystalline state and produce denser and more adherent films. Since a discharge was required for both ion sources to accomplish IBAD, the argon pressure was necessarily increased to 5.8×10^{-4} Torr. The assist or secondary ion source was set at 4.5 mA and 700 V, while the primary source, aimed at the target material, was set to 45.0 mA and 1000 V.

The titanium specimens were sputter coated to specific thicknesses for the requirements of the particular analysis

technique. Specimens for Auger electron spectroscopy were coated for three hours producing coatings of 0.3 and 0.4 μm for the dual-beam and single-beam techniques, respectively. Specimens for bond strength testing were coated for nine hours producing coatings between 1.0 and 1.2 μm . Transmitted electron microscopy specimens were prepared by sputter depositing the Ca-P film onto cleaved NaCl crystals. These specimens were coated for two hours producing films between 0.2 and 0.3 μm in thickness.

Post-Deposition Treatments

Since the process of ion-beam sputter deposition produces particles from the target material in the form of atoms, molecules, and ions, the loss of the crystal structure for a material as complex as hydroxylapatite was not unexpected. Consequently, post-deposition heat treatments were performed in an effort to achieve crystallinity. Following coating, specimens in both the single- and ion-beam assisted groups were set aside to be studied in the as-sputtered form. Other specimens were annealed in air at 600°C for one hour with the intent of both increasing the oxygen content in the films and providing energy for crystallization. This temperature was chosen because it was well below the titanium phase transformation at 882°C. Of those specimens which were annealed, half were allowed to cool within the furnace while the other half were quenched in distilled deionized water at room temperature. Additional samples were sent to the U.S. Army Materials Technology Laboratory in Watertown,

Massachusetts, where they were hot isostatically pressed at 600°C and 117 MPa. Thus, three different post-treatment categories were evaluated for both the single- and ion-beam assisted deposition methods, in addition to the as-sputtered forms of each method. Specimens coated using only sputter deposition were categorized as single-beam as-sputtered (SBAS), quenched (SBQ), furnace cooled (SBFC), or HIP'ed (SBH). Specimens coated by the IBAD process were categorized as dual-beam as-sputtered (DBAS), quenched (DBQ), furnace cooled (DBFC), or HIP'ed (DBH).

Methods

Transmission Electron Microscopy

Transmission electron microscopy specimens were prepared by sputter-depositing the Ca-P film directly onto cleaved NaCl crystals. Prior to deposition the NaCl crystals were sputter cleaned at the same beam parameters as previously described for the titanium substrates; however, only fifteen minutes of cleaning time were used to remove any adsorbed gases, since ion-beam bombardment could cause surface damage to the NaCl crystals.

The salt crystals were coated for two hours to achieve 0.3 μm of coating for single-beam deposition and 0.2 μm for the ion-beam assisted process. Five specimens in each group were set aside to be examined in the as-sputtered form. Ten specimens in each group were placed in the annealing furnace for one hour at 600°C. Following heat treatment five specimens in each group were removed from the furnace and placed on an aluminum block to cool rapidly while the

remaining samples were allowed to cool in the furnace. Water quenching, of course, could not be used with these specimens without dissolving the underlying NaCl substrate. TEM specimens were made by carefully floating the Ca-P film from the NaCl crystal in a water bath. The water bath contained a metal grid suspended just below the water line. A piece of 10 μm filter paper was placed on the grid with a 3 mm, 100 μm mesh copper TEM grid on it. The film was floated above the copper grid while the water level in the bath was carefully lowered to bring the film into contact with the TEM grid. The filter paper was removed and allowed to dry with the grid and film in place. These samples were placed in the TEM and examined for crystallinity visually and with the aid of selected area diffraction.

Energy dispersive spectroscopy (EDS) was also used in the TEM to analyze for the presence of any impurities in these films. Sodium and chlorine were of particular interest because of the nature of the sample preparation. Argon was also analyzed for because the sputtering gas can in some instances be incorporated into the depositing film.

Auger Electron Spectroscopy

Auger depth profiles were performed using intermittent argon ion-beam raster. Several parameters had to be evolved in order to perform successful Auger analyses of these specimens. Since the Ca-P coating on the titanium was an insulator, great care had to be taken to minimize charging of the surface. A tilting stage was required to achieve efficient electron conduction off the coated surface. The 2

mm X 10 mm Ti specimens were used in Auger analyses because this diameter was the proper size for the tilting Auger stage. A coating thickness of 0.4 μm , achieved with a single-beam sputter deposition time of three hours, was found to work best for the Auger analysis. Ion-beam assisted samples were coated for the same length of time, but since the IBAD rate is somewhat slower these films were approximately 0.3 μm in thickness. Early work with the Auger showed this to be the proper thickness to achieve efficient electron conduction from the specimen surface. In performing an Auger depth profile an argon ion beam was used to slowly mill away the material surface as the Auger electrons were analyzed. In this study the ion beam was not run simultaneously with the Auger analysis because it caused charging of the ceramic surface and shifting of the element peaks. Depth profiles were performed using an intermittent argon ion-beam raster of forty seconds per analysis cycle. The beam voltage was kept low at 2.5 keV with a spot size of 5 μm . Current was also kept below 1.15×10^{-7} A to minimize the electron current density and any resultant damage to the samples. The tilting stage was set at an angle of 70 degrees to allow for a more efficient electron conduction path. Background pressure for the Auger was on the order of 10^{-8} Pa.

A total of sixteen specimens, two per category, were analyzed using AES. Depth profiles were performed in two locations on each specimen for consistency.

Energy Dispersive Spectroscopy

Energy dispersive spectroscopy was also used in order to determine the Ca/P ratios of the films. Representative specimens in each category from the adhesion tests were placed in the SEM to examine the interface failure site and check for any remaining calcium or phosphorus in this area. The undamaged area of the coatings away from the fracture site was also examined for calcium and phosphorus content. These results were quantified to determine the percentages of each element present and the ratio of Ca to P. Oxygen was included in the analysis for the purposes of stoichiometry. A portion of the sintered target material was also analyzed to compare the calcium and phosphorus ratios within the coatings to that of hydroxylapatite.

Bond Strength Testing

The Z-axis bond strength testing was performed on the films using a Sebastian Five adhesion testing apparatus manufactured by Quad Group of Spokane, Washington (Riegart 1988). For these tests, the 2 mm X 6.35 mm titanium specimens were used. A 3.6 mm X 12 mm pull stud, supplied pre-coated with a thermal curing epoxy by Quad Group, was clipped to the center of each of the Ca-P sputter-coated titanium specimens. These samples were allowed to cure in an oven at 150°C for one hour. Since the adhesive becomes highly liquid just prior to full polymerization, the pull stud was assured of settling into a perpendicular position on the specimen surface. Figure 8 shows the configuration of the specimen with the pull stud spring-clipped to its

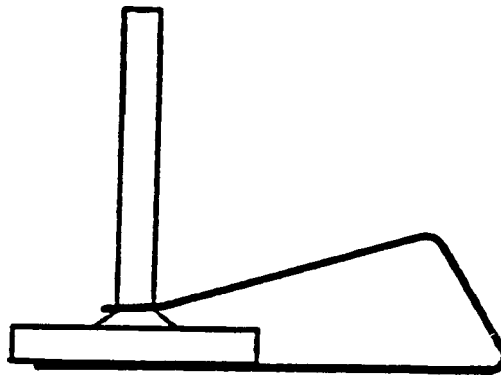
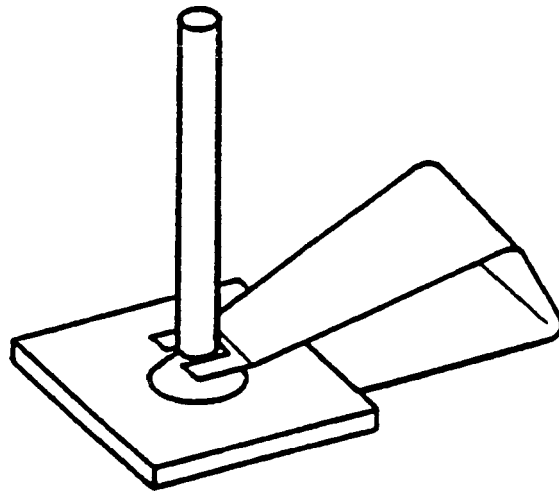


Figure 8. Position of Bond Test Specimen in Spring Clip

surface for curing. Quad Group rated the bond strength of the fully cured epoxy at 70 MPa. The mounted specimens were inserted into the machine platen and gripped. The Sebastian was activated, pulling the stud down against the platen support ridge until failure occurred in the coating or the epoxy bond.

A total of eighty specimens, ten per category, were used in the adhesion tests. Duncan's Multiple Range statistical analysis was performed on these data to determine the significance of any observed differences among the groups (Miller and Freund 1977). Reflected light photomicrographs were taken of the adhesion specimens following testing to determine the location of the bond failure. Specimens were coded according to one or a combination of the following four failure locations: 1) between the titanium substrate and the coating, T/C; 2) within the coating, C; 3) between the coating and the epoxy, C/E; and 4) between the epoxy and the pull stud, E/S.

CHAPTER IV.

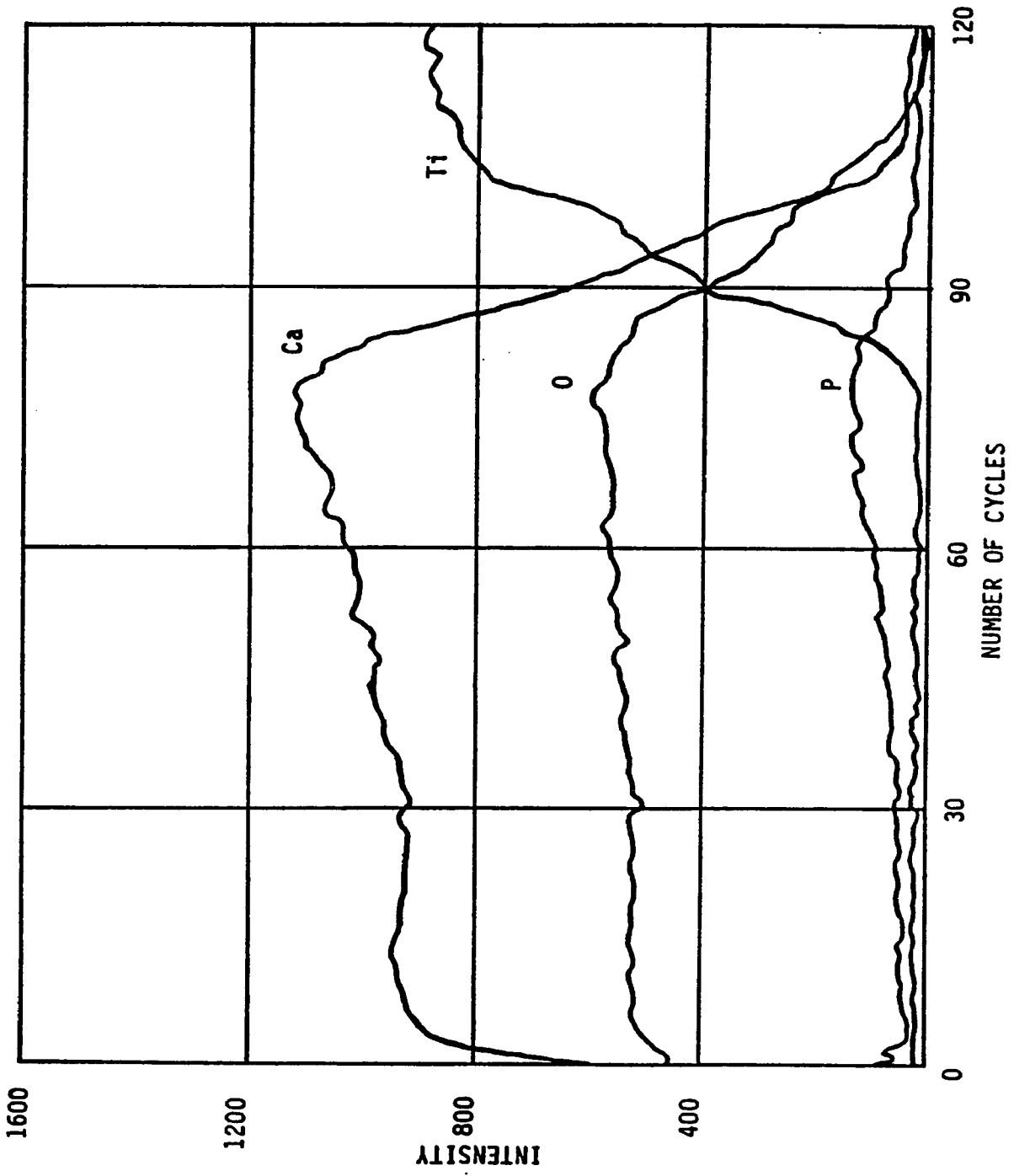
RESULTS

Auger Electron Spectroscopy

Auger electron spectroscopy (AES) was performed to determine coating composition as a function of depth through to the titanium interface. Figure 9 shows a typical AES depth profile obtained from a single-beam as-sputtered (SBAS) specimen. Analyses of these profiles showed the presence of the three major constituents of hydroxylapatite, i.e., Ca, O, and P. The presence or absence of hydrogen could not be measured by AES because the element hydrogen is too light for AES detection.

Since an argon ion beam was used to mill away the coating surface for the Auger depth profile, the milling rate was determined by comparing the rate through a known thickness of the single-beam as-sputtered coating material. It was found to be approximately $180 \text{ \AA}/\text{min}$. at a vacuum chamber pressure of 10^{-7} to 10^{-8} Pa and an ion-beam voltage of 3.0 keV. Because the Ca-P coating was an insulator, all specimens were held at a 70° angle in a tilting Auger stage to prevent charging of the ceramic. As a result, the thickness through to the SBAS interface in Figure 9 represents a distance of 1300 nm, even though the coating

Figure 9. Auger Depth Profile of Single-Beam As-Sputtered Coatings



itself was only 450 nm thick. It required approximately 110 argon ion-beam milling cycles to reach the interface. Since the sputter deposition rate for the IBAD process was somewhat lower than that of single-beam deposition, these coatings were usually only 300 nm thick. The distance through to the interface for DBAS specimens at the 70° angle was 880 nm. Figure 14 shows that it required approximately seventy cycles to reach the DBAS interface. This compares favorably to the argon ion sputter rate of the SBAS specimens.

Phosphorus content was also found to be very low or non-existent in both the SBAS and DBAS profiles until approximately 300 nm from the titanium interface. This was observed in all coated samples independent of the deposition process or the post-deposition treatment. An Auger depth profile performed on the sintered hydroxylapatite target material shown in Figure 10 illustrates how the phosphorus content of the bulk material remained within the background level throughout the depth of the profile. This material was determined by x-ray diffraction and energy dispersive spectroscopy to be stoichiometric hydroxylapatite with a 1.67 atomic ratio of Ca and P. Since there was no titanium interface in this sample, no phosphorus peak was seen.

Figure 11 shows an AES profile of a typical single-beam furnace cooled (SBFC) specimen. These specimens showed a significant increase in oxygen level at the film/Ti interface following the 600°C heat treatment. This increase was sustained into the near surface volume of the titanium

Figure 10. Auger Depth Profile of HA Target Material

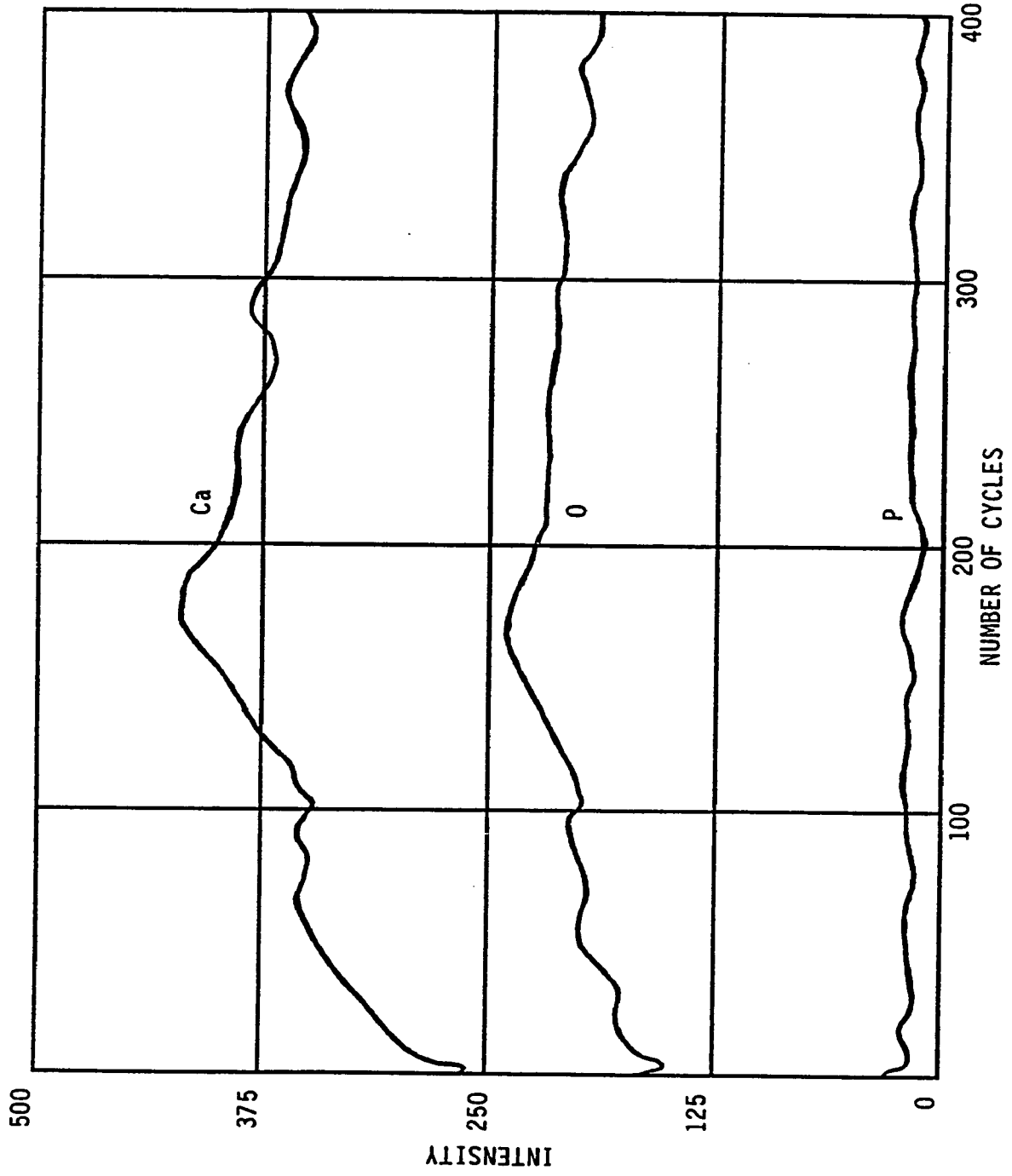
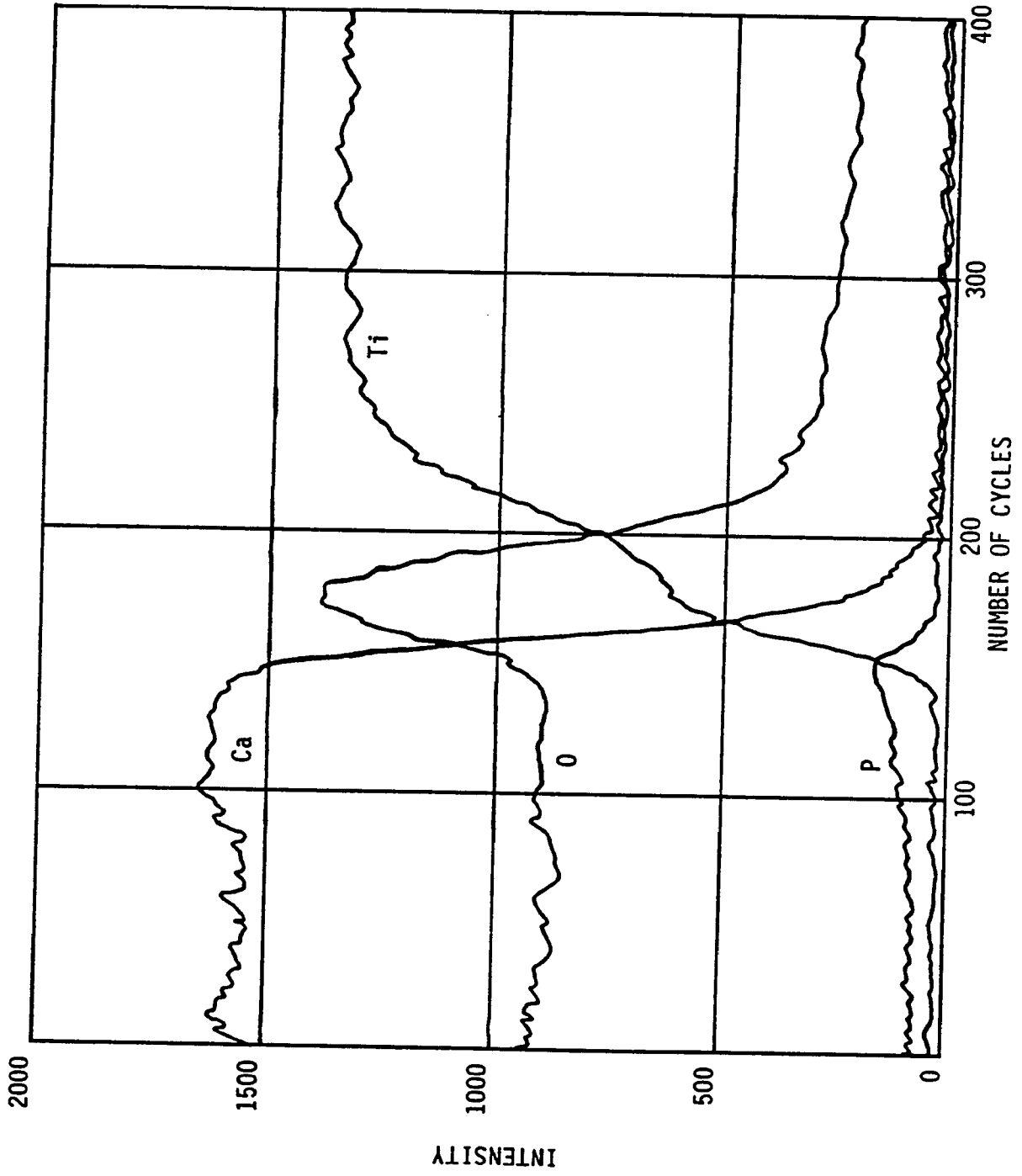


Figure 11. Auger Depth Profile of Single-Beam Furnace Cooled Coatings



substrate. Single-beam quenched (SBQ) specimens shown in Figure 12 appeared similar to the furnace cooled samples with an increase in oxygen at the interface and a sustained oxygen increase into the titanium surface. However, the peak in oxygen at the interface was broader than the oxygen peak in the single-beam furnace cooled specimens. The difference in the shape of the oxygen profiles for the furnace cooled and quenched specimens was most likely due to the difference in cooling rates for these specimens. At the heat treatment temperature of 600°C, oxygen diffused into the titanium substrate because the solubility of oxygen in titanium increased with increasing temperature. The rapid cooling rate of quenching trapped the diffused oxygen in the titanium, hence the broader oxygen profiles in the SBQ and DBQ specimens. Furnace cooling was slow enough to allow much of the oxygen to diffuse out of the titanium, thereby resulting in a higher oxygen content at the coating/substrate interface.

Figure 13 shows the single-beam HIP'ed (SBH) specimens. These specimens exhibited an oxygen increase at the Ca-P/Ti interface, and they also contained a significant amount of carbon in the near surface region of the coating. This was most likely the result of contamination from the graphite furnace used in the hot isostatic pressing procedure. Another interesting observation which should be noted in these specimens was the definite shift in the phosphorus peak from just before the titanium interface to within the interface region.

Figure 12. Auger Depth Profile of Single-Beam Quenched Coatings

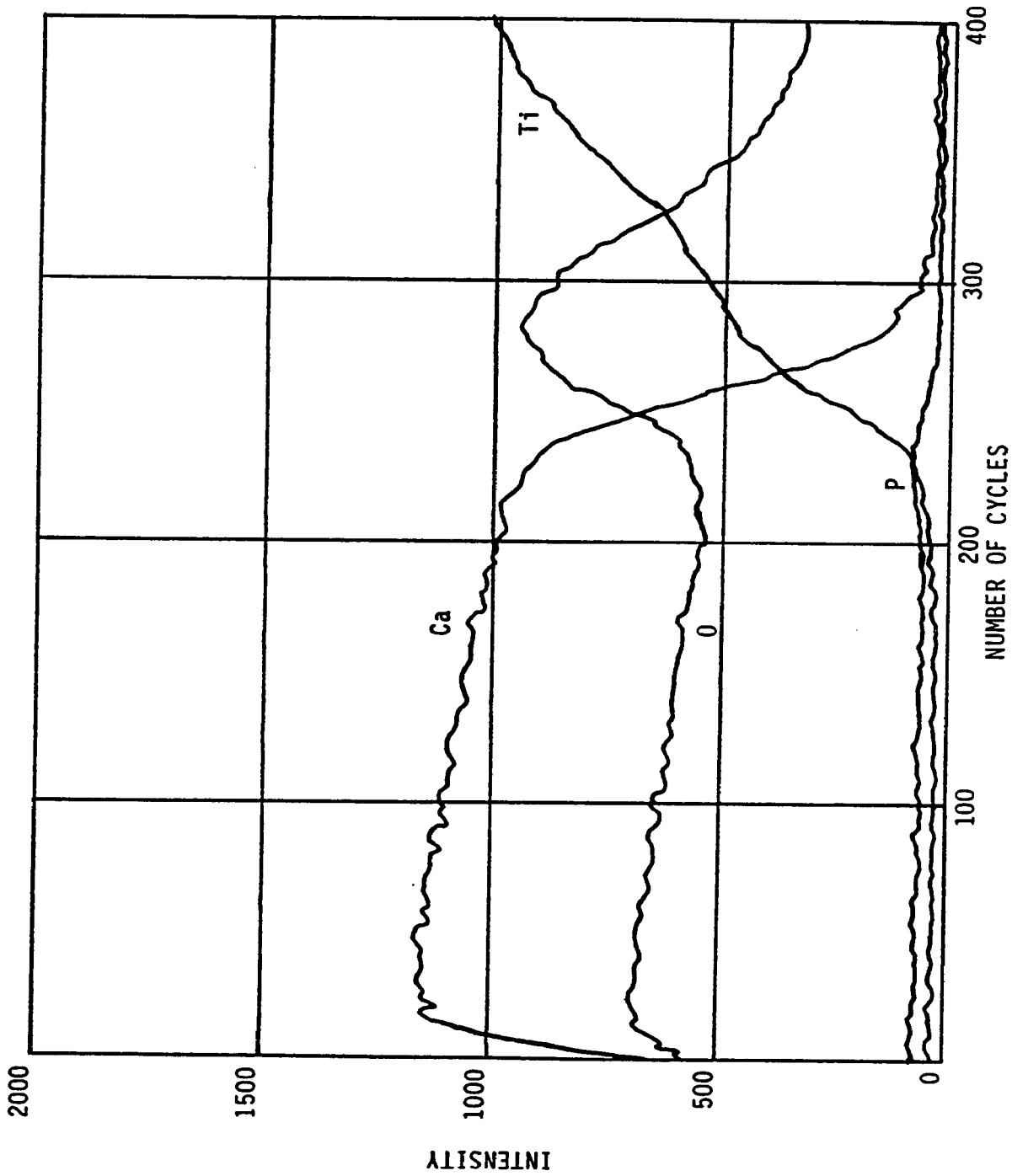


Figure 13. Auger Depth Profile of Single-Beam Hot Isostatically Pressed Coatings

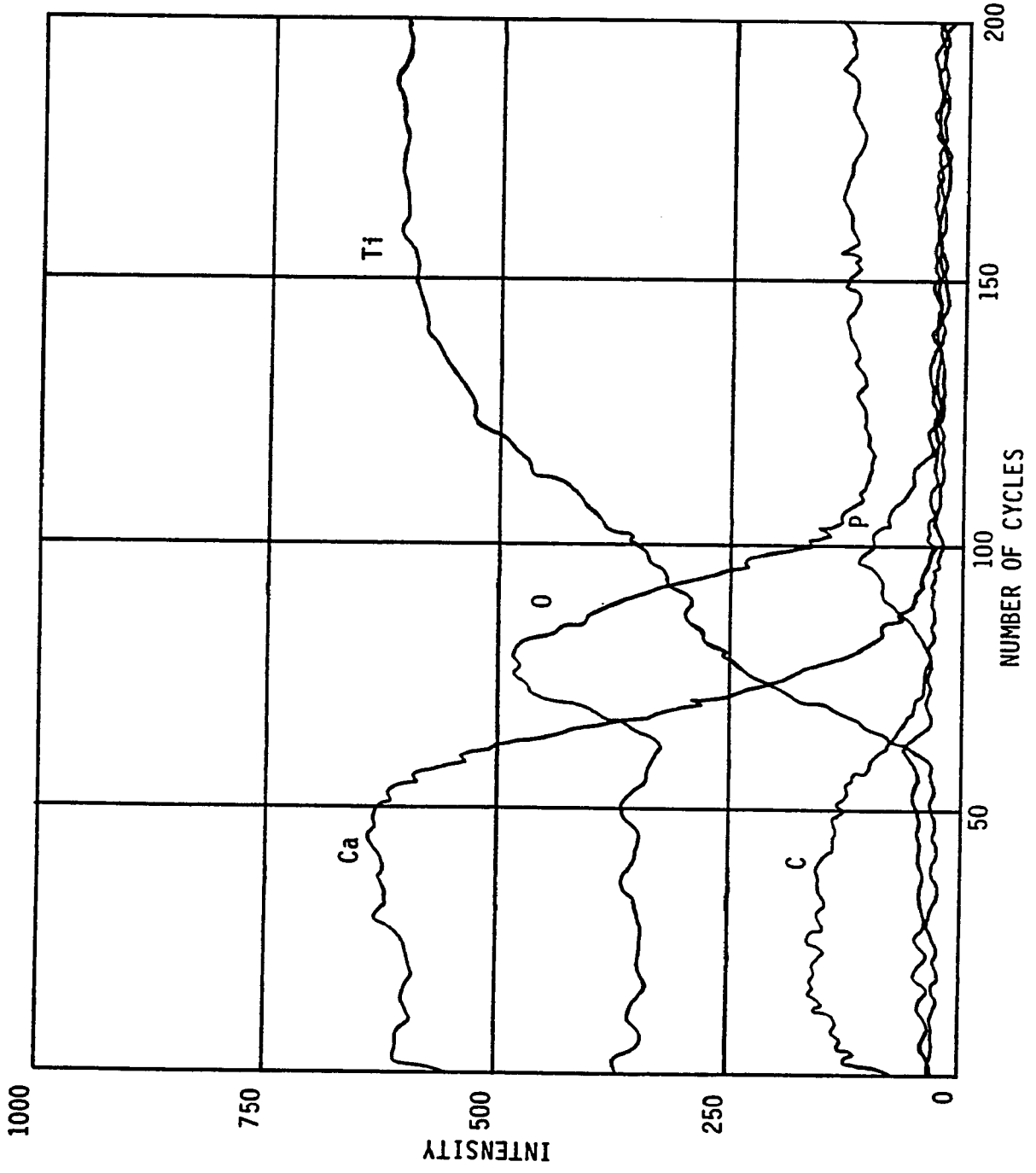
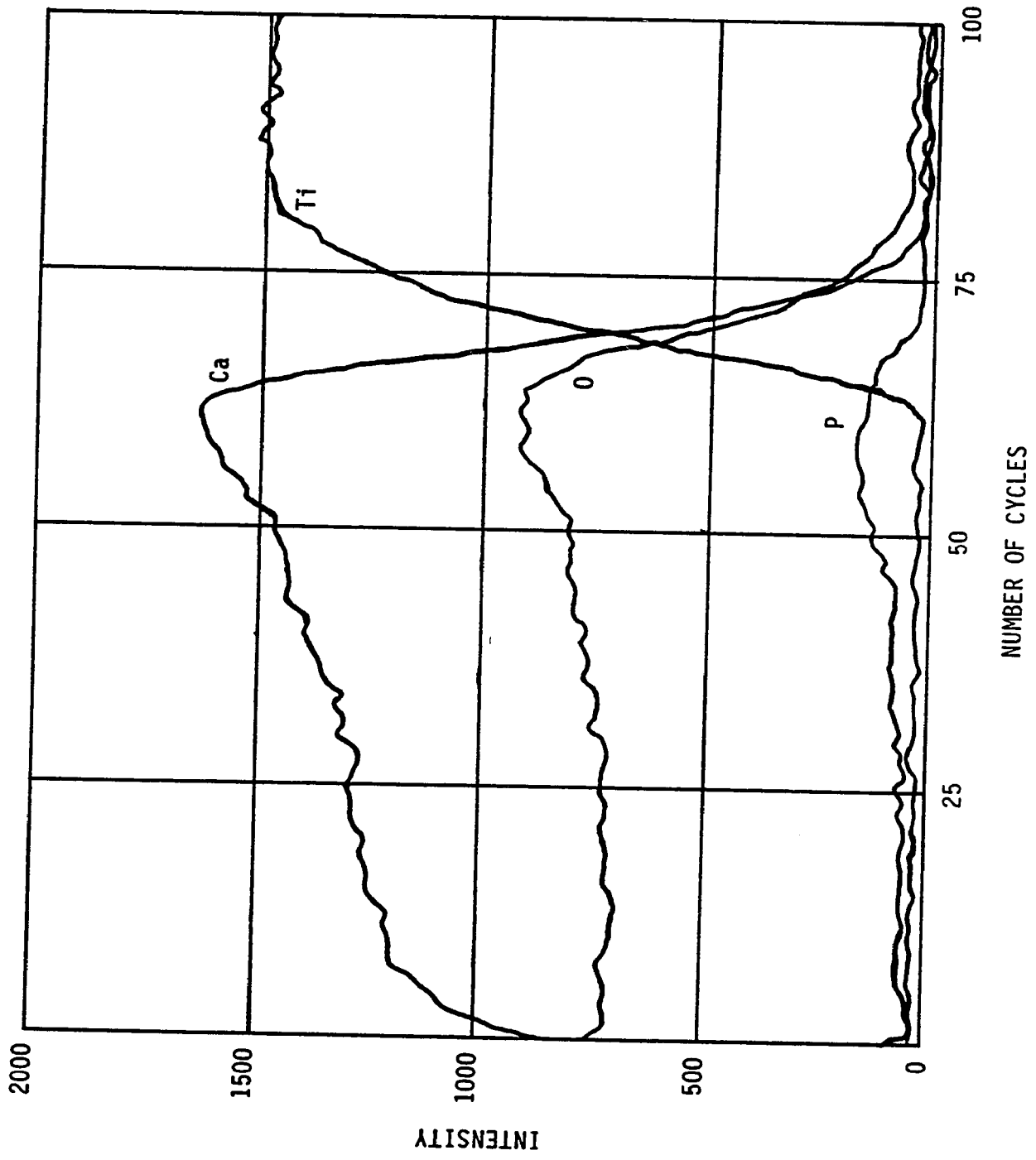


Figure 14. Auger Depth Profile of Dual-Beam As-Sputtered Coatings



The profile for dual-beam as-sputtered (DBAS) specimens, shown in Figure 14, was similar to the single-beam as-sputtered specimens. Once again phosphorus detection was very low until just prior to reaching the coating/substrate interface. Both the dual-beam furnace cooled (DBFC) specimens and the dual-beam quenched (DBQ) specimens shown in Figures 15 and 16, respectively, were found to be similar to their single-beam counterparts, exhibiting an increase in oxygen content at the interface which was sustained into the near-surface volume of the titanium. Both dual-beam heat treated specimens also showed low phosphorus levels until just prior to reaching the titanium interface.

Dual-beam HIP'ed (DBH) specimens also exhibited the same type of carbon surface contamination seen in the single-beam HIP'ed specimens, but the increase in phosphorus content at the interface was not observed for these specimens. The Auger depth profile for DBH specimens is shown in Figure 17. An increase in oxygen at the interface was also noted in the DBH specimens.

Energy Dispersive Spectroscopy

Energy dispersive spectroscopy was performed on each of the films to determine chemical composition and the Ca/P atomic ratio. Table 2 is a listing of the Ca/P ratios determined by EDS for each coating. The as-sputtered coatings are represented by AS in the table. Quenched specimens are represented by Q, furnace cooled specimens by FC, and the hot isostatically pressed specimens are

Figure 15. Auger Depth Profile of Dual-Beam Furnace Cooled Coatings

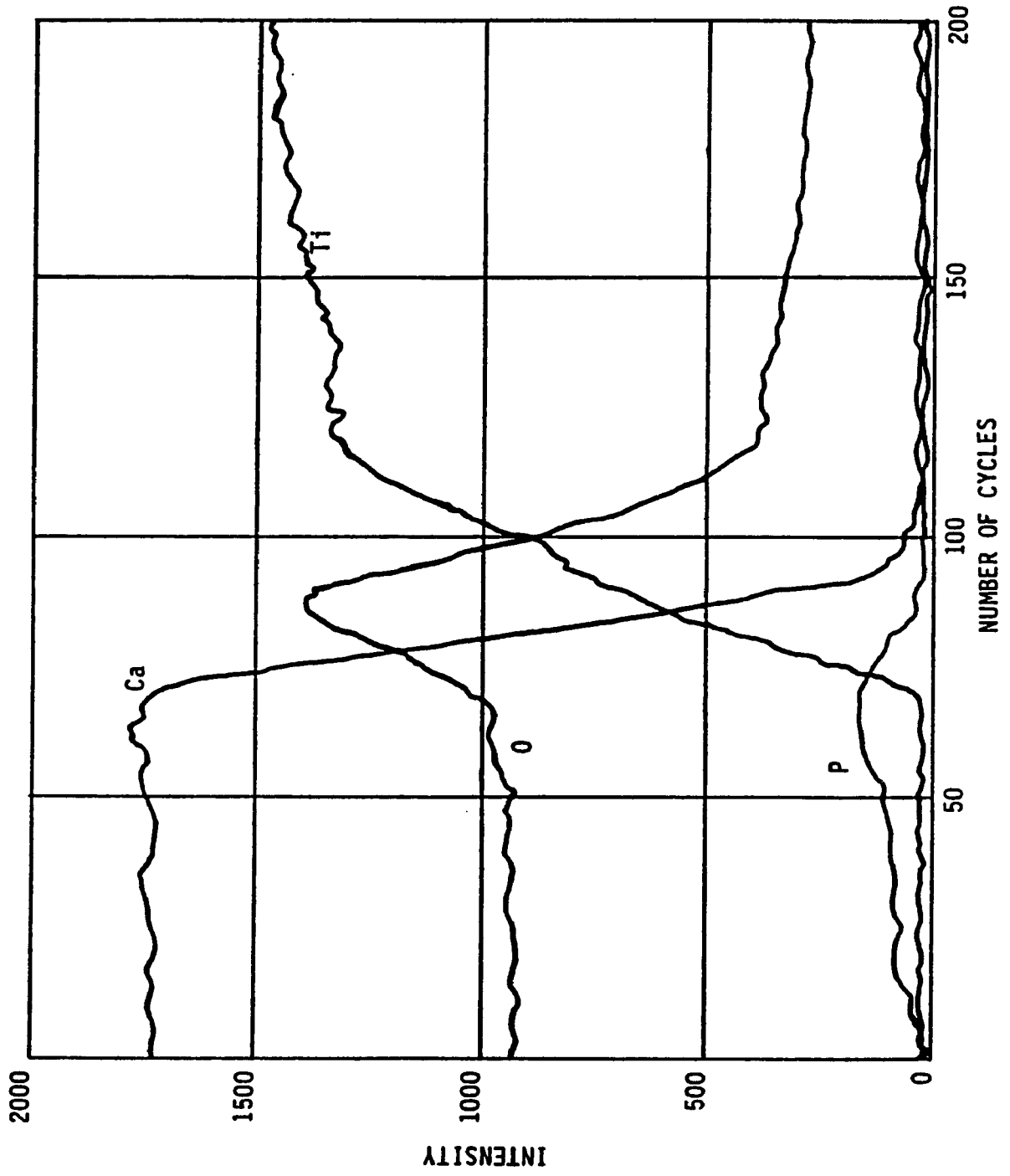


Figure 16. Auger Depth Profile of Dual-Beam Quenched Coatings

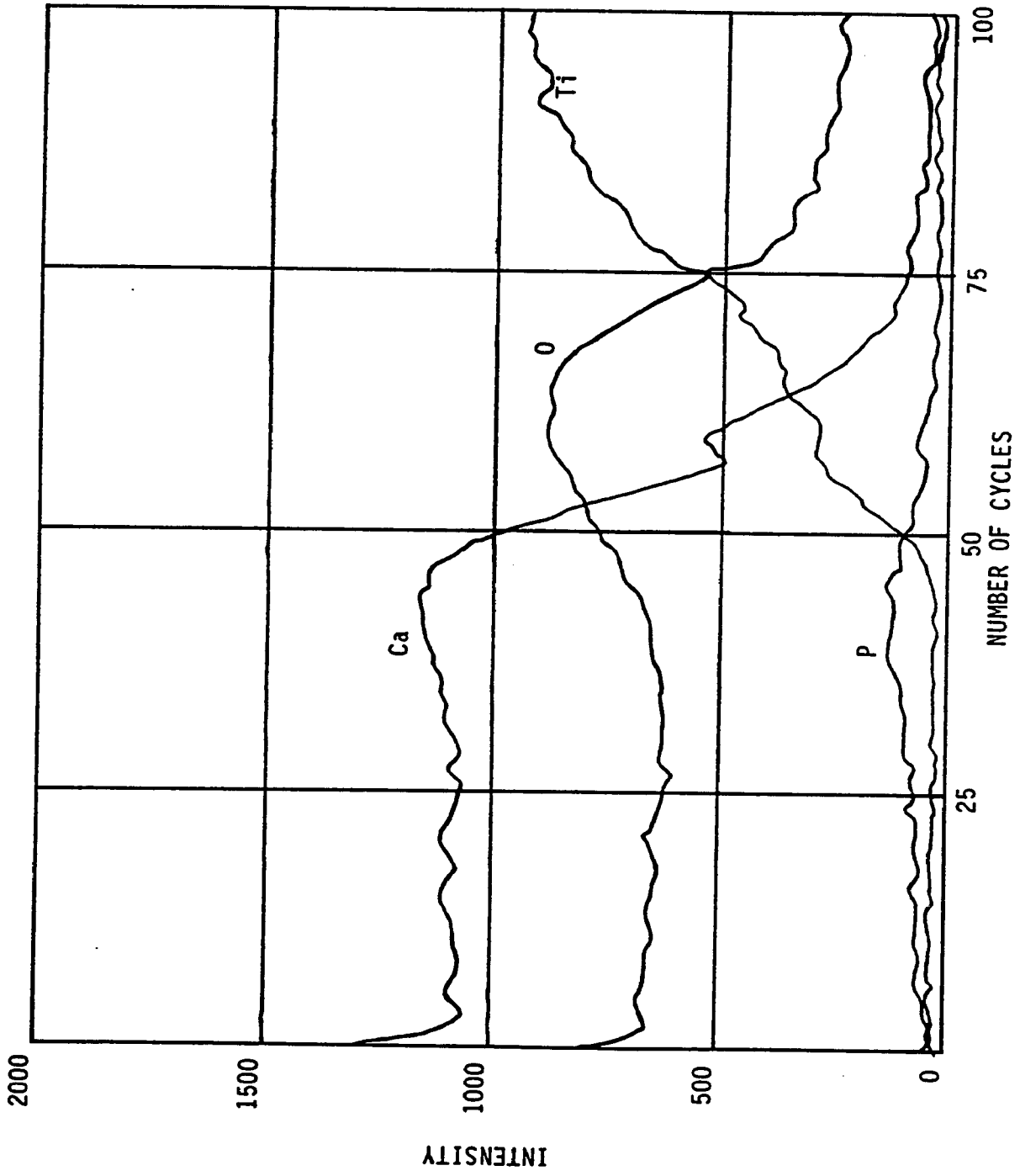
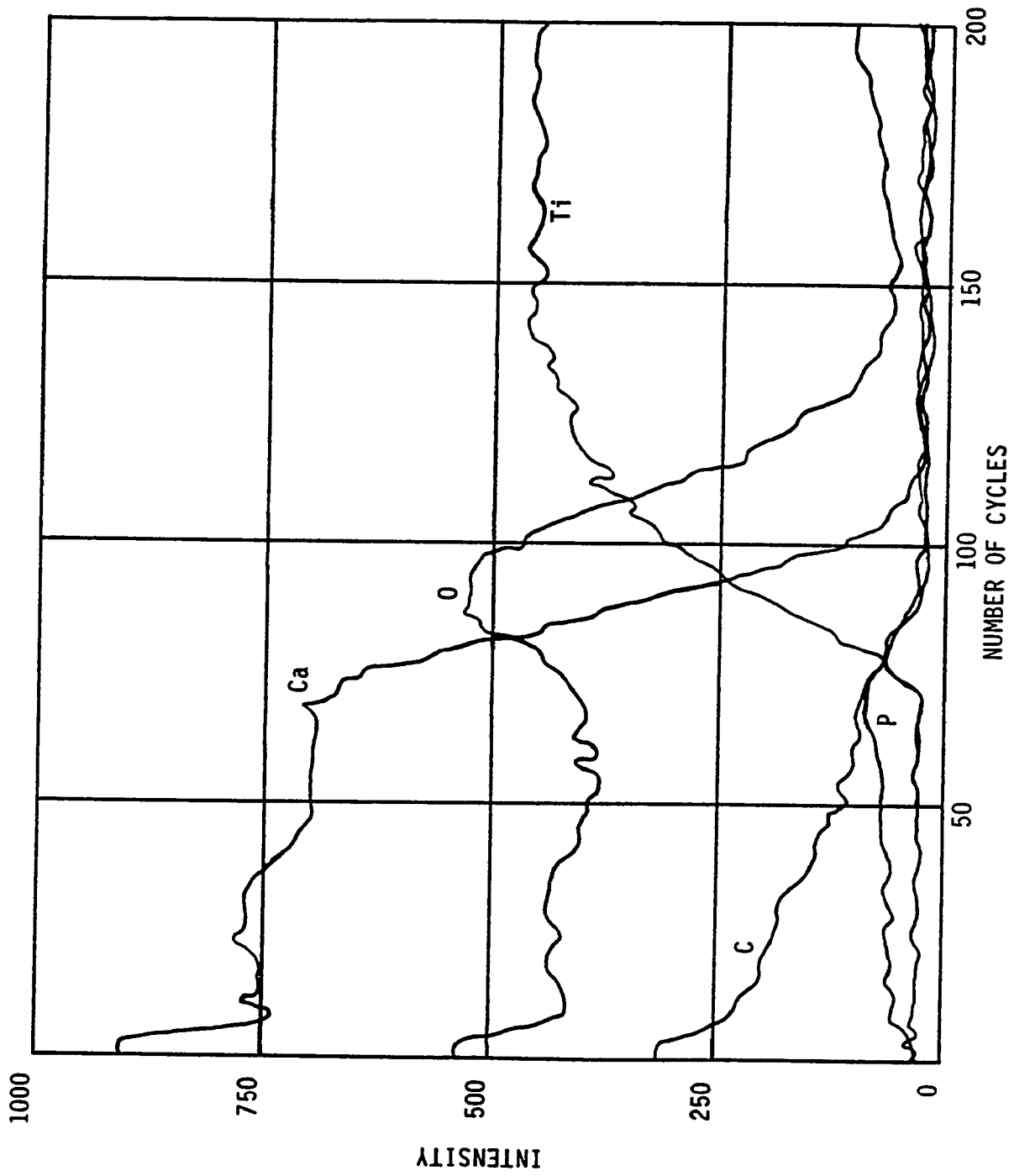


Figure 17. Auger Depth Profile of Dual-Beam Hot Isostatically Pressed Coatings



represented by H. All coatings were found to be enriched in calcium and somewhat deficient in phosphorus. This ranged from a high of 62.14% Ca and 5.7% P in the DBH specimens to a low of 51.08% and 12.45% P in the DBQ specimens. Correspondingly, the Ca/P atomic ratio ranged from 6.66 for the DBH specimen to 2.50 for the DBQ specimen. Overall, the single-beam specimens were closest to the correct Ca/P ratio of 1.67 observed in the starting target material. The SBAS ratio was 2.54. The SBQ ratio was 2.71, and the SBFC ratio was 2.69. The SBH ratio was lower than the DBH ratio, but at 4.08, it was still the highest of the single-beam deposited coatings. Dual-beam as-sputtered coatings had a high ratio of 3.98, and the DBFC coatings a Ca/P ratio of 4.47.

TABLE 2

Ca/P Ratios for the Ion-Beam Sputter Deposited Coatings				
	AS	Q	FC	H
Single-Beam	2.54	2.71	2.69	4.08
Dual-Beam	3.98	2.50	4.47	6.66

Figure 18 shows EDS pattern for an SBAS specimen. Figure 19 shows an EDS pattern for a DBAS specimen. Dual-beam deposited specimens all exhibited a peak for argon, but the single-beam deposited films usually did not. The amount of entrapped argon in the dual-beam films never amounted to more than 1%, but it was present in all the films regardless of the post-deposition heat treatment.

Figure 18. EDS Profile of Single-Beam As-Sputtered Coatings

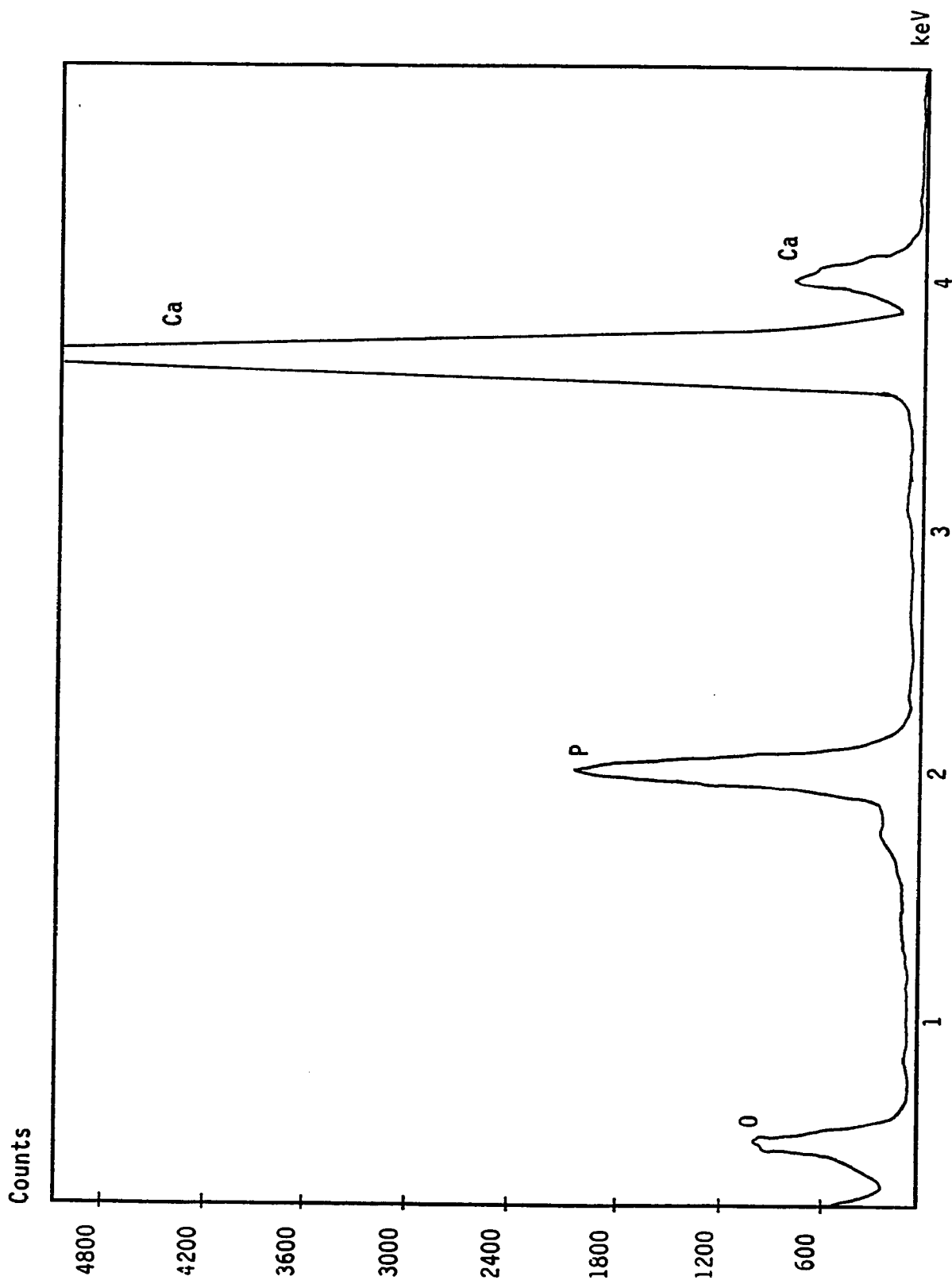
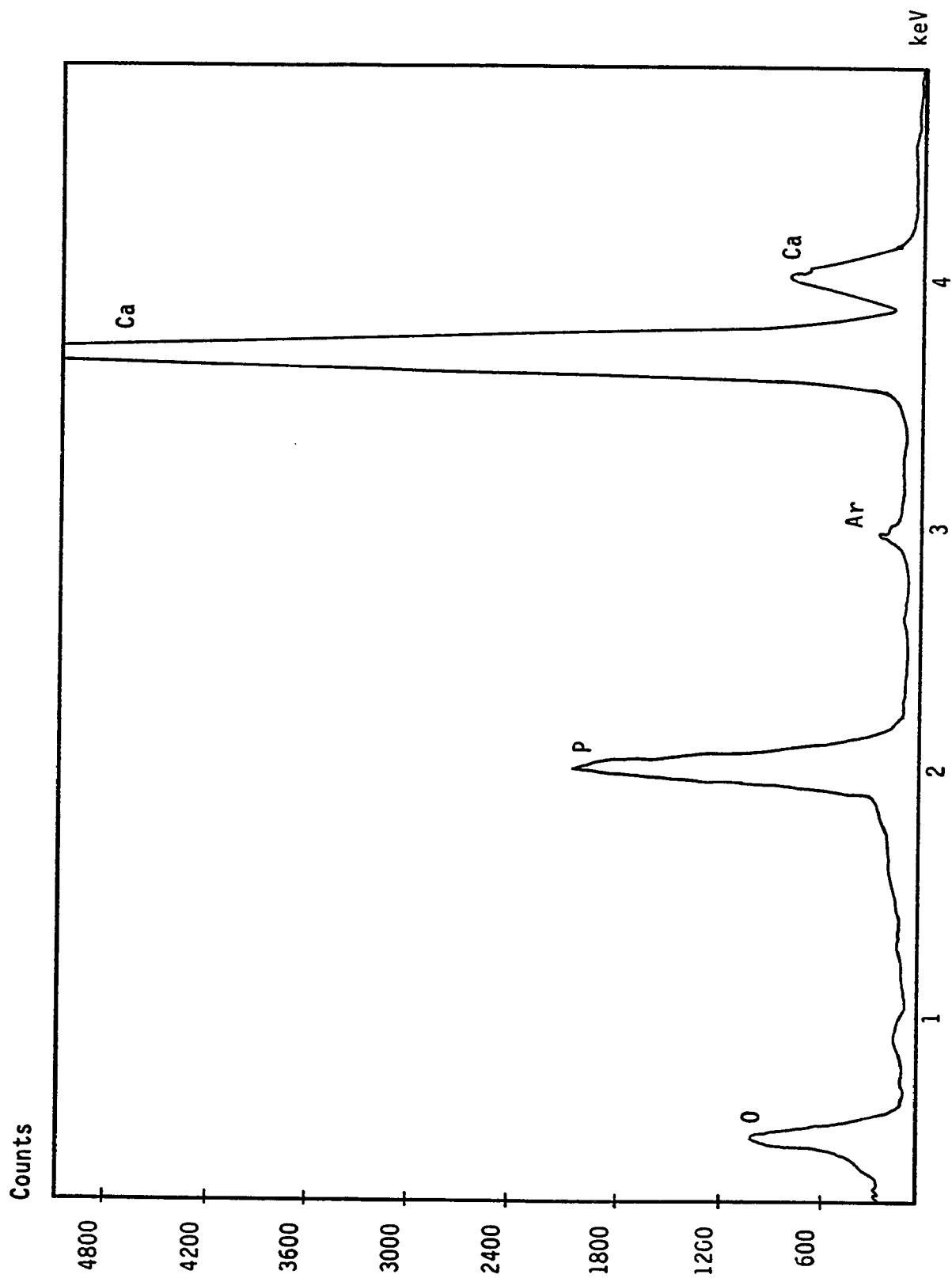


Figure 19. EDS Profile of Dual-Beam As-Sputtered Coatings



Transmitted Electron Microscopy

Figure 20a shows a TEM micrograph typical of SBAS thin films. The enlargement at 20,000X shows that the film was amorphous in its as-sputtered state. No structure or pattern was found in these specimens. Figure 20b is an accompanying selected area diffraction (SAD) pattern for the same area of the SBAS micrograph. The presence of diffuse rings with no clearly defined spot pattern indicates that this material was essentially amorphous with little or no crystalline structure. While observing the specimen under a 200 keV electron beam, however, crystals slowly began to develop. Figure 20c is a micrograph at 25,000X which shows the size and shape of crystals formed during analysis. These crystals were extremely fine grained and fairly diffuse. The spot near the center of the micrograph shows the effect produced by continued electron beam bombardment in a localized area. The crystals grew in size with prolonged analysis. Figure 20d shows the spotty SAD of the area which is indicative of diffuse crystallinity.

Dual-beam as-sputtered films were also featureless and amorphous in appearance when first viewed in the TEM as seen in Figure 21a. Figure 21b is the SAD pattern of the DBAS film which also shows diffuse rings indicative of a lack of crystallinity or only short range order at best. These films began to show the development of small crystals during analysis just as the SBAS specimens did. This is shown in Figure 21c. The SAD pattern shown in 21d was indicative of

Figure 20. TEM/SAD of Single-Beam As-Sputtered Films

- a. TEM of Single-Beam As-Sputtered Film
- b. SAD of Single-Beam As-Sputtered Film
- c. TEM of SBAS Film after Electron Beam Heating
- d. SAD of SBAS Film after Electron Beam Heating

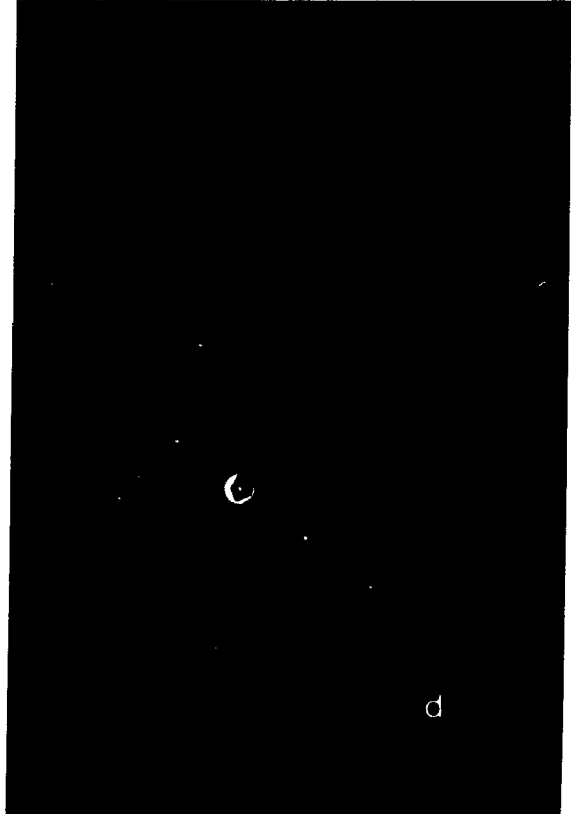
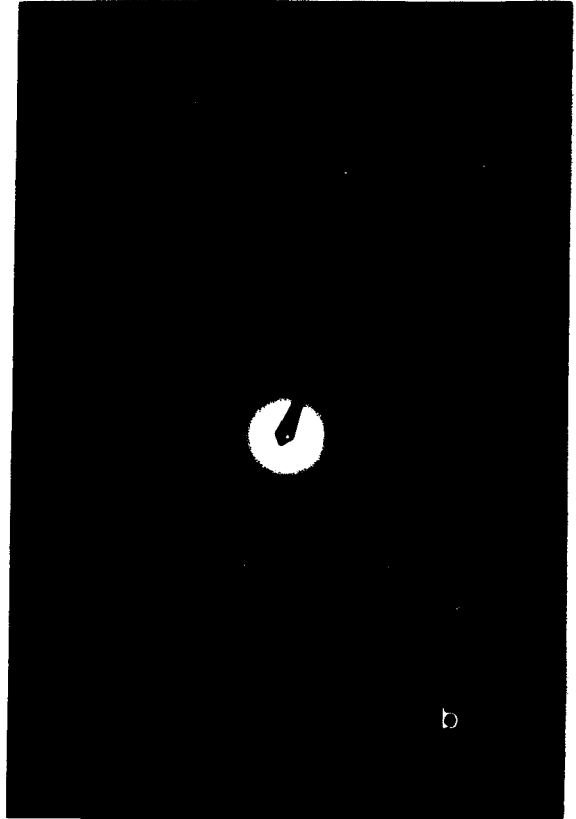
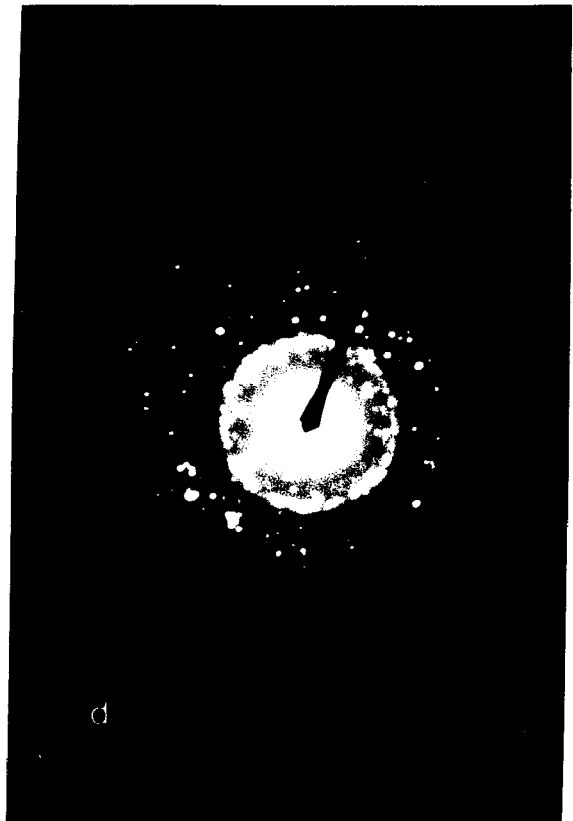
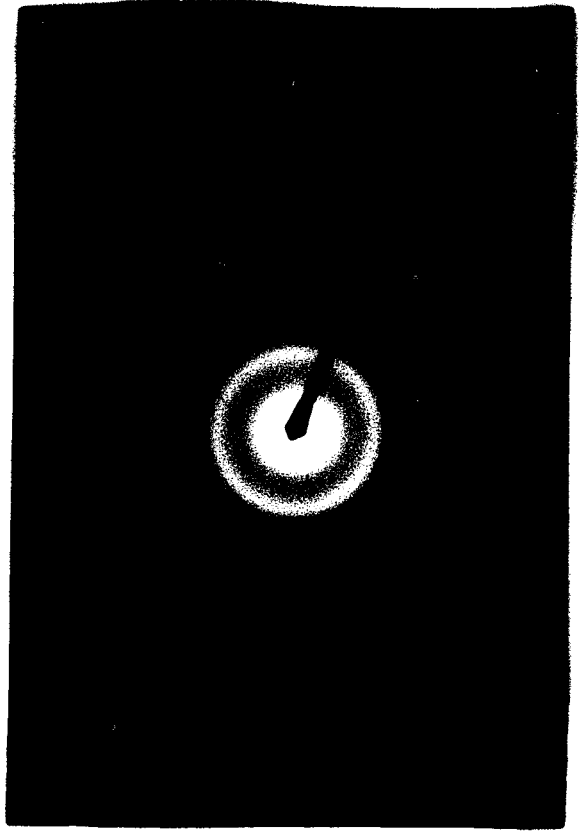


Figure 21. TEM/SAD of Dual-Beam As-Sputtered Films

- a. TEM of Dual-Beam As-Sputtered Film
- b. SAD of Dual-Beam As-Sputtered Film
- c. TEM of DBAS Film after Electron Beam Heating
- d. SAD of DBAS Film after Electron Beam Heating



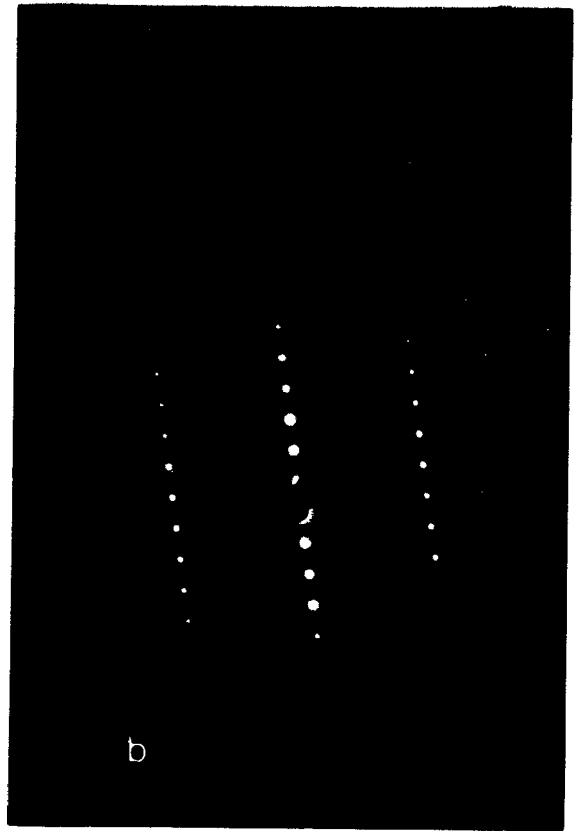
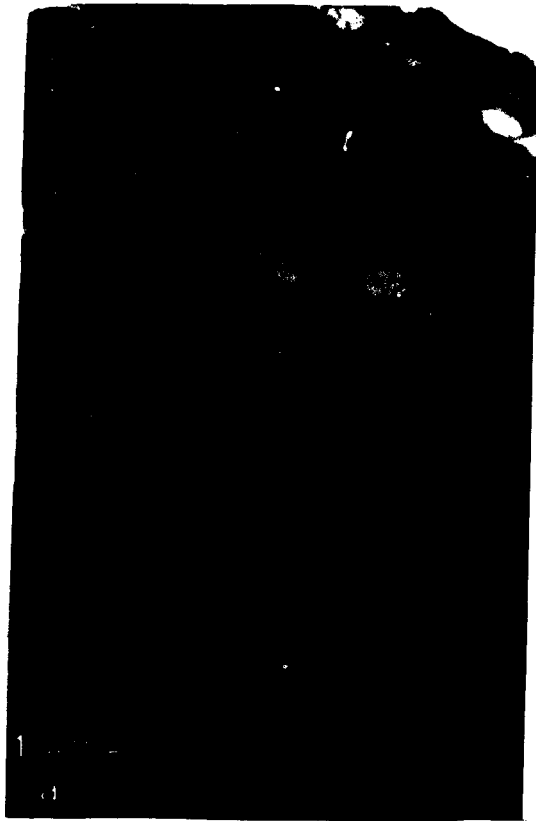
a crystalline structure in the area of the transmission electron beam.

As previously described in the materials and methods chapter, Ca-P films sputter deposited onto NaCl crystals were placed on an aluminum quench block when removed from the furnace. Water quenching would have immediately separated the film from the substrate. This process had to occur under controlled conditions so that the films could be floated onto copper microscope grids to insure conduction within the microscope.

Figures 22a and 22c show TEM micrographs of SBFC and SBQ films, respectively. Both annealed films were definitely crystalline at first analysis. Although Figure 22a and Figure 22c were taken at different magnifications, comparison of the size bar shows that the grain sizes were not the same. The crystals in the SBFC specimens were approximately 1 μm or less in diameter, while the grains in the SBQ specimens were on the order of 2 μm micrometers or less. The corresponding SAD patterns for these specimens are shown in Figures 22b and 22d. Both SAD patterns were taken at the same camera length, so they are comparable. The SAD pattern in Figure 22b is a single crystal pattern. This pattern was only achieved with SBFC films. The pattern appeared to be a hexagonal crystal, which is the structure of both hydroxylapatite and whitlockite $[\text{Ca}_3(\text{PO}_4)_2]$. The measured d-spacings from this pattern were 7.90 \AA , 2.062 \AA , and 2.023 \AA . The closest comparable d-spacings reported for hydroxylapatite are 8.17 \AA for the 100 direction, 2.065 \AA

Figure 22. TEM/SAD of Single-Beam Furnace Treated Films

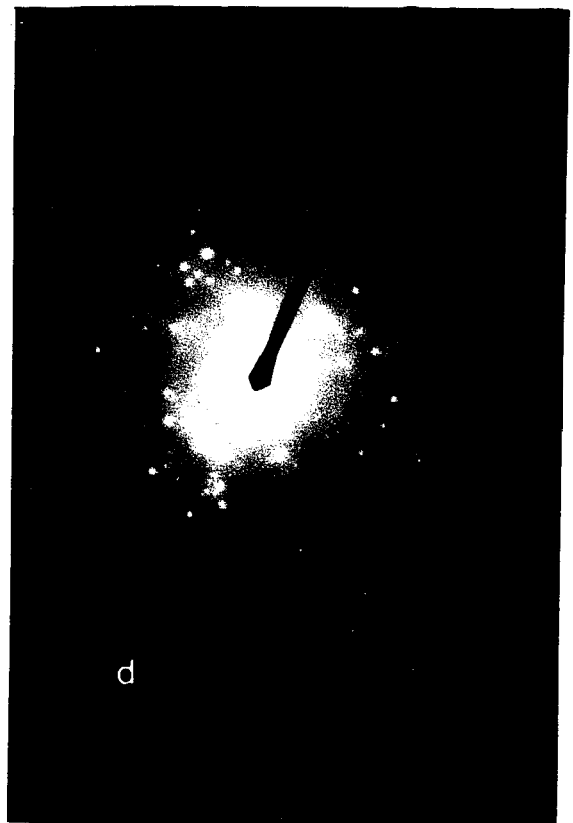
- a. TEM of Single-Beam Furnace Cooled Film
- b. SAD of Single-Beam Furnace Cooled Film
- c. TEM of Single-Beam Quenched Film
- d. SAD of Single-Beam Quenched Film



b



2 μm



d

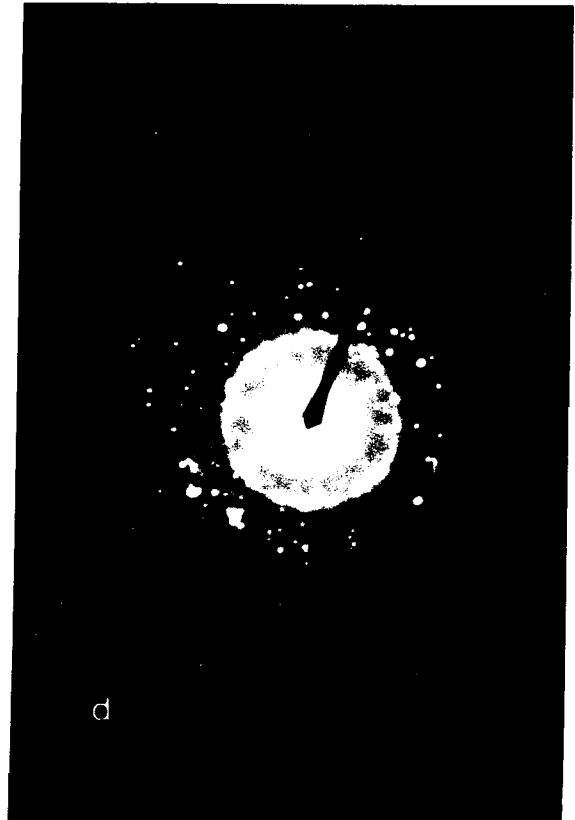
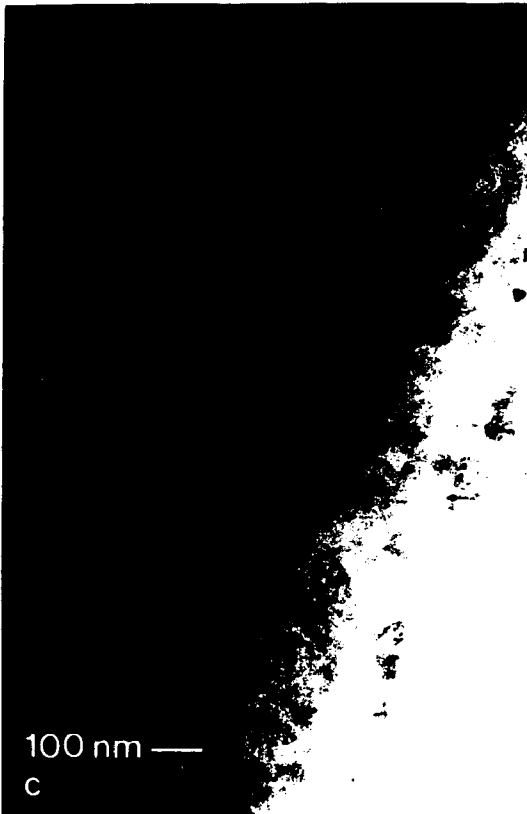
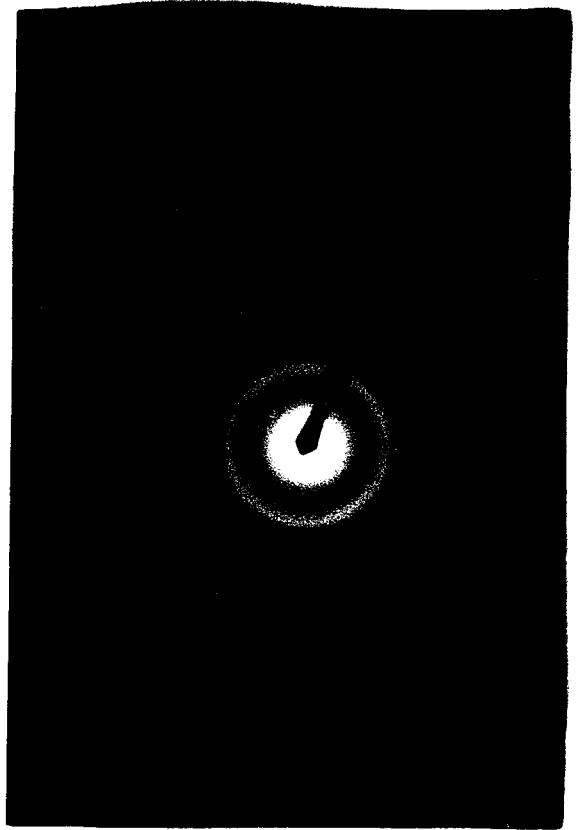
for the 113 direction, and 2.040 \AA for the 400 direction. The reported d-spacings for β - whitlockite or tricalcium phosphate more closely matched the measured values from the film. The d-spacing for the 012 direction is 8.15 \AA . The d-spacing for the 324 direction is 2.023 \AA , and the d-spacing for the 232 direction is 2.061 \AA .

Films sputter deposited onto NaCl crystals were not hot isostatically pressed because it was not possible for the substrate to withstand the high temperature and pressure process environment without deterioration. Additionally, the hypothesis concerning hot isostatic pressing was that it would promote diffusion between the coating and the titanium substrate. Transmission electron microscopy of HIP'ed films on NaCl would not have added appreciable information concerning this hypothesis. However, since a crystalline structure was discovered in films annealed in air at 600°C , it was expected that these films would be crystalline, also.

Figure 23 shows TEM micrographs and SAD patterns of DBFC and DBQ specimens. Dual-beam annealed films were also crystalline at first analysis, and recrystallization frequently occurred under the 200 keV electron beam. Comparison of Figures 23a and 23c shows a finer grain structure for the dual-beam furnace cooled specimen. The grain size for the dual-beam quenched specimens was approximately $2 \text{ }\mu\text{m}$ in diameter, while the furnace cooled specimens were about half that. The large dark square or hexagonal grains shown in Figure 23c are salt crystals remaining from the single crystal NaCl substrate. The shape

Figure 23. TEM-SAD of Dual-Beam Furnace Treated Films

- a. TEM of Dual-Beam Furnace Cooled Film**
- b. SAD of Dual-Beam Furnace Cooled Film**
- c. TEM of Dual-Beam Quenched Film**
- d. SAD of Dual-Beam Quenched Film**



and SAD pattern for the cubic salt crystals were so distinctly different from the crystal structure of the coating that they were easily distinguished. Additionally, the presence of sodium and chlorine was evident in the EDS analyses of these areas.

Bond Strength Test

Z-Axis bond strength tests were performed using the Sebastian Five thin film bond strength apparatus. Pull studs were fixed to the coated Ti disks by means of a special heat cured epoxy. They were then placed in the Sebastian and pulled at a rate of 5 Kg/sec. The force necessary for separation from the substrate was measured. Figure 24 is a histogram showing the bond strengths for each of the eight test categories. Single-beam as-sputtered specimens exhibited the highest average interfacial bond strength of 47.28 MPa. This was followed by the dual-beam as-sputtered specimens with an average interfacial bond strength of 38.67 MPa. In each of the categories, the dual beam specimens exhibited lower bond strengths. The coatings on the heat treated specimens were also less adherent than the as-sputtered specimens.

Single-beam quenched specimens had an average bond strength of 29.57 MPa and the dual-beam quenched specimens averaged 27.79 MPa. The bond strength data collected on the furnace cooled group were still lower than the quenched group. Single-beam furnace cooled specimens averaged 11.48 MPa, while the dual-beam furnace cooled group had an average bond strength of only 8.67 MPa. The hot isostatically

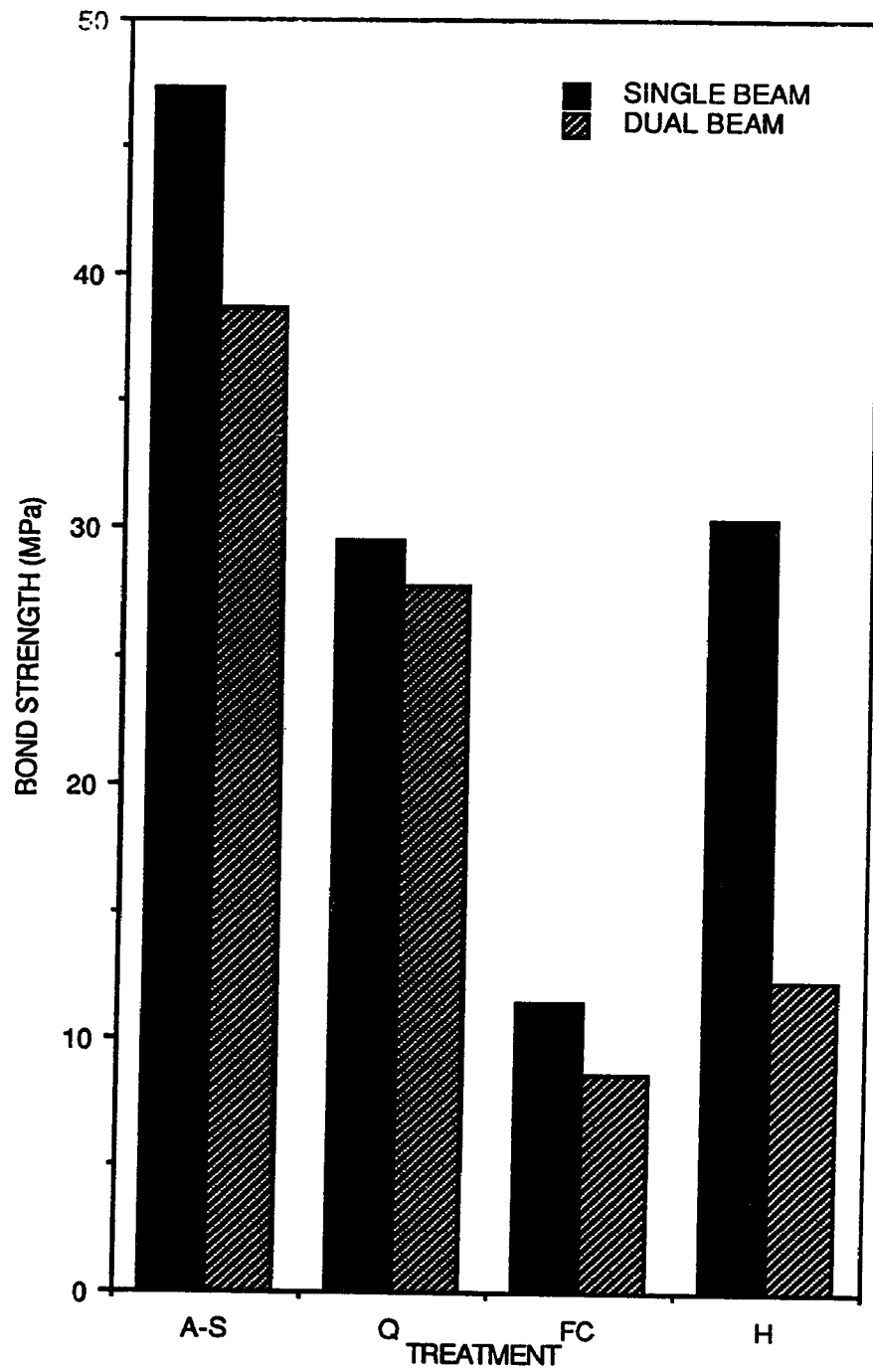


Figure 24. Coating Bond Strength

pressed specimens did not completely follow this trend. Although the bond strength average for the DBH specimens was rather low at 12.241 MPa, the SBH specimens had a much higher average interfacial bond strength of 30.37 MPa.

TABLE 3

Average Bond Strength Values and Statistics	
Group	Mean (MPa)
SBAS	47.28
DBAS	38.67
SBH	30.37
SBQ	29.57
DBQ	27.79
DBH	12.24
SBFC	11.48
DBFC	8.67

Duncan's multiple range test was performed on the bond strength data to determine the level of significance of the differences seen in the data groups. Table 3 is a grouping of the bond strength means according to significance at a confidence interval of 95%. The vertical lines to the right of the means join those data that the test determined were not statistically different from one another. The test indicated a significant difference between the SBAS and DBAS bond strength means. However, there was no significant difference between the SBFC and the DBFC specimens, nor was there any meaningful difference between the SBQ and DBQ groups.

The furnace cooled and quenched groups were also significantly different from one another. The SBQ bond

strength means were statistically different from the DBQ means. In fact, the SBH means fell into the same range as the means of the quenched specimens, while the DBH means were grouped with the furnace cooled samples.

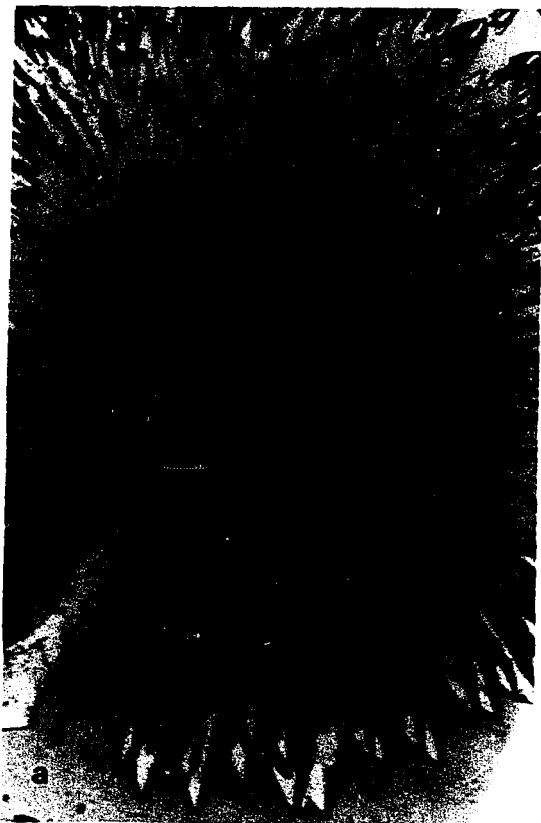
Figure 25 includes a series of reflected light photomicrographs which illustrate the types of interfacial bond failures found in the coating bond strength tests. Figure 25a shows a failure at the interface between the coating and the titanium with fracture lines radiating out from the center of the fracture zone. This type of failure was characteristic of all the as-sputtered specimens, whether they were single-beam or dual-beam deposited. The dark material in the center of the photograph is residual epoxy from the pull stud. Energy dispersive spectroscopy of the fracture site performed in the SEM showed that in many regions of the fracture area the coating was removed completely. Figure 25b shows a failure which occurred within the coating itself. This type of failure was typical of the quenched specimens. Although EDS still picked up amounts of calcium and phosphorus within the fracture zone, it also detected significantly more titanium in this region than in the area outside the fracture.

The furnace cooled specimens generally failed as shown in Figure 25c. These coatings exhibited the lowest bond strength of all the groups. The failure always occurred through the coating/substrate interface. Occasionally, the center of the fracture zone failed at the epoxy/coating interface leaving a region in the center of these specimens

undisturbed. The fracture zone extended from the perimeter of this area out to the edge of the pull stud. In most of the furnace cooled specimens, only small traces of the coating constituents could be detected by EDS in the fracture region. This area was essentially stripped bare to the titanium. The DBH specimens nailed by much the same mode as the furnace cooled specimens.

Figure 25d shows the failure site of an SBH specimen. These samples failed by a combination of the three previous modes. A center region of coating material was occasionally left intact with fracture lines radiating out from that area toward the periphery. The fracture area still contained up to 50% of the coating material as determined by EDS, indicating a failure through the coating.

Figure 25. Photomicrographs of Bond Test Fractures



CHAPTER V.

DISCUSSION

The primary objective of this study was to determine if thin adherent crystalline calcium phosphate coatings could be produced on titanium by ion-beam sputter deposition. Bioactive calcium phosphate coatings have the potential for developing a bond to bone and could, therefore, be instrumental in improving the short-term and long-term fixation of metallic implant systems in dentistry and orthopaedics. Additionally, these coatings may reduce the release of possibly harmful metallic ions from the implant into the surrounding tissues.

Ion-beam sputter deposited coatings produced from complex oxides such as hydroxylapatite at low substrate temperatures are frequently amorphous in the as-sputtered state (Naito et al. 1987; Solnick-Legg and Legg 1989; Yamauchi et al. 1988). All as-sputtered films in this study, whether deposited by single-beam or dual-beam methods, were amorphous when imaged by transmitted electron microscopy and analyzed by selected area diffraction. This confirmed the hypothesis that sputtered particles arriving on the substrate surface did not possess the energy necessary to diffuse across the surface to low energy

nucleation sites and form crystals. Combining this information with the results from EDS and the Auger depth profiles which showed the presence of Ca, P, and O in the film demonstrated that the SBAS films were amorphous calcium phosphate.

Based on the Auger and EDS data, phosphorus appears to be very sensitive to migration under an ion beam. It does not obey the requirement that all the primary constituents of a compound must remain stable in order for stoichiometry to be preserved under ion-beam sputtering. Under the ion-beam bombardment most of the phosphorus in the HA target appears to diffuse out of the surface, leaving the target calcium enriched.

Although the ion-beam assisted deposition process should have been instrumental in supplying the additional energy needed for diffusion to form crystals, it did not under the range of processing variables used in this study. This was probably due to the low ion density (5.0 mA) used for dual-beam bombardment which was intended to minimize resputtering of the depositing coating. An increase in ion current which reflects an increase in ion density could possibly have provided the additional energy necessary to produce an as-sputtered crystalline coating.

The heating of the films by the TEM electron beam was sufficient to produce localized crystal formation in the amorphous single-beam and dual-beam as-sputtered films. These crystals were smaller than those seen in the furnace treated films and the resultant SAD pattern was more

diffuse, indicating some amorphous material remained. However, the heating was not as long in duration within the TEM as it was in the furnace. Such a quick conversion indicated that crystal transformation in these films did not require a great deal of energy.

Other investigators have reported the conversion of amorphous ion-beam deposited films to crystallinity using post-deposition heat treatments. Yamauchi et al. sputter deposited $\text{Ba}_2\text{Si}_2\text{TiO}_8$ films which were stoichiometrically correct but largely amorphous. The authors annealed their films at 750°C for ten hours. Crystals did develop due to the annealing, but the resultant SAD patterns showed only a few bright spots within widely diffuse rings. This indicated that a great deal of amorphous material remained within the film (Yamauchi et al. 1988).

Naito et al. produced films from $\text{YBa}_2\text{Cu}_3\text{O}_7$ which were not correct in composition or structure in their as-sputtered state. The films were enriched in Y, Ba, and Cu but deficient in oxygen and only partially crystalline. The authors were not able to achieve the super-conducting phase they were trying to produce without subsequently annealing the films at $650\text{--}850^\circ\text{C}$ for up to nine hours (Naito et al. 1987).

Annealing at 600°C was performed in this study to try to achieve crystallinity in the amorphous as-sputtered films. Since cooling rate can have an effect on crystal size and the amount of material transformed from amorphous to crystalline, some samples were allowed to cool over 4 1/2

hours within the furnace while other specimens were quenched from the annealing temperature. Following quenching these coatings were examined by light microscopy and scanning electron microscopy to check for cracking or coating delamination. All the coatings were found to be intact following quenching, and no delamination from the substrate was noted. This was a qualitative indicator of the high adhesive strength of the sputter deposited coatings.

The TEM micrographs and SAD patterns shown in Chapter IV demonstrated that the heat treatment followed by either cooling rate was successful in producing crystallinity in both the single-beam and dual-beam films. The difference in grain size seen in the TEM micrographs of furnace cooled and quenched films could have been due to a phase transformation to which the furnace cooled specimens were subjected and the quenched specimens were not. However, the $\text{CaO-P}_2\text{O}_5$ does not have a transformation at 600°C or below under normal conditions. It is more likely that the difference was an artifact due to the continued grain growth experienced by the films under the TEM electron beam.

Resolvable single crystal SAD patterns were only achieved in the single-beam furnace cooled films. Such patterns could have been possible with the other crystalline films, but just as in the as-sputtered films, the 200 keV electron beam produced continued grain growth and, consequently, continually changing patterns. The single crystal SAD patterns, as such, were not always stable enough to successfully photograph.

Two of the three resolved d-spacings shown in Figure 23b matched β -whitlockite, also known as tricalcium phosphate (TCP), a naturally occurring calcium phosphate compound found in the body. The largest d-spacing from the film missed a complete indexing of β -whitlockite by just over 3%. Distortion of lattice dimensions is not unexpected in ion-beam sputter deposited films. Sputter deposited films frequently have a very high defect density. Ziemann and Kay reported lattice distortions of a few per cent in sputter deposited palladium films (Ziemann and Kay 1983).

Analysis of the EDS data indicated that the entire film could not have been tricalcium phosphate because it did not contain enough phosphorus to combine with all the calcium present to form only TCP. If all the phosphorus present in the films did combine with the calcium to form TCP then the remainder of the coating had to be CaO, presuming calcium and oxygen were the only remaining elements left in the coating.

Ducheyne et al. recently reported that plasma spraying can transform hydroxylapatite into a mixture of tetracalcium phosphate and α - and β -tricalcium phosphate. This alteration can greatly affect the mechanical and materials properties of the coating because the chemical reactivity of the transformed materials is higher than that of the hydroxylapatite starting material. The formation of tetracalcium phosphate was not likely in the sputter deposited films because the largest resolved d-spacing of 7.90 Å in the films was more than twice the largest

published d-spacing of tetracalcium phosphate (Ducheyne et al. 1988).

Tricalcium phosphate has been used in many dental applications and some orthopaedic ones (Chae et al. 1988). Since TCP can be resorbable in the body, it has mainly been used as a temporary scaffold material until natural bone could develop to replace it. A resorbable material such as TCP can serve as one localized supply of calcium and phosphorus which is needed for developing new bone. However, at a thickness of less than 2 μm , resorption of these films would probably occur too quickly to be of functional value.

Although the films used in the TEM and SAD studies to determine crystallinity were not deposited onto titanium, comparison with the results for the Auger data indicated that the heat treatments were also effective in producing crystallinity in these coatings. Based on the equivalent argon milling rates determined in the Auger for the SBAS and DBAS specimens, the structures of the as-sputtered coatings would appear to be very similar. As reported by Harper, Cuomo, and Kaufman, milling rate can be indicative of the structure and composition of the material being sputtered (Harper, Cuomo, and Kaufman 1982). These authors have reported that an element bound in a compound sputters more slowly than the single element. Energy from the incident ion beam must be used to overcome the molecular bonds of the compound in addition to the binding energy of the surface.

The argon milling rate for the heat treated specimens, SBFC and SBQ, was not equivalent to that of the as-sputtered material, even though the film thicknesses were similar. This indicated that the structure of the annealed films was not the same as the as-sputtered films. The analyses presented in Figures 12 and 13 showed that it required a longer sputtering time or more sputtering cycles to reach the interface of the SBFC and SBQ specimens than it did for the SBAS specimen. It required approximately 200 cycles to reach the interface of the SBFC specimen and around 300 cycles to reach the SBQ interface. This was an indication that the 600°C annealing cycle did produce a structural change in the single-beam deposited coatings. Although the annealed dual-beam coatings had a somewhat slower sputter rate than the DBAS coating, it was not as dramatic a difference as that seen in single-beam deposited coatings. This difference was most likely due to the inclusion of a small percentage of argon in the dual-beam deposited coatings which would reduce with the density of the coatings.

The transition between the coating and the substrate was also not as sharply defined in the annealed specimens as it was in the as-sputtered ones. The rate of increase of titanium at the interface was broader in the furnace treated specimens with increased oxygen content at the interface. A slump or slowing in the rate of titanium increase occurred in all the annealed specimens at the same time as the oxygen level increased in the interface region. This would seem to

suggest that the oxygen in the interface is present locally as a titanium oxide. The broad oxygen peak at the interface of the quenched specimens would suggest that the oxygen was more widely dispersed in the SBQ and DBQ specimens than in the furnace cooled specimens. A sharp oxygen peak was observed at the interface of the SBFC and DBFC specimens. The slow cooling rate used for the furnace cooled specimens allowed oxygen to diffuse out of the titanium and concentrate at the interface. Since the amount of oxygen relative to the amount of calcium within the coating thickness was the same in all Auger depth profiles regardless of the post-deposition treatment, it was not thought that the increase in oxygen in the interface was due to the absorption of oxygen from the coating. It is likely that the heat treatments produced an overall oxygenation of the coatings and the substrate material as titanium has a very strong affinity for oxygen.

The behavior of phosphorus during Auger analysis was consistent in all specimens. The level of this element was always very low throughout the depth of the coating profile, only increasing as the analysis neared the interface with the titanium substrate. Since phosphorus has a low order Auger transition and therefore a low relative sensitivity factor, it was not thought that this represented a depletion of phosphorus in the coating or an actual increase in phosphorus content near the interface (Jeol 1982). Phosphorus appeared to migrate in advance of the Auger signal until the profile reached the titanium interface. A

peak formed in the region of the interface apparently because the phosphorus could not migrate into the titanium. The AES profile of the stoichiometrically correct target material shown in Figure 11 supported this. Analysis of the coatings using energy dispersive spectroscopy also supported this concept. Data provided in Table 3 showed that although the phosphorus level in all the coatings was below the ideal ratio of 1.67 in the target, it was not as low as that shown in the AES profiles.

Auger analyses of the SBH specimens were similar to the other specimens through the coating depth. Phosphorus readings were still very low in the coating with a slight increase just prior to the interface; however, these specimens had a second stronger phosphorus peak within the near-surface volume of the titanium. This suggested that in this instance Ti-phosphides were formed. Additionally, EDS analysis of the SBH coatings showed a Ca/P ratio of 4.08, which was 60% higher than the other single-beam as-sputtered or annealed coatings. This indicated a real diffusion of phosphorus out of the coating. The SBH coatings also exhibited much higher bond strengths than the DBH coatings, which did not show a diffusion of phosphorus into the titanium. The SBH coatings were also more adherent than either SBFC or DBFC coatings. This was further evidence that a chemical bond was developed between the coating and the substrate due to the formation of Ti-phosphides. Ducheyne and Van Raemdonck noted a similar shifting of phosphorus in their AES studies of electrophoretically

deposited hydroxylapatite (Ducheyne et al. 1986; Van Raemdonck, Ducheyne, and De Meester 1984). Following electrophoretic deposition onto Ti substrates, the authors sintered their coatings at 900°C and 5 MPa or at 950°C and 100 MPa. They were unable to identify the nature of the Ti-phosphide formed due to a continual change in structure and composition through the depth of the interface region.

The carbon contamination seen in the SBH and DBH specimens was probably not as deep as the depth profiles indicated, since carbon atoms are known to recondense rather quickly after being sputtered away, even in an AES vacuum. Erroneously high carbon values would be due to the continued reanalysis of the same carbon as it reformed on the surface during successive analysis cycles.

Energy dispersive spectroscopy indicated that overall the dual-beam coatings were more deficient in phosphorus than the single-beam coatings. Since the energy or heat from the primary ion beam was sufficient to cause phosphorus to diffuse away from the surface of the target, leaving it depleted of this element, it is also likely that the secondary ion beam caused the same diffusion and preferential sputtering of phosphorus from the coating. Only the DBQ specimens listed in Table 2 had Ca/P ratios in the same range as the single-beam specimens. Examination of the deposition process records for these films shows that the control parameters for the secondary ion beam malfunctioned during this production run. These coatings were ion bombarded at 430 V and 15 mA instead of 700 V and 5

mA. This indicated that lower ion energy and higher ion density minimized the resputtering of phosphorus from the coating during ion-beam assisted deposition.

Although the heat treatments were successful at producing crystallinity in the films, they were not beneficial to the coating bond strength. As was shown in Figure 25 and Table 3, the quenched specimens had lower bond strengths than the as-sputtered specimens, while the furnace cooled specimens had still lower bond strengths. The DBH specimens had bond strengths in the same range as the furnace cooled specimens. With the exception of the SBH coatings, bond strengths deteriorated with increased time of exposure to high temperature. This loss of bond strength due to annealing was most likely due to the reduction of the compressive intrinsic stress inherent in most ion-beam sputter deposited coatings. Compressive intrinsic stress would be beneficial to the interfacial bond strength of a ceramic material such as this coating since ceramics are generally stronger in compression. The oxygen increase was more widely dispersed throughout the region between the coating and the substrate in the SBQ and DBQ specimens. This may have been responsible for the higher bond strengths exhibited by the quenched specimens. Additionally, the higher concentration of oxygen in the interface of the furnace cooled specimens was most likely responsible for the weakening of this interface, resulting in lower bond strengths for the SBFC and DBFC samples.

The bond strength values of the single-beam as-sputtered coatings were found to be significantly different from the values of the dual-beam as-sputtered coatings. Although the differences between the single-beam and dual-beam coatings were not statistically significant in the quenched and furnace cooled categories, the dual-beam coatings had lower average bond strengths in each group. This was most likely due to the reduction of compressive intrinsic stress in the dual-beam coatings. Ion-beam assisted deposition has been shown to reduce or modify the intrinsic stress of sputter deposited thin films (Roy et al. 1989). The inclusion of entrapped argon in the dual-beam deposited films could also have contributed to their lower bond strengths.

Filiaggi and Pilliar have recently reported bond strength testing of plasma sprayed HA on a grit-blasted titanium alloy substrate (Filiaggi and Pilliar 1989). The authors found an average tensile bond strength of 6.7 MPa with all failures occurring in the ceramic/metal interface. This result was considerably lower than the 40 MPa tensile bond strength values reported by Kay (Kay 1988). Filiaggi and Pilliar suggested the differences could be ascribed to the penetration of the adhesive into the pores of the other plasma sprayed coatings. This was a situation which Filiaggi and Pilliar carefully avoided. These investigators also subjected the plasma sprayed coatings to a 960°C heat treatment followed by controlled cooling to determine if this would promote diffusion bonding to enhance the tensile

strengths. A considerable improvement was noted. Subsequent bond strengths ranged from 15.0 MPa to 26.0 MPa. Energy dispersive spectroscopy and secondary ion mass spectroscopy indicated at least partially that the improvement in bond strength was due to enhanced diffusion bonding at the ceramic/metal interface.

These values compared favorably with the bond strengths of the sputter deposited coatings. The as-sputtered coatings in this study were at least as adherent as the highest values published for plasma sprayed hydroxylapatite. However, the sputter deposited films were produced on polished surfaces as opposed to grit blasted ones. The rougher substrate surfaces would be responsible for some additional mechanical interlocking between the plasma sprayed coating and its substrate. Additionally, the sputter deposited films were not porous, so there could be no penetration of the epoxy on the pull studs to the titanium substrate.

Summary

In summation, ion-beam sputter deposition produced amorphous randomly oriented thin films of calcium and phosphorus. In comparison to the HA target material, these coatings were deficient in phosphorus and enriched in calcium. Ion-beam assisted deposition, used by many investigators to alter the crystal structure of depositing thin films, was not beneficial in producing as-sputtered crystalline films. The coatings produced by this method were even more deficient in phosphorus than the single-beam

coatings because of preferential phosphorus sputtering from the secondary ion beam.

A furnace heat treatment at 600°C was successful at converting the sputter deposited films to crystallinity. Resolved d-spacings from the SBFC specimen were a relatively close match to the published values for -TCP. Some lattice distortion was not unexpected because of the high defect density of sputter deposited films. No real difference was seen in the TEM micrographs between the quenched and furnace cooled specimens except what appeared to be a smaller grain size in the furnace cooled specimens; however, since recrystallization and grain growth continued to occur in the TEM during the examination, this difference could be ascribed to artifact. The bond strengths of the quenched specimens were significantly higher than the bond strengths of the furnace cooled specimens, which was probably due to the complete annealing of the intrinsic stress from the furnace cooled specimens.

The heat treatment also produced a diffusion of oxygen to the coating/titanium interface. No diffusion of the other HA constituents was apparent from the heat treatment alone. Hot isostatic pressing, however, did promote the diffusion of phosphorus into the near-surface volume of the titanium substrate, leading to the formation of Ti-phosphides. This diffusion was also apparent in the increased bond strengths exhibited by these specimens.

CHAPTER VI.

CONCLUSIONS

Bioactive coatings of calcium phosphate on dental and orthopaedic implants offer an alternative to current methods of implant fixation. A slowly reactive coating of a calcium phosphate such as hydroxylapatite may bond directly with living bone, forming a stronger and more biocompatible implant/tissue interface than is available through more traditional methods of implant fixation. A more rapidly reactive material such as tricalcium phosphate, ideally, will resorb and become incorporated into new bone as it develops adjacent to the implant. Work has continued on the development of processes to apply bioactive coatings to implant surfaces which do not adversely affect the bioactive nature of the material to be applied and which do not produce detrimental metallurgical changes in the implant substrate. At the same time the coating must have exceptional bond strength to the implant in order to withstand the interfacial shear and tensile forces it must endure in the body.

Four conclusions based on the original hypotheses of this study are as follows:

1. The coatings produced on titanium substrates by ion-beam sputter deposition for this study were composed of

amorphous calcium phosphate. Preferential sputtering of phosphorus resulted in calcium-rich, phosphorus-depleted coatings.

2. Argon ion-beam assisted deposition did not provide the additional energy needed to produce as-sputtered crystalline calcium phosphate coatings. Additionally, the process resulted in argon entrapment in all coatings produced in this manner.
3. Post-deposition heat treatments at 600°C were successful in supplying the energy needed to transform the amorphous coatings into crystalline β -tricalcium phosphate and CaO. The heat treatment also increased the level of oxygen at the coating/titanium interface, forming titanium oxide. Cooling rate had no apparent effect on the amorphous to crystalline transformation.
4. Ion-beam sputter deposition produced very adherent amorphous coatings which compared very favorably with the published bond strength data for plasma sprayed hydroxylapatite coatings. Ion-beam assisted deposition lowered the bond strength of the coatings because it reduced the beneficial compressive stresses responsible for good adhesion in ceramic sputter deposited coatings. The heat treatments also annealed the intrinsic stress from the coating, further reducing the bond strength of the coatings. Hot isostatic pressing produced a diffusion of phosphorus into the titanium, forming titanium phosphides. Although diffusion led to increased chemical bonding between the coating and the

substrate, the diffusion process further depleted the coating of phosphorus.

Ion-beam sputter deposition did not produce the form of bioactive calcium phosphate desired in this study; however, the process shows great promise. By controlling process variables such as target material, substrate temperature, and ionizing gas, a slowly reactive biocompatible coating could be produced using ion-beam sputter deposition.

CHAPTER VII.

RECOMMENDATIONS

In order for a 1-2 μm bioactive coating to be successful as an aid to implant fixation, it must be a less soluble form of calcium phosphate than what has been developed here. A major point of development for future work must be the production of the correct stoichiometry of the coating material. A method of retaining the hydroxyl group or restoring it to the sputtered coating must be devised if the more slowly active form of calcium phosphate, hydroxylapatite, is to be coated in this manner. Even hydroxylapatite, though, might be completely resorbed within a year in vivo at coating thicknesses which are practicable by ion-beam sputter deposition. Perhaps the most beneficial coating produced by this method is one that would be reactive at its surface but nearly insoluble through the depth to the substrate. By altering the deposition parameters and target materials, such a coating could possibly be developed by ion-beam sputter deposition. The following are suggested areas of research for the future.

1. The substrate stage should be heated to provide sufficient energy for surface diffusion of the sputtered particles as they arrive on the substrate.

As-sputtered crystalline coatings could be produced using a heated substrate.

2. Reduction of the incident ion-beam energy could possibly limit the diffusion of phosphorus from the target surface and, therefore, reduce the preferential sputtering of this element. According to Thornton, the incident ion beam can be reduced to as low as 600 eV without seriously lowering the sputter deposition rate (Thornton 1982a). However, such a reduction in energy has been shown to be beneficial in reducing preferential sputtering in alloys and compounds where this is a problem. Reduction of the ion-beam energy used in the IBAD process will also reduce the resputtering of phosphorus caused by this method.
3. The use of other target materials, perhaps with higher phosphorus content, should be investigated in order to control the final chemistry of the coating.
4. Ion-beam assisted deposition using reactive gases such as oxygen should also be investigated as a method of controlling the final chemistry of the coating.
5. Other post-deposition treatments should be investigated which would convert the TCP and CaO found in this study to a less soluble form of calcium phosphate. Tricalcium phosphate and CaO have been shown to react to form HA in the presence of humid air at 1000°C; however, the process is a slow one and would subject the substrate to a metallurgically detrimental temperature (Bonel et al. 1988).

6. Additional SAD studies should be performed on the ion-beam sputter deposited films using a liquid nitrogen cooled specimen stage to try to control electron beam induced grain growth.
7. Investigations should be performed on sputter coated titanium specimens using TEM to more fully characterize the interface between the calcium phosphate coating and the titanium substrate. Such a study could provide information on the diffusion mechanisms of oxygen and phosphorus during heat treatments.

LIST OF REFERENCES

- Bachman, P.K.; Gartner, G.; and Lydtin, H. (1988): Plasma-Assisted Chemical Vapor Deposition Processes, Materials Research Society Bulletin, 13:52-59.
- Beirne, O.R.; Curtis, T.A.; and Greenspan, J.S. (1986): Mandibular Augmentation with Hydroxyapatite, Journal of Prosthetic Dentistry, 55:362-367.
- Besmann, T.M.; Stinton, D.P.; and Lowden, R.A. (1988): Chemical Vapor Deposition Techniques, Materials Research Society Bulletin, 13:45-50.
- Blocher, J.M. (1982): Chemical Vapor Deposition. In: Deposition Technologies for Films and Coatings, R.F. Bunshah, Ed., Park Ridge, N.J.: Noyes Publications, pp. 335-364.
- Bonel, G.; Heughebaert, J.-C.; Heughebaert, M.; Lacout, J.L.; and Lebugle, A. (1988): Apatitic Calcium Orthophosphates and Related Compounds for Biomaterials. In: Bioceramics: Material Characteristics Versus In Vivo Behavior, P. Ducheyne and J.E. Lemons, Eds., New York: The New York Academy of Sciences, pp. 115-130.
- Bonfield, W. (1988): Biomechanical Stability and Design: Strength. In: Bioceramics: Material Characteristics Versus In Vivo Behavior, P. Ducheyne and J.E. Lemons, Eds., New York: The New York Academy of Sciences, pp. 287-291.
- Bunshah, R.F. (1982a): Deposition Technologies: An Overview. In: Deposition Technologies for Films and Coatings, R.F. Bunshah, Ed., Park Ridge, N.J.: Noyes Publications, pp. 1-18.
- Bunshah, R.F. (1982b): Evaporation. In: Deposition Technologies for Films and Coatings, R.F. Bunshah, Ed., Park Ridge, N.J.: Noyes Publications, pp. 83-169.
- Bunshah, R.F. and Deshpandey, C.V. (1988): Evaporation Processes, Materials Research Society Bulletin, 13:33-39.

- Busemi, P. and Hench, L.L. (1978): An Immersion Process for Coating Metal Implants with Bioglass. An Investigation of Bonding Mechanisms at the Interface of a Prosthetic Material. Contract No. DAMD 17-76-C-6033. Supported by the U.S. Army Medical Research and Development Command, Washington, D.C., pp. 55-61.
- Carosella, C.A.; Hubler, G.K.; Van Vechten, D.; and Donovan, E.P. (1989): $B_{(1-x)}N_x$ Alloy Films Prepared by Ion Beam Assisted Deposition. In: Processing and Characterization of Materials Using Ion Beams, L.E. Rehn, J. Greene, and F.A. Smidt, Eds., Pittsburgh: Materials Research Society, pp. 79-84.
- Chae, J.C.; Collier, J.P.; Mayor, M.B.; and Suprenant, V.A. (1988): Efficacy of Plasma-Sprayed Tricalcium Phosphate in Enhancing the Fixation of Smooth Titanium Intramedullary Rods. In: Bioceramics: Material Characteristics Versus In Vivo Behavior, P. Ducheyne and J.E. Lemons, Eds., New York: The New York Academy of Sciences, pp. 81-90.
- Chang, A.L. and Kant, R.A. (1989): Characterization of TiN Films Prepared by Ion Beam Assisted Deposition. In: Processing and Characterization of Materials Using Ion Beams, L.E. Rehn, J. Greene, and F.A. Smidt, Eds., Pittsburgh: Materials Research Society, pp. 433-438.
- Cook, S.D.; Kay, J.F.; Thomas, K.A.; and Jarcho, M. (1987): Interface Mechanics and Histology of Titanium and Hydroxylapatite-Coated Titanium for Dental Implant Applications, The International Journal of Oral and Maxillofacial Implants, 2:15-22.
- Cook, S.D.; Thomas, K.A.; Kay, J.F.; and Jarcho, M. (1988): Hydroxyapatite-Coated Titanium for Orthopedic Implant Applications, Clinical Orthopaedics and Related Research, 232:225-243.
- Cuomo, J.J. (1986): Synthesis by Reactive Ion Beam Deposition. In Ion Plating and Implantation, Applications to Materials, R.F. Hochman, Ed., Atlanta: American Society for Metals, pp. 25-30.
- Davies, J.P. and Harris, W.H. (1989): Severe Weakness of Bone Cement Retrieved After In Vivo Service in Man. In: Transactions of the 15th Annual Meeting of the Society for Biomaterials, Society for Biomaterials, April 28-May 2, 1989, p. 52.
- de Groot, K.; Geesink, R.G.T.; Wolke, J.G.C.; and Klein, C.P.A.T. (1988): Plasma Sprayed HA Coatings on Metallic Implants. In: Transactions of the Third World Biomaterials Congress, 11:306.

- de Putter, C.; de Groot, K.; and Sillevius Smitt, P.A.E. (1982): Implants of Dense Hydroxylapatite in Prosthetic Dentistry. In: Clinical Applications of Biomaterials, A.J.C. Lee, T. Albrektsson, and P.-I. Branemark, Eds., New York: John Wiley and Sons, pp. 123-132.
- Deutchman, A.H. and Partyka, R.J. (1989): Diamond-Film Deposition: A Gem of a Process, Advanced Materials and Processes, 135:29-33.
- Donovan, E.P.; Carosella, C.A.; and Van Vechten, D. (1989): Thermal Annealing Investigation of the Optical Properties of $Si_{1-x}N_x$ Films Fabricated by Ion Beam assisted Deposition. In: Processing and Characterization of Materials Using Ion Beams, L.E. Rehn, J. Greene, and F.A. Smidt, Eds., Pittsburgh: Materials Research Society, pp. 501-506.
- Driessens, F.C.M. (1988): Physiology of Hard Tissues in Comparison with the Solubility of Synthetic Calcium Phosphates. In: Bioceramics: Materials Characteristics Versus In Vivo Behavior, P. Ducheyne and J.E. Lemons, Eds., New York: The New York Academy of Science, pp. 131-136.
- Ducheyne, P. (1985): Bioglass Coatings and Bioglass Composites as Implant Materials, Journal of Biomedical Materials Research, 19:273-291.
- Ducheyne, P.; Cuckler, J.M.; Radin, S.; Healy, K.E.; and Nazar, E. (1988): Bioactive Calcium Phosphate Ceramic Linings on Porous Metal Coatings for Bone Ingrowth. In: Transactions of the Third World Biomaterials Congress, 11:309.
- Ducheyne, P.; Van Raemdonck, W.; Heughebaert, J.C.; and Heughebaert, M. (1986): Structural Analysis of Hydroxyapatite Coatings on Titanium, Biomaterials, 7:97-103.
- Feenstra, L. and de Groot, K. (1983): Medical Use of Calcium Phosphate Ceramics. In: Bioceramics of Calcium Phosphates, K. de Groot, Ed., Boca Raton, Fla: CRC Press, pp. 131-142.
- Filiaggi, M.J. and Pilliar, R.M. (1989): Interfacial Characterization of a Plasma-Sprayed Hydroxyapatite/Ti-6Al-4V Implant System. In: Transactions of the Tenth Annual Meeting of the Canadian Society for Biomaterials, Vol. 10.
- Ghate, P.B. (1982): Deposition Techniques and Microelectronic Applications. In: Deposition Technologies for Films and Coatings, R.F. Bunshah, Ed., Park Ridge, N.J.: Noyes Publications, pp. 514-548.

- Glang, Reinhard (1970): Vacuum Evaporation. In: Handbook of Thin Film Technology, L.I. Maissel and R. Glang, Eds., New York: McGraw-Hill Book Company, pp. 1.1-1.30.
- Greenwald, A.C.; Hirvonen, J.K.; and Jaggi, N.K. (1989): Ion Beam Deposition of Diamond-Like Carbon. In: Processing and Characterization of Materials Using Ion Beams, L.E. Rehn, J. Greene, and F.A. Smidt, Eds., Pittsburgh: Materials Research Society, pp. 109-112.
- Harper, J.M.E. (1978): Ion Beam Deposition. In: Thin Film Processes, J.L. Vossen and W. Kern, Eds., New York: Academic Press, pp. 175-208.
- Harper, J.M.E.; Cuomo, J.J.; and Kaufman, H.R. (1982): Technology and Applications of Broad-Beam Ion Sources Used in Sputtering. Part II. Applications, Journal of Vacuum Science Technology, 21:737-756.
- Heimke, G. and Griss, P. (1983): Tissue Interactions to Bone Replacement Materials. In: Bioceramics of Calcium Phosphates, K. de Groot, Ed., Boca Raton, Fla.: CRC Press, pp. 79-98.
- Hench, L.L. (1988): Bioactive Ceramics. In: Bioceramics: Material Characteristics Versus In Vivo Behavior, New York: New York Academy of Science, pp. 54-71.
- Herman, H. (1988): Plasma Spray Deposition Processes, Materials Research Society Bulletin, 13:60-67.
- Hirvonen, J-P. and Hirvonen, J.K. (1989): Analysis of Nitrogen, Boron, and Hydrogen of i-BN Films Fabricated by the Ion Beam Assisted Deposition. In: Processing and Characterization of Materials Using Ion Beams, L.E. Rehn, J. Greene, and F.A. Smidt, Eds., Pittsburgh: Materials Research Society, pp. 85-90.
- Huang, T.C.; Lim, G.; Parmigiani, F.; and Kay, E. (1985): Effect of Ion Bombardment During Deposition on the X-Ray Microstructure of Thin Films, Journal of Vacuum Science and Technology, A3:2156-2166.
- Hubler, G.K.; Vanvechten, D.; Donovan, E.P.; and Kant, R.A. (1989): Ion Beam Assisted Deposition of Titanium Nitride. In: Processing and Characterization of Materials Using Ion Beams, L.E. Rehn, J. Greene, and F.A. Smidt, Eds., Pittsburgh: Materials Research Society, pp. 55-60.
- Jaulin, M.; LaPlanche, G.; Delafond, J.; and Pimbert-Michaux, S. (1989): A New Apparatus for Dynamical Ion Beam Mixing. In: Processing and Characterization of Materials Using Ion Beams, L.E. Rehn, J. Greene, and F.A. Smidt, Eds., Pittsburgh: Materials Research Society, pp. 91-100.

- Jeol, Ltd. (1982): Handbook of Auger Electron Spectroscopy, Tokyo: Jeol, Ltd.
- Jiankun, Z.; Xianghuai, L.; Youshan, C.; Zhihong, Z.; Wei, H.; Zuyao, Z.; and Shichang, Z. (1989): Investigation of Titanium Nitride Synthesized By Ion Beam Enhanced Deposition. In: Processing and Characterization of Materials Using Ion Beams, L.E. Rehn, J. Greene, and F.A. Smidt, Eds., Pittsburgh: Materials Research Society, pp. 73-78.
- Jones, D.W. (1988): Coatings of Ceramics on Metals. In: Bioceramics: Materials Characteristics Versus In Vivo Behavior, P. Ducheyne and J.E. Lemons, Eds., New York: The New York Academy of Science, pp. 19-37.
- al-Jumaily, G.A.; Mooney, T.A.; Spurgeon, W.A.; and Dauplaise, H.M. (1989): Properties of Silicon Oxynitride and Aluminum Oxynitride Coatings Deposited Using Ion Assisted Deposition. In: Processing and Characterization of Materials Using Ion Beams, L.E. Rehn, J. Greene, and F.A. Smidt, Eds., Pittsburgh: Materials Research Society, pp. 61-66.
- Kant, R.A.; Dillich, S.A.; Sartwell, B.D.; and Sprague, J.A. (1989): The Causes of Property Variations of IBAD-Titanium Nitride. In: Processing and Characterization of Materials Using Ion Beams, L.E. Rehn, J. Greene, and F.A. Smidt, Eds., Pittsburgh: Materials Research Society, pp. 427-432.
- Kataoka, I.; Yamada, I.; Eto, K.; and Ito, K. (1989): Evaluation of Multilayers for Soft X-Ray Fabricated by Ion Beam Sputtering. In: Processing and Characterization of Materials Using Ion Beams, L.E. Rehn, J. Greene, and F.A. Smidt, Eds., Pittsburgh: Materials Research Society, pp. 513-518.
- Kaufman, H.R. (1978): Technology of Ion Beam Sources Used in Sputtering, Journal of Vacuum Science Technology, 15:272-278.
- Kaufman, H.R. (1984): Fundamentals of Ion-Source Operation, Fort Collins, Colo.: Front Range Research.
- Kaufman, H.R.; Cuomo, J.J.; and Harper, J.M.E. (1982): Technology and Application of Broad-Beam Ion Sources Used in Sputtering. Part I. Ion Source Technology, Journal of Vacuum Science Technology, 21:725-736.
- Kaufman, M.J.; Biancaniello, F.S.; and Kreider, K.G. (1988): The Annealing Behavior of Sputter-Deposited Al-Mn and Al-Mn-Si Films, Journal of Materials Research, 3:1342-1348.

- Kay, J.F. (1988): Bioactive Surface Coating for Hard Tissue Biomaterials. In: Transactions of the Third World Biomaterials Congress, 11:307.
- Kay, J.F.; Jarcho, M.; Logan, G.; and Liu, S.T. (1986): The Structure and Properties of Hydroxylapatite Coatings on Metal, Society for Biomaterials Transactions, 12:13.
- Kay, E.; Parmigiani, F.; and Parrish, W. (1987): Effect of Energetic Neutralized Noble Gas Ions on the Structure of Ion Beam Sputtered Thin Metal Films, Journal of Vacuum Science Technology, A5:44-51.
- Lacefield, W.R. (1988): Hydroxylapatite Coatings. In: Bioceramics: Material Characteristics Versus In Vivo Behavior, P. Ducheyne and J.E. Lemons, Eds., New York: The New York Academy of Science, pp. 72-80.
- Lau, W.M. (1989): Ion Bombardment Effects on GaAs Using 100 eV Nitrogen Ions. In: Processing and Characterization of Materials Using Ion Beams, L.E. Rehn, J. Greene, and F.A. Smidt, Eds., Pittsburgh: Materials Research Society, pp. 695-700.
- Lee, N.L.; Fisher, G.B.; and Schulz, R. (1988): Sputter Deposition of a Corrosion-Resistant Amorphous Metallic Coating, Journal of Materials Research, 3:862-871.
- Legg, K.O. and Solnick-Legg, H. (1988): Ion Beam and Plasma Enhanced Hydroxylapatite Films. In: Ion Implantation and Plasma Assisted Processes, R.F. Hochman, H. Solnick-Legg, and K.O. Legg, Eds., Atlanta: ASM International, pp. 57-62.
- Lichtenwalner, D.J.; Anderson, A.C.; and Rudman, D.A. (1989): Plasma-Activated Ion Beam Reactive Sputtering of NbN Thin Films. In: Processing and Characterization of Materials Using Ion Beams, L.E. Rehn, J. Greene, and F.A. Smidt, Eds., Pittsburgh: Materials Research Society, pp. 67-72.
- Lince, J.R. and Fleischauer, P.D. (1987): Crystallinity of rf-sputtered MoS₂ films, Journal of Material Research, 2:827-838.
- Maissel, L.I. (1970): Application of Sputtering to the Deposition of Films. In: Handbook of Thin Film Technology, L.I. Maissel and R. Glang, Eds., New York: McGraw-Hill Book Company, pp. 4.1-4.44.
- Mattox, D.M. (1982): Adhesion and Surface Preparation. In: Deposition Technologies for Films and Coatings, R.F. Bunshah, Ed., Park Ridge, N.J.: Noyes Publications, pp. 63-82.

- Menis, D.L.; Wixson, R.L.; and Lautenschlager, E.P. (1989): Fatigue of Two Dental Acrylics and Simplex-P Bone Cement. In: Transactions of the 15th Annual Meeting of the Society for Biomaterials, Society for Biomaterials, April 28-May 2, p. 51.
- Miller, I. and Freund, J.E. (1977). Probability and Statistics for Engineers, 2nd edition, Englewood Cliffs, N.J.: Prentice Hall, p. 352.
- Miller, R.A. (1984): Oxidation-Based Model for Thermal Barrier Coating Life, Journal of the American Ceramic Society, 67:517-521.
- Nagakubo, M.; Yamamoto, T.; and Naoe, M. (1989): Soft Magnetism and Morphology of Fe Films by Dual Ion Beam Sputtering. In: Processing and Characterization of Materials Using Ion Beams, L.E. Rehn, J. Greene, and F.A. Smidt, Eds., Pittsburgh: Materials Research Society, pp. 29-34.
- Naito, M.; Hammond, R.H.; Oh, B.; Hahn, M.R.; Hsu, J.W.P.; Rosenthal, P.; Marshall, A.F.; Beasley, M.R., Gabelle, T.H.; and Kapitulnik, A. (1987): Thin-Film Synthesis of the High- T_c Oxide Superconductor $YBa_2Cu_3O_7$ by Electron-Beam Codeposition, Journal of Materials Research, 2:713-725.
- Neugebauer, C.A. (1970): Condensation, Nucleation, and Growth of Thin Films. In: Handbook of Thin Film Technology, L.I. Maissel and R. Glang, Eds., New York: McGraw-Hill Book Company, pp. 8.3-8.44.
- Nowak, W.B.; Levy, M.; and Chang, F. (1986): Ion Plating for Corrosion Control. In: Ion Plating and Implantation: Applications to Materials, R.F. Hochman, Ed., Atlanta: American Society for Metals, pp. 71-74.
- Ogino, M.; Ohuchi, F.; and Hench, L.L. (1980): Compositional Dependence of the Formation of Calcium Phosphate Films on Bioglass, Journal of Biomedical Materials Research, 14:55-64.
- Pantano, Jr., C.G.; Clark, Jr., A.E.; and Hench, L.L. (1974): Multilayer Corrosion Films on Bioglass Surfaces, Journal of the American Ceramic Society - Discussions and Notes, 57:13-14.
- Picha, G.J. and Siedlak, D.J. (1984): Ion-Beam Microtexturing of Biomaterials, MD&DI, April:39-42.
- Riegart, R.P. (1988): Future Physical Testing of Interconnect Technology, Printed Circuit Assembly, 2:5-7.

- Rizzo, H.F.; Echeverria, A.; Massalski, T.B.; and Baxi, H. (1989): Amorphous and Metastable Phase Formation in Systems with Positive Heats of Mixing Using High-Rate Sputter Deposition. In: Processing and Characterization of Materials Using Ion Beams, L.E. Rehn, J. Greene, and F.A. Smidt, Eds., Pittsburgh: Materials Research Society, pp. 231-236.
- Rossnagel, S.M. and Cuomo, J.J. (1988): Ion Beam Deposition, Film Modification and Synthesis, MRS Bulletin, 13:40-45.
- Rossnagel, S.M. and Kaufman, H.R. (1987): Charge Transport in Magnetrons, Journal of Vacuum Science Technology, A5:2276-2279.
- Rossnagel, S.M. and Kaufman, H.R. (1988): Current-Voltage Relations in Magnetrons, Journal of Vacuum Science Technology, A6:223-229.
- Roy, R.A.; Petkie, R.; Yee, D.S.; Karasinski, J.; and Boulding, A. (1989): Stress Modification in Tungsten Films Deposited by Ion-Assisted Evaporation. In: Processing and Characterization of Materials Using Ion Beams, L.E. Rehn, J. Greene, and F.A. Smidt, Eds., Pittsburgh: Materials Research Society, pp. 17-22.
- Sarikaya, M.; Thiel, B.L.; Aksay, I.A.; Weber, W.J. and Frydrych, W.S. (1987): Microstructural Characterization of $\text{YBa}_2\text{Cu}_3\text{O}_{7-x}$, Journal of Materials Research, 2:736-742.
- Seaward, K.L.; Barbee, Jr., T.W.; and Tiller, W.A. (1986): The Synthesis of SiC_x Films by Dual Source Sputter Deposition, Journal of Vacuum Science and Technology, A4:31-37.
- Solnick-Legg, H. and Legg, K. (1989): Ion Beam and Plasma Technology for Improved Biocompatible Surfaces, MRS Bulletin, 14:27-30.
- Taga, Y. and Ohwaki, T. (1989): Effects of Sputtered Particle Energy on the Properties of SiO_2 Films. In: Processing and Characterization of Materials Using Ion Beams, L.E. Rehn, J. Greene, and F.A. Smidt, Eds., Pittsburgh: Materials Research Society, pp. 41-46.
- Tetreault, T.G.; Hirvonen, J.K.; and Parker, G. (1989): The Friction and Wear Behavior of Ion Beam Assisted Nitride Coatings. In: Processing and Characterization of Materials Using Ion Beams, L.E. Rehn, J. Greene, and F.A. Smidt, Eds., Pittsburgh: Materials Research Society, pp. 439-444.

- Thomas, K.A.; Kay, J.F.; Cook, S.D.; and Jarcho, M. (1987): "The Effect of Surface Macrotecture and Hydroxylapatite Coating on the Mechanical Strengths and Histologic Profiles of Titanium Implant Materials, Journal of Biomedical Materials Research, 21:1395-1414.
- Thornton, J.A. (1982a): Coating Deposition by Sputtering. In: Deposition Technologies for Films and Coatings, R.F. Bunshah, Ed., Park Ridge, N.J.: Noyes Publications, pp. 170-243.
- Thornton, J.A. (1982b): Plasmas in Deposition Processes. In: Deposition Technologies for Films and Coatings, R.F. Bunshah, Ed., Park Ridge, N.J.: Noyes Publications, pp. 19-62.
- Thornton, J.A. and Penfold, A.S. (1978): Cylindrical Magnetron Sputtering. In: Thin Film Processes, J.L. Vossen and W. Kerns, Eds., New York: Academic Press, pp. 76-114.
- Tucker, Jr., R.C. (1982): Plasma and Detonation Gun Deposition Techniques and Coating Properties. In: Deposition Technologies for Films and Coatings, R.F. Bunshah, Ed., Park Ridge, N.J.: Noyes Publications, pp. 454-489.
- Van Mullem, P.J. and Maltha, J.C. (1983): Histology of Bone: A Synopsis. In: Bioceramics of Calcium Phosphate, Boca Raton, Fla.: CRC Press, pp. 53-78.
- Van Raemdonck, W.; Ducheyne, P.; and De Meester, P. (1984): Auger Electron Spectroscopic Analysis of Hydroxylapatite Coatings on Titanium, Journal of the American Ceramic Society, 67:381-384.
- Vossen, J.L. and Cuomo, J.J. (1978): Glow Discharge Sputter Deposition. In: Thin Film Processes, J.L. Vossen and W. Kern, Eds., New York: Academic Press, pp. 12-75.
- Waits, R.K. (1978): Planar Magnetron Sputtering, In: Thin Film Processes, J.L. Vossen and W. Kerns, Eds., New York: Academic Press, pp. 131-174.
- Webb, D.J.; Dietrich H.-P.; Gfeller, F.; Moser, A.; and Vettiger, P. (1989): Passivation of GaAs Laser Mirrors by Ion-Beam Deposited Al₂O₃. In: Processing and Characterization of Materials Using Ion Beams, L.E. Rehn, J. Greene, and F.A. Smidt, Eds., Pittsburgh: Materials Research Society, pp. 507-512.
- Wehner, G.K. and Anderson, G.S. (1970): The Nature of Physical Sputtering. In: Handbook of Thin Film Technology, L.I. Maissel and R. Glang, Eds., New York: McGraw-Hill Book Company, pp. 3.1-3.38.

- Westwood, W.D. (1988): Sputter Deposition Processes, MRS Bulletin, 13:46-51.
- Williams, F.L.; Boyer, L.L.; Reicher, D.W.; McNally, J.J.; Al-Jumaily, G.A.; and McNeil, J.R. (1989): In: Processing and Characterization of Materials Using Ion Beams, L.E. Rehn, J. Greene, and F.A. Smidt, Eds., Pittsburgh: Materials Research Society, pp. 483-494.
- Woltgens, J.H.M. (1983): Formation and Decay of the Tooth. In: Bioceramics of Calcium Phosphate, K. de Groot, Ed., Boca Raton, Fla.: CRC Press, pp. 33-52.
- Yamamuro, T.; Jitsuhiko, S.; Kakutani, Y.; Yoshii, S.; Kitsugi, T.; and Ono, K. (1988): Novel Methods for Clinical Applications of Bioactive Ceramics. In: Bioceramics: Material Characteristics Versus In Vivo Behavior, P. Ducheyne and J.E. Lemons, Eds., New York: The New York Academy of Sciences, pp. 107-114.
- Yamauchi, H.; White, R.J.; Ayukawa, M.; Murray, T.C.; and Robinson, J.W. (1988): The Structure of Thin Films Sputter Deposited from a $Ba_2Si_2TiO_8$ Ceramic Target, Journal of Materials Research, 3:105-111.
- Ziemann, P. and Kay, E. (1983): Correlation Between the Ion Bombardment During Film Growth of Pd Films and Their Structural and Electrical Properties, Journal of Vacuum Science and Technology, A1:512-516.
- Zuhr, R.A.; Pennycook, A.J.; Haynes, T.E.; and Holland, O.W. (1989): Metal Silicides Formed by Direct Ion Beam Deposition. In: Processing and Characterization of Materials Using Ion Beams, L.E. Rehn, J. Greene, and F.A. Smidt, Eds., Pittsburgh: Materials Research Society, pp. 47-54.

GRADUATE SCHOOL
UNIVERSITY OF ALABAMA AT BIRMINGHAM
DISSERTATION APPROVAL FORM

Name of Candidate E. Douglas Rigney Jr.

Major Subject Biomedical Engineering

Title of Dissertation Characterization of Ion-Beam Sputter-Deposited
Calcium-Phosphate Films

Dissertation Committee:

Dr. Bill Lacefield, Chairman

William Lacefield

Dr. Linda Lucas

Linda C. Lucas

Dr. Rose Andrews

Rose Andrews

Dr. Jack Lemons

Jack Lemons

Dr. Ray Thompson
Director of Graduate Program

Raymond G. Thompson
Martin J. McEntee

Dean, UAB Graduate School

Arthur Hamel

Date August 3, 1989